UNIVERSITÀ
DEGLI STUDI
DI PADOVA

Sede Amministrativa: Università degli Studi di Padova

Dipartimento di Scienze Chimiche

_____

CORSO DI DOTTORATO DI RICERCA IN: Scienze Molecolari

CURRICOLO: Scienze Chimiche

CICLO: XXXV°

Ultrafast relaxation dynamics of Fucoxanthin Chlorophyll Protein: the carotenoid perspective

Coordinatore: Ch.mo Prof. Leonard Prins

Supervisore: Ch.ma Prof. Elisabetta Collini

Dottorando: Giampaolo Marcolin

Questa stanza di luce

È cattedrale per le mie intuizioni

Nascoste tra le nocche delle dita

Tra le intercapedini delle mani

È il non saperti spiegare

Perché tra queste nere mura

Tutto ciò che so si abbandona

Al gesto minuscolo delle articolazioni

Queste non sono più le mie dita

Queste non sono più le mie mani

Sono qualcosa di condiviso

E io, tra i fasci di luce, gli specchi e le brugole

Non sono più solo io

INDEX

Abstract

Fucoxanthin Chlorophyll Protein (FCP) is a Light Harvesting Complex that can be found in diatoms and brown algae, crucial for the photosynthesis process in the marine environment. Thanks to the presence of specific chromophores (fucoxanthin, chlorophyll *a* and chlorophyll *c*), it is able to capture the blue-green part of the light spectrum. The recent discovery of the 3D structure of FCP coming from different organisms, resolved by crystallography (from the diatom *Phaeodactylum tricornutum*) and electron microscopy (from the diatom *Chaetoceros gracilis*), helped to understand how the pigments are arranged in the protein scaffold. This knowledge is a fundamental tool for characterizing and analyzing the spectroscopic feature of FCP. In this Ph.D. thesis, the ultrafast relaxation dynamics of FCP are investigated through Two-Dimensional Electronic Spectroscopy (2DES), with a particular focus on the characterization of the role of fucoxanthin. In particular, I tried to answer a new question arising from the disclosure of structural data: the spatial closeness between fucoxanthin and chlorophyll *c* suggests an interaction between these two molecules, but no sign of such an interaction has been found so far. I found evidence of this interaction in an ultrafast signal appearing in 2DES maps, attributable to an ultrafast delocalization of the excitation among the chromophores. Preliminarily to these measurements, I performed a solvent-dependent characterization of isolated fucoxanthin with 2DES, studying the features related to its Intramolecular Charge Transfer (ICT) state. As a result, I found new experimental evidence related to an instant population of the ICT state, explainable using a model in which the ICT is coupled with the S_2 state rather than the S_1 state, as generally considered. This preliminary characterization helped me to gain insight into the spectroscopic features of fucoxanthin, and it turned out to be of crucial importance before the characterization of FCP.

Abstract (italiano)

La Fucoxanthin Chlorophyll Protein (FCP) è una proteina antenna che si può trovare in diatomee e alghe marroni, ed è cruciale per i processi di fotosintesi che avvengono nell'ambiente marino. Grazie alla presenza di cromofori come fucoxantina, clorofilla a e clorofilla c, questa proteina è in grado di assorbire la parte blu-verde dello spettro della luce solare che filtra sott'acqua. Recentemente, la pubblicazione della struttura 3D di vari complessi di FCP ottenuti da organismi diversi, risolta tramite cristallografia (per la diatomea *Phaeodactylum tricornutum*) e microscopia elettronica (per la diatomea *Chaetoceros gracilis*), ha permesso di capire come i pigmenti sono disposti all'interno della proteina. Inoltre, la conoscenza di questa struttura è uno strumento fondamentale per caratterizzare e analizzare le proprietà spettroscopiche di FCP. In questa tesi di dottorato, ho studiato le dinamiche di rilassamento ultraveloce di FCP tramite la spettroscopia elettronica bidimensionale (2DES), con particolare attenzione alla caratterizzazione del ruolo della fucoxantina. In particolare, ho provato a rispondere a nuove domande che sono emerse dai dati strutturali: infatti la vicinanza spaziale tra fucoxantina e clorofilla c suggerisce una possibile interazione fra di loro, anche se non esistevano ad oggi prove sperimentali a supporto. In questa tesi, ho trovato la prova di questa interazione nella presenza di un segnale ultraveloce nelle mappe 2DES che ho attribuito a un'eccitazione ultraveloce delocalizzata tra i vari cromofori. Prima delle misure su FCP, mi sono dedicato alla caratterizzazione 2DES della fucoxantina disciolta in diversi solventi, con l'obbiettivo di studiare le caratteristiche legate ad uno stato a trasferimento di carica intramolecolare (ICT). Come risultato, sono riuscito a trovare una nuova evidenza sperimentale legata alla formazione istantanea di una popolazione dello stato ICT, spiegabile attraverso un modello in cui lo stato ICT è accoppiato allo stato S_2, piuttosto che allo stato S_1, come generalmente si considera. Questo studio preliminare è stato fondamentale per comprendere meglio le caratteristiche spettroscopiche della fucoxantina e si è rivelato di cruciale importanza prima delle misure su FCP.

Chapter 1

Introduction

How is it possible to gain information about what surrounds us? Every day humans interact with their environment through the five senses. With sight, for example, we are able to investigate the shapes of the objects and how they evolve in time, thanks to the photons that hit them and then reach our retina. Over the centuries, we expanded the possibility for our eyes to interact with bigger objects (for example, a night sky with a telescope) or smaller objects (for example, insects with magnifying glasses or even further, microbes with microscopes). But also modern optical microscopes have their limits and cannot go below a certain resolution (10^{-7} m). Chemistry deals with molecules so small that cannot be detected by human sight, even if helped through magnification tools. If we want to understand the features of the molecules that form everything that surrounds us, we have to use other tools, such as more advanced non-optical imaging techniques or spectroscopy.

Similarly to our sight, spectroscopy uses the interaction between matter and light to investigate molecules and their features and how they evolve over time. A lot of spectroscopic techniques exist to satisfy different tasks; during my Ph.D. project, I've been learning and working on Two-Dimensional Electronic Spectroscopy (2DES), an advanced optical technique that operates with laser pulses in the visible region of the electromagnetic spectrum and that can trace the evolution of the explored systems in a femtosecond time regime (10^{-15} s).[1–3] In this way, we are able to experience the small world of molecules and macromolecules, but also the ultrafast world of the processes that govern them. In fact, with 2DES it is possible to follow the ultrafast relaxation dynamics of the excited states of the systems under investigation and to see how these states can interact with each other, leading for example to energy transfer processes and internal conversions, or with the solvent / environment, leading to dephasing and damping processes.[4]

What kind of systems would be worth investigating with 2DES? Since the advent of this technique, about twenty years ago, *Light Harvesting Complexes* (LHCs) belonging to the vast world of photosynthesis[5] are one of the most studied systems.[6–10] Photosynthesis is one of the most remarkable and crucial processes that happen in nature, as many living beings found their main vital functions on it. In fact, plants and other autotrophic organisms are able to convert sunlight and carbon dioxide into energy, oxygen and biomass through this phenomenon, which is organized in many different phases. The first one is called

light harvesting. This process is promoted by LHCs, proteins that embed chromophores such as chlorophylls and carotenoids that absorb the sunlight and then transfer it to the reaction center, where the chemical reactions occur.[11] This process is generally described in the wider context of Excitation Energy Transfer (EET) models, but the fine details that characterize the entire photosynthetic process are still not fully clear.[12]

The scientific community has always been very interested in comprehending this phenomenon. One of the most intriguing developments suggested that some aspects of biological light-harvesting might be explained through the use of quantum mechanics. This hypothesis, related also to other biological processes, has contributed to the birth of the emergent field of *quantum biology*.[13] In this framework, 2DES represents the optimal technique to investigate and observe this kind of phenomenon. In fact, one of the most important achievements of this technique is the observation, even at room temperature, of long lived oscillations in the energy transfer dynamics of different light-harvesting complexes, suggesting the involvement of quantum electronic coherence in the process.[14–16]

During my Ph.D. I wanted to focus on a particular kind of LHC, crucial for the production of oxygen in the ocean, that recently gained a lot of attention because of the characterization of its crystallographic structure: the Fucoxanthin Chlorophyll Protein (FCP).[17,18] As the name suggests, FCP is a LHC characterized by the presence of two chromophores: fucoxanthin (a carbonyl carotenoid) and chlorophyll (*a* and *c*). It can be found in underwater organisms such as diatoms and brown algae. Because of the challenging light conditions experienced by these organisms, the photosynthetic process has evolved towards high efficiency levels of light harvesting, and, more precisely, EET processes. For this reason, FCP and other similar LHCs have been widely studied over the years to understand the fine details that govern the energy transfer dynamics of its pigments. Nonetheless, a clear view of the energy relaxation pathways and the interplay between the excited states at play is not clear yet.[19]

In this context, the aim of my Ph.D. project is to investigate FCP's ultrafast relaxation dynamics through 2DES, with a particular focus on carotenoid's characterization. To this aim, I followed a slightly different approach than the one employed in previous spectroscopic characterizations. Rather than exploiting spectroscopic data to gain information about the structure of the protein and the arrangement of the chromophores,[20,21] I took into account the recently published structure of FCP for a more thorough interpretation of the 2DES measurements, trying to solve new challenges arisen from the knowledge of the structure.

Because of the complexity of the specific mechanisms involved in the antenna multi-chromophoric systems, it is pivotal to have a very precise preliminary knowledge of the photophysical properties of the individual molecular species involved.[22] Having this in mind, the first part of my Ph.D. project was dedicated to the 2DES exploration of the ultrafast relaxation dynamics of fucoxanthin *in vitro*, with a solvent-dependent characterization. In fact, the possibility of comparing the signals of fucoxanthin *in vitro* and *in protein* has been very helpful in the characterization of the FCP dataset: carotenoids, and fucoxanthin in particular, are molecules quite challenging to investigate spectroscopically, because of the multiple electronic states involved in their dynamics, some of which are not even excitable directly. In fact, a clear view of the ultrafast relaxation dynamics of these molecules is still missing.[23,24] As it will be described in depth in the following parts of this thesis, this original approach allowed to unveil relevant details about the interaction and the dynamic processes between fucoxanthin and chlorophyll chromophores.

This thesis is divided into eight chapters. This first introductory chapter outlines the overall organization of my project, where the common thread is represented by the fucoxanthin molecule, the real protagonist and fulcrum of my studies and research. The second chapter lays the groundwork to understand the theoretical background governing the light-matter interaction and, specifically, which kind of signal a 2DES experiment yields. The third chapter describes the 2DES experimental setup used for data acquisition, processing and analysis. Chapter four summarizes the current state-of-the-art knowledge on the isolated chromophores under investigation: fucoxanthin and chlorophyll; in particular, the spectroscopic features characterized up to now and the controversies they raised are reported. Chapter five, instead, summarizes the state-of-the-art of the FCP and the recent findings about its crystallographic structure. The sixth and seventh chapters are devoted to the analysis of the experimental data of fucoxanthin and FCP and their interpretation, respectively. Finally, chapter eight collects the most relevant conclusive remarks on my Ph.D. project and its future perspectives.

Chapter 2

Theory Notes

Two-Dimensional Electronic Spectroscopy (2DES) is an ideal tool to investigate the relaxation dynamics of the excited electronic states of molecules that happen in the ultrafast time scale. To understand the type of information and signals that a 2DES measure provides, a theoretical background that describes the physics of the light–matter interaction that controls these processes is needed.[25]

2.1 Density Matrix

In this spectroscopic framework, the most convenient way to treat the light–matter interaction is to use a *semi-classical* approach, where the light is described classically by Maxwell's equations, while the matter is treated quantum-mechanically. More precisely, the system can be more generally described as a statistical ensemble of different quantum states, that cannot be identified by a single wavefunction. A theoretical approach particularly suitable for treating this kind of systems involves the Density Matrix formalism. The first tool that is used in this approach is the density operator for a pure state (i.e. a state that can be described using only a single wavefunction $\psi(t)$), defined as the outer product of the wavefunction with its conjugate, labelled as *ket* and *bra*, respectively:[25,26]

$$\hat{\rho}(t) \equiv |\psi(t)\rangle\langle\psi(t)| \tag{1.1}$$

It works as a projection operator, acting both on the right and on the left side of a given observable. This operator can also be expressed in a matrix representation where the matrix elements are written as:[25,26]

$$\rho_{ij} = \langle i|\psi(t)\rangle\langle\psi(t)|j\rangle \tag{1.2}$$

where i and j are elements (rows and columns) of the density matrix. Two different types of matrix elements can be distinguished in the matrix representation of the density operator: in-diagonal elements, called *populations*, and off-diagonal elements, called *coherences*. Populations represent the probability of the system of being described by the *i-th* eigenstate, whether the coherences represent the probability of being described by a superposition of different states, oscillating with a frequency that depends on the energy of the states involved.

The density matrix formalism is particularly useful in measuring of observables, which are estimated as the expectation value of a given operator $\langle \hat{A} \rangle$. In fact, everything is reduced to the calculation of the trace of the density matrix, i.e. the sum of the diagonal elements:

$$\langle \hat{A} \rangle = Tr[A\rho] \tag{1.3}$$

This means that the only difficulty we might encounter, concerns the actual definition of $\hat{\rho}(t)$, which can vary, for example, in the case that the system is in a pure state or in a statistical ensemble of different states. Since 2DES is a time-dependent spectroscopic technique, we have to take into account the temporal evolution of the density matrix. This is defined by the Liouville-Von Neumann equation, here written in the interaction picture:[25,26]

$$\frac{\partial \hat{\rho}^I(t)}{\partial t} = -\frac{i}{\hbar}[\hat{V}^I(t), \hat{\rho}^I(t)] \tag{1.4}$$

where the square brackets delimit a commutator operator and $\hat{V}^I(t)$ represents the time-dependent part of the Hamiltonian that describes the system. Eq. 1.4 can be solved by integrating it iteratively to obtain the perturbative expansion of the density operator. In this way, we can select the order of the solution by choosing the number of iterations, i.e. the time steps needed to describe the time evolution of the system. In the next section, we'll see how this approach can be applied to a third-order spectroscopic technique like 2DES.

2.2 Response Theory

The response theory introduces the concept of the response function that quantifies the system's response to a generic time-dependent perturbation. The perturbation interacts with an internal variable of the system and this interaction generates a measurable observable. In non-linear optics, the generic perturbation is the electric field (originated by the laser pulse), the internal variable is the transition dipole moment of the system and the observable is the expectation value of the transition dipole moment, i.e. the macroscopic polarization. In the interaction picture of the density matrix formalism, the *n-th* order polarization can be written as:[25,26]

$$P^{(n)}(t) = Tr[\mu^I(t)\rho^{I(n)}(t)] = \langle \hat{\mu}^I(t)\hat{\rho}^I(t) \rangle \tag{1.5}$$

where μ^I and $\rho^{I(n)}$ are the matrix representations in the interaction picture of the transition dipole moment and the *n-th* order density operator, respectively.

Instead, the perturbation can be described by the time-dependent part of the Hamiltonian $\hat{V}^I(t)$, expressed in the dipole approximation:

$$\hat{V}^I(t) = -\hat{\mu}^I(t)E(t) \tag{1.6}$$

Now we can insert the expression of the polarization and the perturbation in the integrated form of Eq. 1.4. In this way we obtain an equation that links the non-linear polarization with the density matrix operator, a useful tool that connects the macroscopic vision of the light-matter interaction with the quantum mechanical microscopic point of view of the density matrix. As 2DES is a third-order spectroscopic technique, this means that we can stop the iterations at the third step, calculating the third-order polarization:

$$\begin{aligned} P^{(3)}(t) = \left(-\frac{i}{\hbar}\right)^3 \int_{t_0}^{t} d\tau_3 \int_{t_0}^{\tau_3} d\tau_2 \int_{t_0}^{\tau_2} d\tau_1 E(\tau_3)E(\tau_2)E(\tau_1) \cdot \\ \cdot Tr\left[\hat{\mu}^I(t)\left[\hat{\mu}^I(\tau_3),\left[\hat{\mu}^I(\tau_2),\left[\hat{\mu}^I(\tau_1),\hat{\rho}^I(-\infty)\right]\right]\right]\right] \end{aligned} \tag{1.7}$$

It is essential to have a clear understanding of the time variables used to characterize the time order of the third-order light-matter interaction, that are τ_1, τ_2 and τ_3. They represent the absolute times at which the three pulses (the electric fields) arrive on the system. After the three interactions, the system emits a signal at time t. A more advantageous way to treat the light-matter interactions is to implement a new set of time variables: t_1, t_2 and t_3, which represent the time intervals between the pulses and not the absolute times at which they arrive. This means that t_1 is the interval between the first and the second pulse, t_2 the one between the second and the third pulse and t_3 is the interval between the third pulse and the emission of the signal.

Eq. 1.7 can, thus, be rewritten following the response theory, where the third-order polarization (the observable) can be expressed as the convolution of three external electric fields (the perturbation) with the third-order response function $S^{(3)}(t_3, t_2, t_1)$, using the new time variables discussed before:

$$\begin{aligned} P^{(3)}(t) = \int_{0}^{\infty} dt_3 \int_{0}^{\infty} dt_2 \int_{0}^{\infty} dt_1 E(t-t_3) \cdot \\ \cdot E(t-t_3-t_2)E(0) \times S^{(3)}(t_3, t_2, t_1) \end{aligned} \tag{1.8}$$

We can now infer the form of the response function:

17

$$S^{(3)}(t_3, t_2, t_1) = \left(-\frac{i}{\hbar}\right)^3 \cdot$$

$$\cdot Tr\left[\hat{\mu}^I(t_1 + t_2 + t_3)\left[\hat{\mu}^I(t_1 + t_2), [\hat{\mu}^I(t_1), [\hat{\mu}^I(0), \hat{\rho}^I(-\infty)]]\right]\right] \tag{1.9}$$

At this point, the response function for a third-order spectroscopic technique can be calculated. First, the nested commutator must be solved: it is composed of 2^3 terms; the trace of every one of them with $\hat{\rho}^I(-\infty)$ represents one of the possible pathways of interaction that the field can promote on the system.

These pathways are called Liouville pathways. Since every pathway (R_j) has its corresponding conjugated complex (R_j^*), four terms are enough to describe the response function:

$$S^{(3)}(t_3, t_2, t_1) = \left(-\frac{i}{\hbar}\right)^3 \sum_{j=1}^{4} (R_j - R_j^*) \tag{1.10}$$

2.3 Double-sided Feynman diagrams

The eight terms originated from R_j and R_j^* represent the eight Liouville pathways that can describe the total response function for a third-order spectroscopy. In this section, I will discuss how these pathways differ from one another and what kind of signals we expect from them. Their mathematical notation can get quite challenging, but there is a simpler way to represent the eight pathways in a graphical manner, the so-called double-sided Feynman diagrams.[27,28] In this way, it is possible to follow the temporal evolution of the density matrix after each interaction with the electromagnetic field. All the relevant pathways represented by the Feynman diagrams are summarized in figure 2.1.

As the name suggests, double-sided Feynman diagrams are composed of two vertical lines: the left one represents the *ket* part of the density matrix, whereas the right line represents the *bra*. The time evolution of the system goes upwards: before the first interaction, the density matrix, which is in equilibrium conditions, is represented by the letters "gg", indicating that both the *ket* and the *bra* are in the ground state. Each interaction with the electric field is pictured by an arrow. The arrows can point towards the two vertical lines, representing an absorption, or outwards the vertical lines, representing an emission. The arrows on the left side are interactions with the *ket*, instead, the ones on the right are interactions with the *bra*.
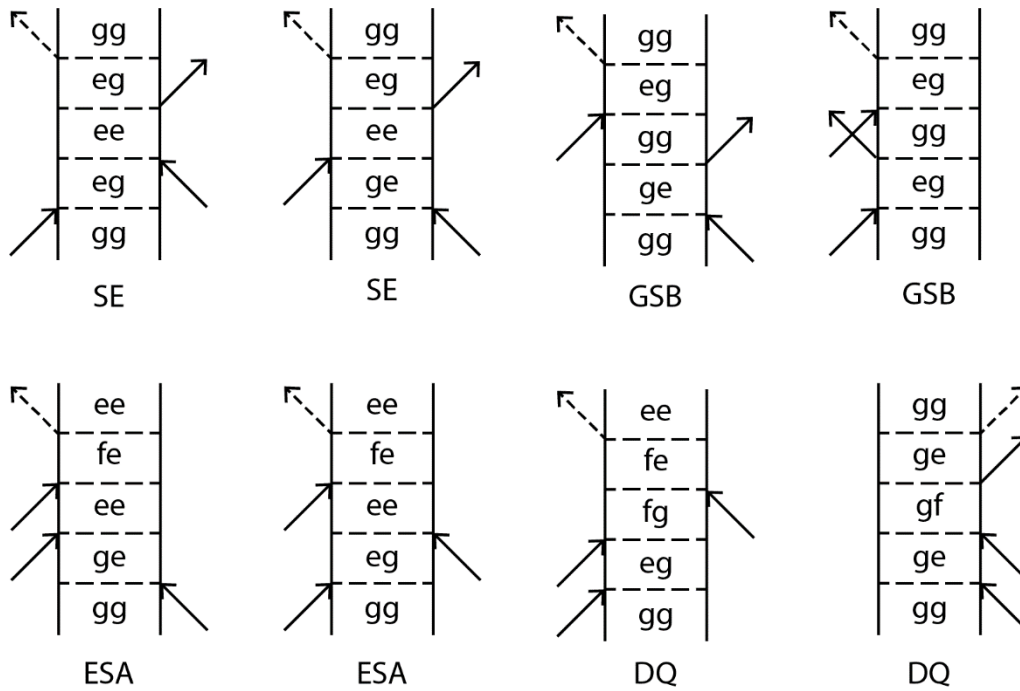
Figure 2.1 -Double-sided Feynman diagrams summarising all the possible contributions to the third-order response function.

SE = stimulated emission; GSB = ground state bleaching; ESA = excited state absorption; DQ = double quantum.

After each interaction, the two letters (like "gg") that represent the indexes of the density matrix change according to the kind of interaction that occurred. In figure 2.1, the time evolution of the system also involves two different excited states labelled with the letters "e" and "f". The last arrow is drawn with a dashed line: that is the generation of the signal and, since it is an emission of radiation, it points away from the vertical lines. During the temporal evolution of the density matrix, i.e. between two arrows, the system can be found either in a coherence, if the *bra* and the *ket* are in different states, or in a population, if both *bra* and *ket* are found in the same state.

Moreover, it is possible to determine whether a particular laser pulse has a positive or a negative frequency field. Here we adopt the convention that arrows pointing to the left (outward on the *ket* side, inward on the *bra* side) represent an interaction with a positive frequency field, $E^+(t)$, whereas, arrows pointing to the right (inward on the *ket* side, outward on the *bra* side) represent an interaction with a negative frequency field, $E^-(t)$. By analyzing the sign of the three interactions with the system described by that particular Liouville pathway, we can understand from the Feynman diagrams which will be the frequency of the emitted signal.[26]

With this information in mind, it is now possible to analyze the different kinds of Liouville pathways in figure 2.1. The two pathways labelled SE are associated with a process known as Stimulated Emission. The first two interactions generate a population in the excited state; the third one causes an emission from

this excited state and then the signal is emitted, restoring the ground state population. Further on, GSB stands for Ground State Bleaching: differently from SE, after the first two pulses, the system is found again in the ground state population. These first four pathways emit a positive signal. Instead, the pathways known as Excited State Absorption (ESA) are characterized by a negative amplitude. In this case, the first two pulses are identical to the SE processes: they generate an excited state population, but the third interaction promotes another absorption to a higher excited state, and then the signal restores the population of the excited state. The last two pathways are associated with a process called double-quantum coherence (DQ), where there is a coherence between the ground state and a double-excited state after the second pulse interaction.

2.4 Two-Dimensional Electronic Spectroscopy

With the theoretical knowledge acquired in the previous sections, it is now possible to describe the response obtained in an experiment of 2D Electronic Spectroscopy, the main spectroscopic technique exploited during my Ph.D. 2DES is a third-order nonlinear experiment, and all the information that can be gathered from it is stored in the third-order response function, $S^{(3)}(t_1, t_2, t_3)$, which is a three-dimensional function oscillating in time. The physical meaning of $S^{(3)}(t_1, t_2, t_3)$ is hard to understand intuitively. In order to have a function easier to manipulate, the time domains t_1 and t_3 are Fourier transformed:

$$S^{(3)}(\omega_1, t_2, \omega_3) = \iint_{-\infty}^{\infty} dt_1 dt_2 \, S^{(3)}(t_1, t_2, t_3) e^{-i\omega_1 t_1} e^{-i\omega_3 t_3} \tag{1.11}$$

In this way, the response function is easier to visualize: the result of a 2DES experiment is a series of two-dimensional frequency-frequency maps that evolve along the population time, t_2, which is the time interval between the second and the third pulse. Considering each 2D map, the x-axis corresponds to the excitation frequency ω_1 and the y-axis corresponds to the emission frequency ω_3. This is why this spectroscopic technique is called "two dimensional" electronic spectroscopy. The excitation axis gives information about the first excited coherence that evolves during the first delay time t_1, and its frequency is the measure of the energy difference between the states involved. The emission axis, similarly, provides information about the coherence evolving during the third delay time t_3. Thus, signals can appear in different parts of the map, having different x and y coordinates.

The first distinction that must be made is between diagonal peaks and off-diagonal (cross) peaks. A diagonal peak is characterized by the same excitation and emission frequency, so it refers to a population of a specific state and it describes, along t_2, the decay dynamics of this state. A cross-peak, instead, has a different excitation and emission frequency; this means that the state from which the signal is emitted is different from the one initially excited. The presence of cross-peaks thus signals the presence of coupling between different states (energy and charge transfer, vibronic coupling, relaxation, etc.). The possibility of distinguishing cross-peaks (and the associated coupling mechanisms) and following their dynamics in time, separately from the populations' diagonal signals, is one of the main strengths of 2DES with respect to other conventional 1D time-resolved techniques.[2,29–32]

Analyzing the diagrams in figure 2.1, it is possible to ascertain that ESA processes appear as cross-peaks, GSB as diagonal peaks, while SE processes can contribute either as diagonal or cross peaks. ESA will be the main peaks that will be discussed in this thesis, as this kind of signals strongly dominates the third-order response function of carotenoids in the investigated spectral region.

Chapter 3
Setup and Data Analysis

In this chapter, we will focus on the experimental details surrounding the 2DES measurements. The optical layout of the technique will be discussed, starting from the laser source generating the exciting pulse train, its propagation along the optical table and how it eventually interacts with the sample. Consequently, the resulting signal is captured by a detector and then it can be processed and elaborated through home-made software routines, ready to be analyzed and discussed for the interpretation of the data.

3.1 Experimental Setup

2DES was developed about twenty years ago, making it relatively young among other techniques.[1–3] As already mentioned in the previous chapter, 2DES is a third-order non-linear spectroscopic technique: this means that the experiment is characterized by the presence of three different laser pulses that interact with the system under investigation. The three pulses are separated both spatially and temporally, and with 2DES it is possible to reach a sub-10 femtosecond time resolution. Since it is possible to control the different delay times between pulses independently, the ultrashort time resolution of 2DES does not cause an indetermination on the excitation frequency, due to the Heisenberg indetermination principle, because time resolution and excitation frequency can be decoupled thanks to the Fourier Transform methodology.[31]

The particular spatial arrangement (phase matching conditions) chosen for the pulses in our setup is known as BOXCARS geometry. The peculiarity of this geometry setting is that the three pulses propagate parallel one to another along the three vertices of an imaginary square. Then, thanks to a spherical mirror, they are focalized on the sample. Following the phase-matching rules of non-linear spectroscopy, the resulting signal is emitted along the fourth vertex of the imaginary square. This means that the signal can be captured background-free as it does not share its direction with any other laser pulse, increasing the signal-to-noise ratio substantially; on the other hand, this feature requires high levels of phase stability, whose lack leads to signal degradation.[33] In figure 3.1 I report a schematic representation of the whole experimental setup of the 2DES built in our lab,[34] inspired by Nemeth *et al.*[35] Each of its elements will be described in the following subsections.
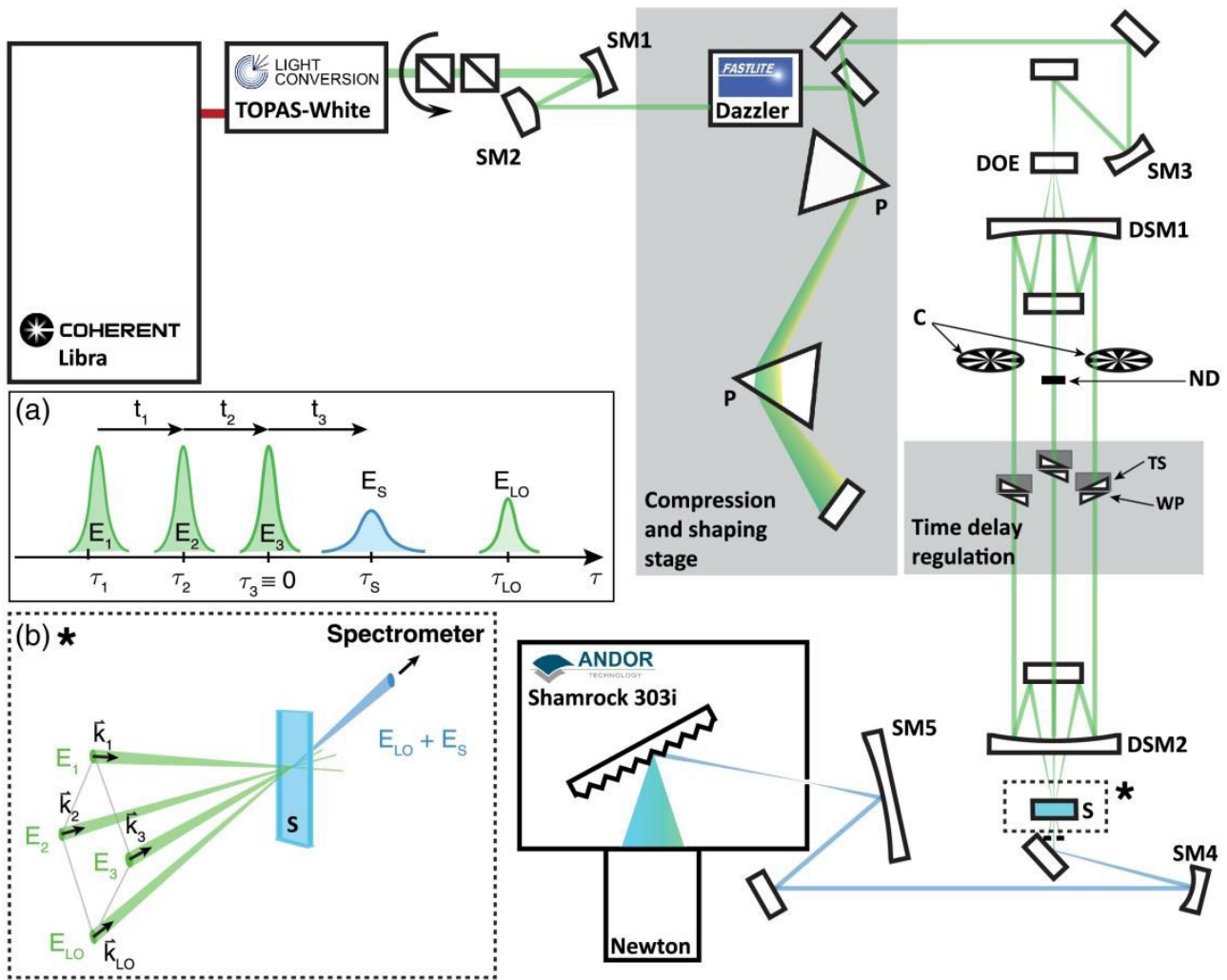
Figure 3.1 - Schematic representation of the 2DES setup. Abbreviations: SM – spherical mirror, P – prism, DOE – diffractive optical element, DSM – donut spherical mirror, C – chopper, ND – neutral density filter, WP – wedge pairs, TS – transitional stage, S – sample. Panel a) time order of pulses, panel b) BOXCARS geometry representation. Reproduced from Bolzonello et al.[34]

3.1.1 Laser Source

The first component of our experimental setup is the laser source. The laser pulses are generated by a Coherent® Libra laser system. It is based on an amplified Ti:Sapphire system and composed of three subunits:

1. a Ti:Sapphire oscillator (*Vitesse*), which generates a train of pulses at 800 nm after being pumped by a green laser (*Verdi*). The train of pulses has a repetition rate of 80 MHz and each pulse is characterized by a bandwidth of ~12 nm, an energy of 3.5 nJ and a duration of 100 fs. These pulses are known as "seed" pulses;

2. a Nd:YAG laser (*Evolution*), which emits nanosecond pulses at 527 nm;

3. a regenerative optical amplifier (*Regen Cavity*) with a Ti:Sapphire rod, which amplifies the seed pulses up to 100.000 times. The cavity works in a population inversion regime guaranteed by the *Evolution* that acts as a pump.

Before entering in the *Regen Cavity* the seed pulses are stretched in time by a stretcher grating to preserve the rod from high peak power. After the amplification, the pulses are then restored to the initial duration by a compressor grating. The final output of the Libra system is a train of pulses at 800 nm with a repetition rate of 3 KHz, power of ~1.7 W and time duration of 100 fs.

3.1.2 Non–collinear Optical Parametric Amplifier

Successively, the laser beam enters the Light Conversion® TOPAS White, a non–collinear optical parametric amplifier (NOPA) that allows to tune the wavelength of the pulses from 500 nm to 1100 nm. The idea is to amplify a specific spectral range of a supercontinuum (white) light through the interaction with 400 nm pump beams on a barium–boron–oxide (BBO) crystal ($Ba(BO_2)_2$) through non–linear effects. Firstly, the 800 nm beam is split in two by a beam splitter. One of the beams is the 1% of the total, and it is focused on a sapphire plate that generates a white–light continuum. Then the white light is collimated and focused into a pulse shaper that controls the chirp and the bandwidth of the final amplified pulse. The remaining 99% passes through a first BBO crystal that converts the 800 nm pulse into a 400 nm pulse through second harmonic generation. This beam is, in turn, split into two other beams, that constitute the pump beams: a 5% acts as a pre-amplification beam while the other 95% is the main pump amplification beam.

Then the white light and the two pump beams converge on a second BBO crystal, where the three pulses interact to amplify a specific part of the white light. It can be selected and maximized by changing the incident angle between the pulses and their reciprocal time delay, i.e., through fine control of the superposition of the pulses both in time and space. Finally, the amplified beam is collimated with a mirror telescope and exits the TOPAS. The output is a train of pulses with a bandwidth of ~100 nm centered at the wanted wavelength. Each pulse has a time duration of about 20 fs and an energy between 1 and 30 μJ. During my Ph.D. project, I investigated different samples that required the selection of different spectral ranges. In the following chapters, these systems and the bandwidth selected for their characterization will be described in detail.

3.1.3 Pulse Shaping

The output of the TOPAS is a train of broadband ultrashort pulses. Dealing with this kind of pulses requires particular precaution as their phase and time duration can be easily distorted during the propagation in the optical elements along the optical path. The primary distortion happens when the broadband pulse passes through a transmissive optical medium with a wavelength-dependent refractive index: the different frequency components of the pulse acquire different speeds when they travel in the medium, that is, the blue component propagates slower than the red one.

A different speed of the components leads to a phase distortion of the wavefront and consequently the time duration of the pulse increases. This non-linear deviation is called "temporal chirp" and it can strongly affect the final shape of the 2DES maps.[34,36] The goal is to excite the optical sample with the shortest pulse possible, i.e., with all the different frequency components of the pulse arriving at the same moment. This condition is the so-called transform-limited (TL) pulse.

In our setup, it is possible to compensate for the phase distortions thanks to two different systems: a prism compressor and an Acousto-Optic Programmable Dispersive Filter (AOPDF, Fastlite® Dazzler). The prism compressor is composed of a couple of prisms made of a material with a known wavelength-dependent refractive index. The pulse passes through the first prism that diffracts the different frequency components of the pulse, which are later restored by the second one. The idea is that, varying the incident angle and the distance between the two prisms, the different light components experience different pathways which can be optimized to compensate for the overall temporal chirp of the laser pulse.

This method is particularly useful for broadband pulses, where the only AOPDF method is not enough for the chirp compensation. Nonetheless, the AOPDF is used in parallel with the prism compressor system, as it allows finer and independent control over the phase. The AOPDF in fact, contains an acoustic-optic crystal coupled to a piezoelectric device that generates acoustic waves.

The pulses pass inside the crystal and interact with the acoustic waves longitudinally, allowing complete control over the phase and amplitude of the pulses. The phase can be monitored by using an integrated software that controls the acoustic waves that "soak" the crystal. The Dazzler allows also to control the "frequency" shape of the pulse, besides its temporal chirp.

3.1.4 BOXCARS Geometry and Time Delay Regulation

The next step of the experimental setup is the implementation of the BOXCARS geometry. The laser beam passes through a diffractive optic element (DOE) that splits the beam into four identical replicas with the same phase and time delay. The four beams propagate parallelly along the four vertices of a square and then are refocused on the optical sample, as shown in figure 3.1b. Three of the four beams represent the three exciting pulses that generate the third-order polarization signal in 2DES. The fourth pulse, instead, is known as the local oscillator (LO) and is used for detection purposes. The spatial separation of the three exciting pulses is not only needed for the phase matching condition that guarantees the emission of the signal in a specific detectable direction, but also allows to monitor the relative delay times between pulses. In a 2DES experiment, the time ordering of the excitation pulses allows to separate different contributions of the total optical response, known as *rephasing* and *non-rephasing* experiments.

It is possible to manage the time delays of the pulses thanks to three couples of antiparallel 4° CaF_2 25 mm wedges. One wedge of each pair is placed on a translational stage (Aerotech® Ant95), controlled by a computer software. The translation permits to manage the quantity of medium that the laser pulses encounter, thanks to the peculiar shape of the wedges; thus, passing through the medium, the laser pulses are slowed down, and their time delay can be controlled with a precision of 0.07 fs. On the contrary, LO does not need a time delay modulation; its pathway is only characterized by the presence of an OD4 graduated neutral density filter, that attenuates its power by a 10^4 factor. Its time arrival is fixed, and it is used as a temporal reference.

With phase matching conditions, the emission of the signal propagates in the same direction as the LO. This allows to obtain an "heterodyne detection": the signal interacts with the LO and their interference is detected, increasing the intrinsic signal-to-noise ratio of the data. The last step of the setup consists of detecting the LO-signal interference. Firstly, it passes through a spectrometer (Andor® Shamrock 303i) that separates the contribution of each wavelength. The signal is then recorded by the Andor® Zyla 5.5 sCMOS (scientific Complementary Metal-Oxide Semiconductor) camera with 5.5 megapixels.

3.2 Data Processing

Data are collected in the form of a three-dimensional matrix that represents the interference between the signal and LO as function of coherence time (t_1), population time (t_2) and the emission frequency (ω_3). This raw dataset cannot be analyzed directly: before the data elaboration, a preliminary step of data

processing is needed. The final goal is to obtain a 3D matrix in the form of a series of frequency-frequency (ω_1, ω_3) maps that evolve in time along the third t_2 dimension. To convert the raw dataset into this kind of matrix, a home-written MATLAB® routine was used. The preliminary processing procedure is quite complex, and a detailed description can be found in Bolzonello *et al.*[34]

The 2DES technique is phase-dependent: this means that the collected data must be phased to have a physical significance. The signal is complex, i.e. it contains both a real and an imaginary part: through the choice of an appropriate phase one can retain only one of the parts. Typically, spectroscopists are interested in the real part of the signal, as it carries information about the absorptive phenomena that take place in the system during the experiment.

Once the most accurate phase is chosen, all the repeated *rephasing* (R) and *non-rephasing* (N) datasets are averaged, forming two unique R and N 3D matrixes, which then are summed together to obtain the *total* (T) signal. At this point the R, N and T matrixes are ready for the analysis and interpretation. In figure 3.2, the total dataset after the data processing is represented by a 3D matrix where the information of the signals is stored. The 2D maps can be interpreted as slices of the matrix at given t_2 values, and the traces of the signals can be followed along the t_2 axis at specific coordinates of ω_1 and ω_3.
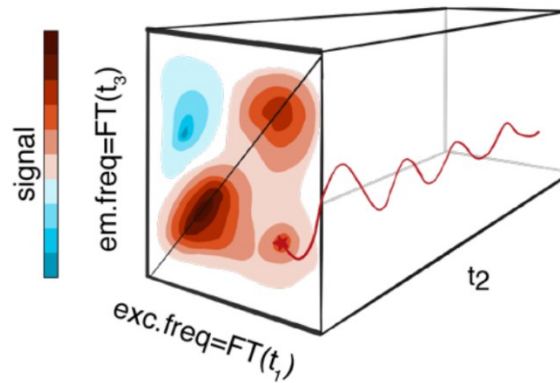

Figure 3.2 - Visual representation of the 3D matrix of the total dataset, where the total signal of the 2DES measurement is stored. The three axes identify the excitation frequency (ω_1 = FT(t_1)) the emission frequency (ω_3 = FT(t_3)) and the population time (t_2). Picture adapted from Collini.[37]

3.3 Data Analysis

The 2DES signals evolve along the time dimension t_2 and their dynamics are characterized by non-oscillating and oscillating contributions. Recalling the theoretical outline discussed in chapter 2, a signal that does not oscillate during t_2 represents a population and its time evolution can be described by an

exponential decay; whereas, a signal that oscillates along t_2 represents a coherence, i.e. the superposition of two different (electronic or vibrational) states, that also decays with a characteristic dephasing rate. The overall relaxation dynamics of the studied system can be unraveled from the analysis of the complete 3D-matrix data through different methodologies. In our research group, a complex multi-exponential global fitting model is employed,[38] that has the power to characterize simultaneously both oscillating and non-oscillating contributions by fitting the signal with a sum of complex exponential functions. The fitting procedure is based on the search for the best solution to a minimization problem built upon the variable projection algorithm. The results of the fitting provide the populations' decay times and the frequency and dephasing times of coherences. An intuitive way to visualize the fitting results is using amplitude maps.

These are known as decay-associated spectra (DAS), that show in a 2D map the amplitude distribution associated with a particular time constant, as emerging from the fitting of the non-oscillating signals; analogously, the coherent decay-associated spectra (CAS) show amplitudes related to the fitting of the oscillating signals. Every decay component, characterized by a time constant (and a frequency, in the case of oscillating components), used to define the fitting function, has its own map. A DAS describes the evolution of populations that can rise or decay over time. The color spectrum of the peaks in a DAS depends on whether the signal is defined by exponentials with a positive or a negative amplitude. In case a signal in the original 2D map has a positive amplitude (like in GSB or SE signals), a corresponding positive (negative) peak in a DAS at the same coordinates implies that, overall, the signal at those coordinates is decaying (rising). The opposite is true for a signal with negative amplitude (like in the ESA signals): a negative peak in the DAS is related to a decaying component and a positive peak is related to a rising component.[38] A CAS, on the other hand, gives information both in terms of amplitude modulus and phase of a particular beating. The former shows where a specific oscillation contributes to the signal on the 2D map, and the latter provides the phase of the oscillating contributions at $t_2 = 0$ fs.[39]

The characterization of oscillations can also be performed in other ways. For example, it is possible to perform a preliminary global fitting with only non-oscillatory decays, in order to remove those contributions and obtain the matrix of oscillating residues. The simplest way to analyze these residues is to integrate along both the excitation and emission frequencies and then Fourier-transform along t_2. The result is a power spectrum of frequencies, an intensity-frequency graph where the oscillating signals are separated according to their frequency. If all the coherences are vibrational, the power spectrum is analogous to a Raman spectrum.[40] The comparison between the two spectra allows to identify other

possible oscillating contributions, in addition to the vibrational ones, such as electronic coherences or solvent contributions. Moreover, Fourier (FT) maps are used to gather information about the distribution of different beatings on the 2D map for a fixed value of ω_2, when also the t_2 dimension is Fourier-transformed.[41–43] Another method is based on time-frequency transforms (TFT) that allows to visualize, through a complex bi-linear transform procedure, oscillating signals both in time (t_2) and frequency on a two-dimensional plot, which gives direct access to their dephasing times.[44,45] To analyze the datasets collected during my Ph.D. project, I explored all these different methods.

Chapter 4

Isolated Chromophores

Building on the wealth of knowledge on spectroscopic theory, experimental setup and data analysis description presented in the previous two chapters, we can now address the various systems I investigated during my Ph.D. In this chapter, the photophysical properties of the main chromophores found in FCP will be discussed in detail, to understand their current state of the art, the future perspectives and what questions still need answers.

4.1 Structure and Properties of Fucoxanthin

Fucoxanthin (structure depicted in figure 4.1) is a molecule that belongs to the class of carotenoids. Carotenoids (Cars) are molecules that can be easily found in nature and play many different roles in biological processes. Their main feature is that they absorb light in the ultraviolet-visible part of the electromagnetic spectrum, which makes them classifiable as chromophores or pigments. In fact, they are red-orange colored and contribute to the color of many plants, vegetables and fruits, such as carrots, pumpkins, tomatoes and radishes.[46] One of the main biological process in which they exploit their light-absorbing features is light harvesting, which is the first step of photosynthesis. During light-harvesting, Cars work as antennas for sunlight inside particular kinds of proteins (I will talk about them in the next chapters) and they transfer the absorbed energy to chlorophylls, in a series of ultrafast energy-transfer steps that channel the energy into the reaction center, in order to transform sunlight into chemical energy. Other relevant biological functions performed by Cars are: (i) photoprotection, involving both singlet and triplet states, a process in which carotenoids dissipate energy when in excess, and prevent harmful oxidation reactions that could damage the organism in which they are placed; (ii) structural stabilization in light harvesting complexes and core complex of Photosystem II.

Structurally, Cars can be recognized thanks to their long backbone of alternated single and double carbon bonds, forming a wide conjugated π-electron system. The number of conjugated carbons can range from seven (peridinin, fucoxanthin) to thirteen (spirilloxanthin) for the most common Cars. This feature plays an important role in the unique spectroscopic properties of Cars, guaranteeing a vast variety of biological functions.[23,47]
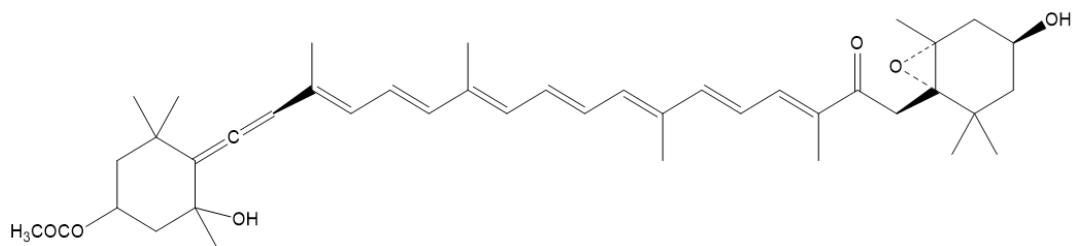
Figure 4.1 - Molecular structure of fucoxanthin.

Spectroscopically speaking, one of the most peculiar features of Cars is the presence of dark states in their excited states manifold. A dark state is an electronic state that cannot be probed directly with a light source, i.e. it is spectroscopically forbidden. This knowledge dates back to 1972, when it was demonstrated that the absorbing state of longer polyenes is not the first excited state, but another excited state higher in energy.[48,49] So, the first excited state (S_1) is dark and it is located between the ground state and the absorbing state, labeled as the second excited singlet state (S_2). Historically, the ground state → first excited state transition (from now on $S_0 \rightarrow S_1$) has never been directly observed, and all the information about the energy and the relaxation dynamics of S_1 had to be measured indirectly, populating S_1 from S_2 relaxation, in two-photon processes.[50–52] Recently, however, a study conducted on deoxyperidinin, showed evidence of the forbidden transition in certain organic solvents.[53]

Historically, this feature was explained through the use of group theory, which works for Cars with high symmetry, but it is not entirely suitable for asymmetric Cars like fucoxanthin. A recent study on highly asymmetric carotenoids concludes that the optical inactiveness is not due to symmetry restrictions and could have a different physical origin. It is difficult, however, to identify what this origin could be; one of the most supported proposals is a considerable electronic–vibrational coupling leading to the breakdown of the Born-Oppenheimer approximation.[54]

Because of this elusive character, gaining information about the energy and the lifetime of the S_1 state is particularly challenging and many techniques have been employed to try to achieve this goal over the years.[23] Moreover, Fx has another important structural feature, namely, the presence of a carbonyl group near the polyene chain. The spectroscopic implications of this detail will be commented in depth in the next paragraphs.

4.2 Probing Excited States of Carotenoids

Most of the spectroscopic information we have on carotenoids comes from in-solution analysis. Typically, these molecules are soluble in organic solvents, showing different solubilities depending on the solvent polarity and their structure.[55]

4.2.1 Linear Absorption Spectra and the S_2 State

The simplest technique to investigate the optical properties of molecules is linear absorption spectroscopy. The absorption spectra of Cars present a strong absorption band (molar absorptivity, $\varepsilon \sim 10^5$ M^{-1} cm^{-1}) in the UV-visible region, from about 350 to 550 nm, attributed to the $S_0 \rightarrow S_2$ transition.[46] Figure 4.2 shows the absorption spectrum of fucoxanthin in toluene, one of the samples that I prepared for the investigation of isolated Fx with 2DES.
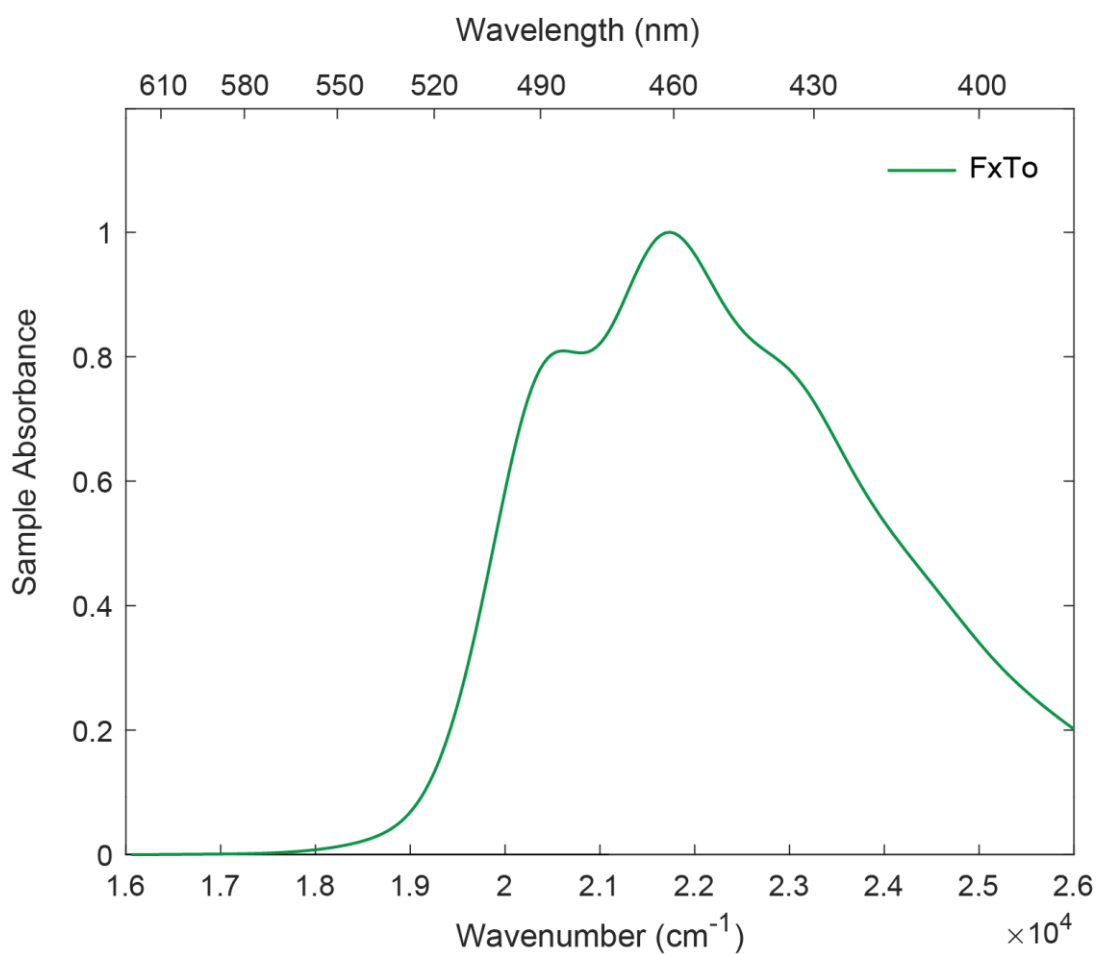

Figure 4.2 – Normalized linear absorption spectrum showing the $S_0 \rightarrow S_2$ transition of fucoxanthin dissolved in toluene.

It is possible to notice a marked vibronic structure due to a strong vibronic coupling: the transition from the ground state can populate also the excited vibrational states of the S_2 state. The separation between the three distinct vibrational bands is ~1300 cm^{-1} and it is the result of a combination of the stretching frequencies of the C-C and C=C bonds.

Many factors influence the excitation energy of the $S_0 \rightarrow S_2$ transition. The most important are: the conjugation length,[56] the carotenoid structure[23] and the solvent polarizability.[57] Besides excitation energy, there are a lot of properties that characterize the relaxation dynamics of the S_2 state. It was observed that the S_2 state violates Kasha's rule if the conjugation system involves more than eight conjugated C=C bonds.[58] However, when the S_2 state is populated, the main process that takes place is internal conversion to the S_1 state;[56] this process has a sub-picosecond time scale, thus, ultrafast spectroscopic techniques are necessary for its characterization. The lifetime of the S_2 state was measured by ultrafast time-resolved fluorescence up-conversion method and it was placed in the range of 100-300 fs.[59–61] The exact value of these time constants should critically depend on the $S_2 - S_1$ energy gap, but it is not the only crucial factor, as stated by studies on carotenoids with different conjugation length.[23]

4.2.2 Transient-Absorption Spectra and the S_1 State

The most common way to probe the S_2 lifetime is through pump-probe (PP) spectroscopy, a third-order technique that gives responses analogous to 2DES but in a mono-dimensional fashion. PP spectroscopy is widely used in the characterization of carotenoids, and so far, it has provided crucial information on their photophysics.

The result of a PP measure is a transient-absorption spectrum in which the Stimulated Emission (SE), Ground State Bleaching (GSB) and Excited State Absorption (ESA) signals, described in chapter 2, can be distinguished. These signals are the same ones that can be found in a 2DES experiment, as both 2DES and PP are third-order non-linear spectroscopic techniques. The main difference between the techniques is that in PP the time interval t_1 (equal to zero) is not scanned, leading to a mono-dimensional spectrum that evolves in time, without the possibility of separating the excitation and the emission frequencies.[31,37] In figure 4.3a we report an example of transient-absorption spectrum obtained for fucoxanthin, adapted from Kosumi et al.[62]

The spectra are dominated by a strong ESA signal, which can be understood considering the associated Feynman Diagram, pictured in figure 4.3b.
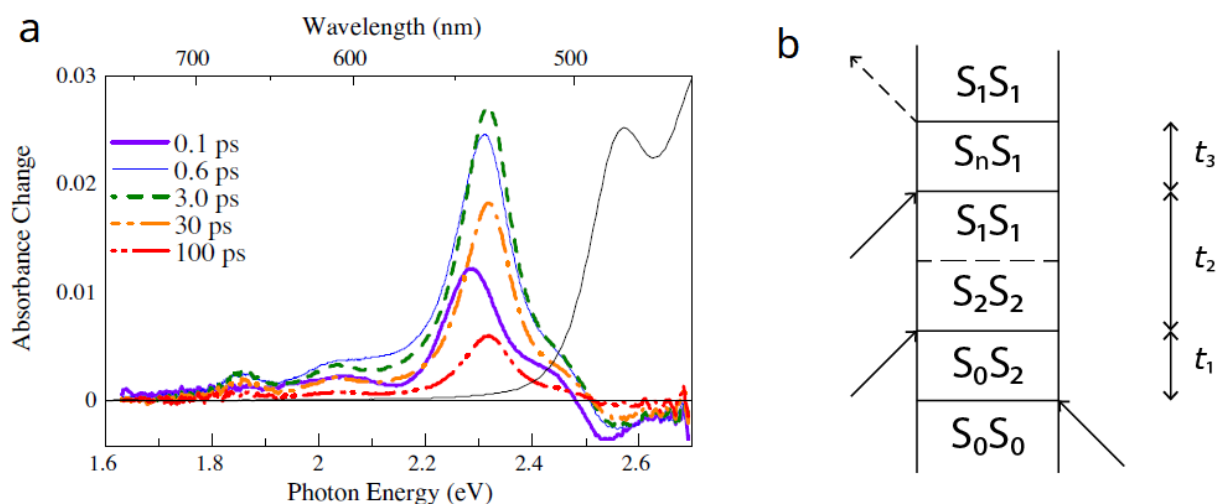
Figure 4.3 – a) Transient-absorption spectra of fucoxanthin in cyclohexane at different values of t_2: the strong positive band represents the ESA signal, the weak negative band below 500 nm represents both the GSB and the SE signals. The figure is adapted from Kosumi et al.[62] b) Feynman diagram of an ESA pathway for a carotenoid.

The first two interactions populate the S_2 state, then, in the time interval t_2, the population of S_2 is transferred via internal conversion to the S_1 state and at last the third pulse causes the transition from S_1 to S_n: a higher excited state, whose identity is still unclear. This particular Feynman Diagram is different from the ones depicted in chapter 2: during the time interval t_2 the system explores two different states. A dashed line is used to indicate that a transfer of population happens from S_2 to S_1 through a process known as internal conversion. The information stored in the ESA signal can be used to unravel indirect information about the excited states of carotenoids.

First, the previously discussed S_2 lifetime can be inferred by the rising of the ESA band. Indeed, as the population relaxes from S_2 to the S_1 state, the ESA from S_1 is promoted. Therefore, the kinetics of the rising of the ESA signal corresponds to the lifetime of the S_2 state. Additionally, some studies have found a transient-absorption feature in the near-infrared region attributable to an ESA directly from the S_2 state.[63]

Moreover, a lot of properties concerning S_1 lifetime were measured through the analysis of the $S_1 \rightarrow S_n$ ESA signal: the decay of the signal itself is a measure of the relaxation timescale of the S_1 state to the ground state. All the carotenoids have an S_1 lifetime in the order of picoseconds, depending on parameters such as conjugation length,[47,56] temperature[64,65] and functional groups interacting with the π-electron system.[23] The ESA signal, however, is not very useful in the characterization of the S_1 energy, because it gives information only about the $S_1 - S_n$ energy gap.

4.3 The Role of the Carbonyl Group

In this section I will discuss why all the aforementioned information about excited–state energies and relaxation dynamics must be revisited when dealing with a carbonyl carotenoid. Differently from other functional groups, carbonyl plays an important role in the photophysics of carotenoids as it is directly linked to the π-electron system. This is the reason why Cars with the carbonyl group, such as fucoxanthin, are treated as a separate class of Cars called 'ketocarotenoids'. In figure 4.4 the linear absorption spectra of the three samples used for the 2DES measurements are shown. The three samples were prepared by dissolving fucoxanthin in three different solvents with different polarity: Methanol (FxMe), Acetone (FxAc) and Toluene (FxTo).
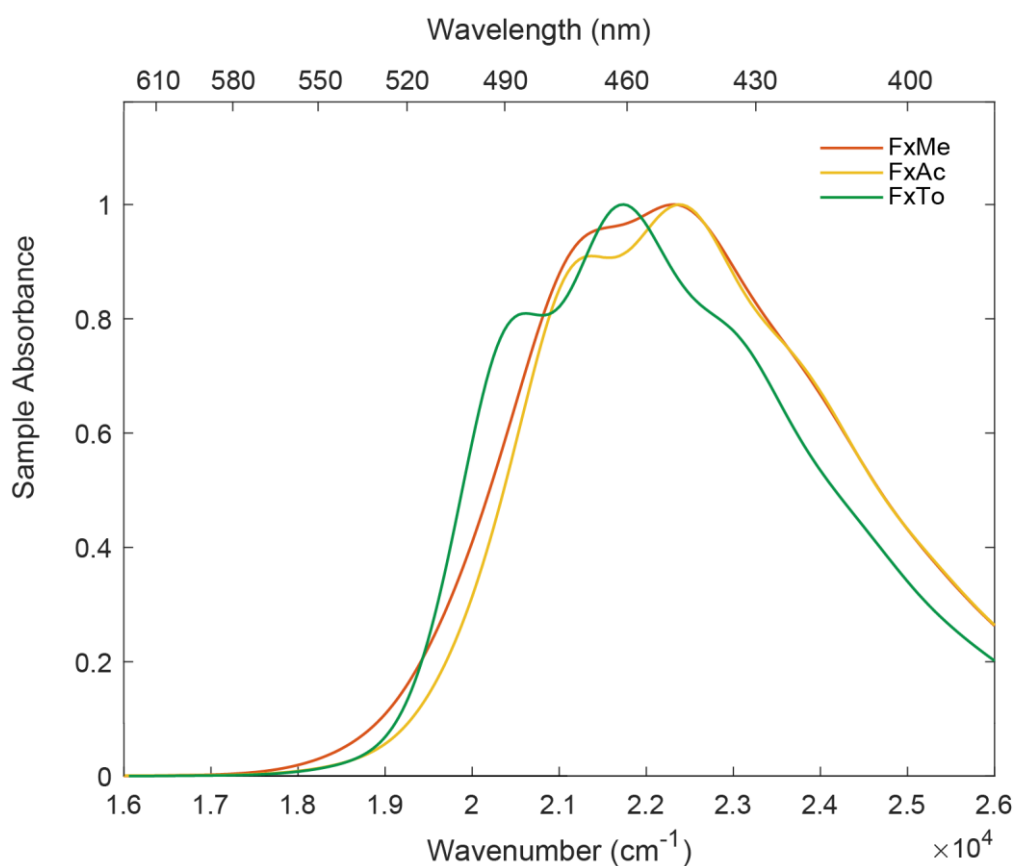

Figure 4.4 – Normalized linear absorption spectra showing the $S_0 \rightarrow S_2$ transition of fucoxanthin in different solvents. Red: fucoxanthin in methanol (FxMe), yellow: fucoxanthin in acetone (FxAc), and green: fucoxanthin in toluene (FxTo).

Note that the three spectra change primarily according to the polarity of the chosen solvent. As reported before, in the FxTo sample the vibronic structure is preserved; whereas, going towards higher polarity solvents, a loss of the vibronic structure and a slight blue–shift are detected. For ketocarotenoids, the solvent dependence and other spectroscopic features, that we will discuss later on, are explained introducing the presence of an Intramolecular Charge Transfer state (ICT) among the excited states.[57,66,67]

An ICT state is a particular kind of electronic state that is characterized by a partial charge separation, hence the solvent polarity dependence. There are several theoretical models based on peridinin, the most iconic carbonyl carotenoid, that aim to describe the origin of this charge separation: firstly, the separation is manifested as a shift of electronic density from the carbonyl to the polyene chain, leading to a partial negative charge on the oxygen of the carbonyl group and a partial positive charge delocalized along the polyene chain;[67] moreover, the charge separation could be enhanced by dispersive interactions between the transition dipole moment and the environment,[68] and also the formation of hydrogen bonds between the carbonyl and the solvent.[69] It was also suggested that the allene group, present in both fucoxanthin and peridinin, could play an important role in the ICT state, as it would act as an electron donor with the carbonyl as the acceptor, enhancing the solvent dependence of the excited state; in this case the partial positive charge would be localized on the allene group.[70]

The energy of the ICT state has been calculated and measured to be similar to the S_1 state, but it is not clear yet whether they are two distinct electronic states or if they form a single coupled S_1/ICT state. Experimentally, early studies reported identical dynamics for both the spectroscopic features assigned to the S_1 and ICT states, suggesting that the two states are actually coupled.[57] However, a recent experimental study by Kosumi *et al.* on fucoxanthin with two-photon PP spectroscopy revealed that the two electronic states are distinct, as the spectral features assigned to the two states can be promoted selectively by changing the energy of the exciting pulses.[62] The main problem with this kind of experimental characterization is the assignment of spectral features, which is not always so straightforward. Another recent interpretation describes the ICT state as a mixing of S_1 and S_2 with a barrier of potential that depends on solvent polarity, as seen in figure 4.5.[71] This proposal is particularly interesting in the analysis of our spectroscopic data, as I will discuss in the next chapters. Hereafter I will refer generically to these states as "S_1/ICT state", even if its true nature is unknown. Different interpretations of the S_1 and ICT nature are summarized in figure 4.5, adapted from Wagner *et al.*[71]

As already mentioned earlier, carbonyl carotenoids exhibit interesting solvent-dependent spectroscopic features even in the steady-state absorption spectra. Increasing the polarity of the solvent, the $S_0 \rightarrow S_2$ absorption band is broadened and the vibronic structure is lost, as shown in figure 4.4. It is possible to notice that the broadening is asymmetric, as a "red" tail appears at low energies. The broadening and the red tail are explained by an increase of the charge-transfer character of the ground state, stabilized in polar solvents, producing a distribution of various conformers that causes the loss of the vibronic features.[57,66,67,72–74]
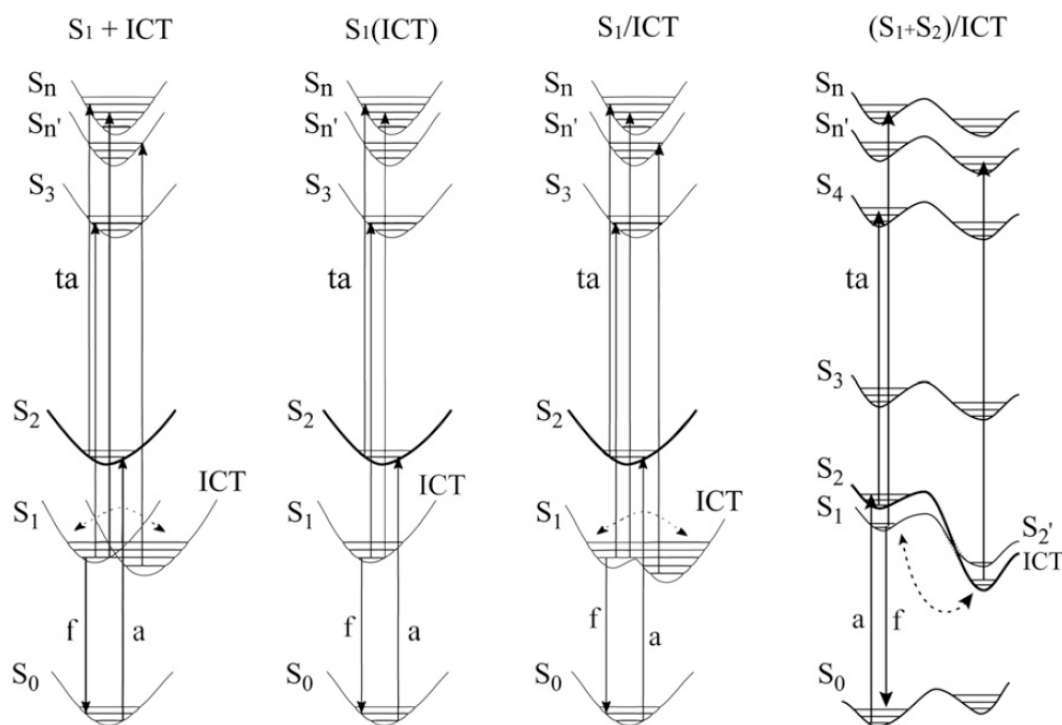
Figure 4.5 -Possible interpretations of the nature of the S_1 and the ICT state, from left to right: S_1 and ICT are two distinct states; S_1 and ICT are the same state; S_1 and ICT are coupled; S_1, S_2 and ICT are coupled. The figure is adapted from Wagner et al.[71]

Another explanation has been proposed recently by Kosumi et al.[75]: the asymmetric red–shift in methanol is caused by a peculiar conformation of the Fx molecule (the "red" form, as we will see in the next paragraphs) with strong ICT character. Also the transient absorption spectra in the $500 - 750$ nm range are quite different from non-carbonyl carotenoids and have strong solvent-dependent features. In this spectral region, there is a strong ESA signal, due to the strongly allowed $S_1 \rightarrow S_n$ transition. Besides, carbonyl carotenoids also present another ESA band between $600 - 750$ nm, which is enhanced by increasing the polarity of the solvent. In figure 4.6 we can see the same PP reported earlier for fucoxanthin by Kosumi *et al.*[62] but this time the solvent is methanol and not cyclohexane.

The origin of this band is not clear at all: the studies that assume that S_1 and ICT are two distinct states, assigned this band to a transition from the ICT state to another S_n state (usually denoted as $S_{n'}$),[23] because this kind of spectral behavior was similar to that of ADMA (Anthyldimethylaniline) and other related compounds.[76,77] This would explain why the intensity changes with polarity: polar solvents stabilize the ICT state to the point that it could lie underneath the S_1 state; thus in the relaxation process, the ICT would be populated more and the intensity of the ICT $\rightarrow S_{n'}$ transition would be higher. On the other hand, non-polar solvents cannot stabilize the ICT state, which would lie above the S_1 state, making its population not significantly relevant.
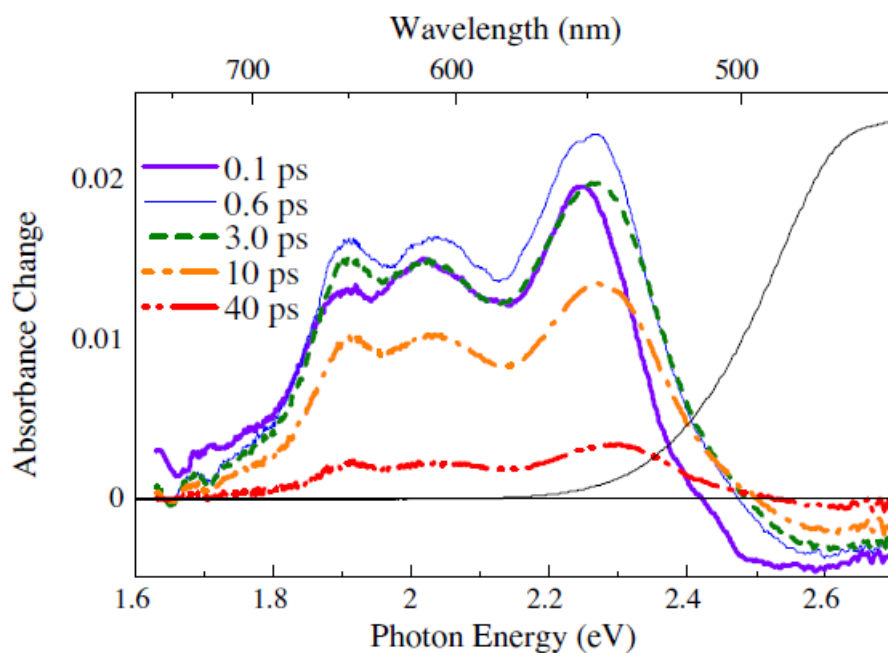
Figure 4.6 - Transient-absorption spectra of fucoxanthin in methanol at different values of t_2: the strong positive band at circa 550 nm represents the ESA signal from S_1, while the positive signal above 600 nm represents the ESA from the ICT state. The figure is adapted from Kosumi et al.[62]

Conversely, the studies that embrace the hypothesis of the S_1/ICT coupling refer to this feature as a "polarity-induced ESA", not specifying what states could be involved, but recognizing the contribution of the ICT state.[72] Another enigmatic aspect of this diatribe is that it is not clear why this new spectral feature changes in intensity as a function of the solvent polarity, whereas its energy position does not.

Solvent polarity also affects the kinetics of carbonyl carotenoids: the lifetime of the S_1/ICT ESA band is significantly reduced if the solvent is polar. For example, fucoxanthin lifetime shifts from 60 ps in non-polar solvents to 30 ps in polar ones.[72] The lifetime dependence on solvent polarity suggests that the presence of the ICT state plays an important role in the relaxation dynamics processes of carbonyl carotenoids. A recent study adds another piece to the puzzle of the photophysics of carbonyl carotenoids: it was shown that fucoxanthin, dissolved in a polar and protic solvent like methanol, exhibits a strong dependence on excitation energies.

When excited at high energies, the correspondent transient absorption spectrum is similar to non-carbonyl carotenoids, as it does not present the low energy ESA band. On the other hand, when excited at lower energies, on the red tail of the absorption spectrum, it shows the spectroscopic features assigned to the presence of the ICT state. This suggested that fucoxanthin in methanol may assume two different molecular forms: the "blue" and the "red" one. Even if the blue form has no ICT spectral features, its lifetime is still reduced, which leads to the hypothesis that it also exhibits a certain ICT character.[75]

4.4 Carotenoids Characterization through 2DES

2DES is a relatively recent spectroscopic technique, so it is not a surprise that to date there are only a few specific 2DES characterizations of carotenoids in the literature. My Ph.D. project aims precisely at contributing to filling this gap.

Electronic Double Quantum (DQ) 2D spectroscopy conducted on β-carotene suggested the presence of an ESA from the S_2 state to another state which is double in energy, denoted as S_{n2}. It was proposed that this state could play a role in the ultrafast dynamics (the first 100 fs) of carotenoid and that it should be considered in the description of relaxation processes.[78] Another 2DES experiment was conducted on β-carotene, analyzing the GSB/SE + ESA band region, stressing the importance of considering the ESA from S_2.[79] Theoretical models for the third-order spectroscopy of carotenoids were proposed, that could account for population and system-bath interactions and their relationship with the molecular structure. Even in this case, the presence of the ESA signal from both S_1 and S_2 emerged as crucial in interpreting the experimental results.[80] It is important to remember that 2DES spectroscopy is at its early stages, and year after year there are new improvements that increase the reach of this technique. It is clear that early 2DES experiments, as the ones performed on carotenoids, must be taken with this awareness in mind.

4.5 Spectroscopic Characterization of Chlorophylls

Although chlorophylls (Chls) are not the focus of the measurements I conducted during my Ph.D., it is essential to understand what kind of signal we should expect from them in a 2DES experiment. In fact, as we said in the introduction to this chapter, Chls are one of the main chromophores in FCP, and their signals cannot be ignored in the overall analysis of the protein behavior. Chlorophylls play a crucial role in the photochemistry processes taking place in oxygenic photosynthetic systems of organisms such as terrestrial plants or algae.[81] Together with carotenoids, they act like antennas that capture the sunlight and transfer its energy to the reaction center of the photosystems.

There are several types of Chls. Generally, their structure is based on a macrocyclic porphyrin system, with four pyrrole rings labeled with letters from A to D. Next to the C ring, an additional isocyclic ring (E) is present. In the center of the molecule, coordinated with the four nitrogen atoms of the macrocycle, there is a Mg^{2+} ion. Structurally, the different kinds of Chls have specific hydrocarbon substituents attached to the macrocyclic ring.[82]
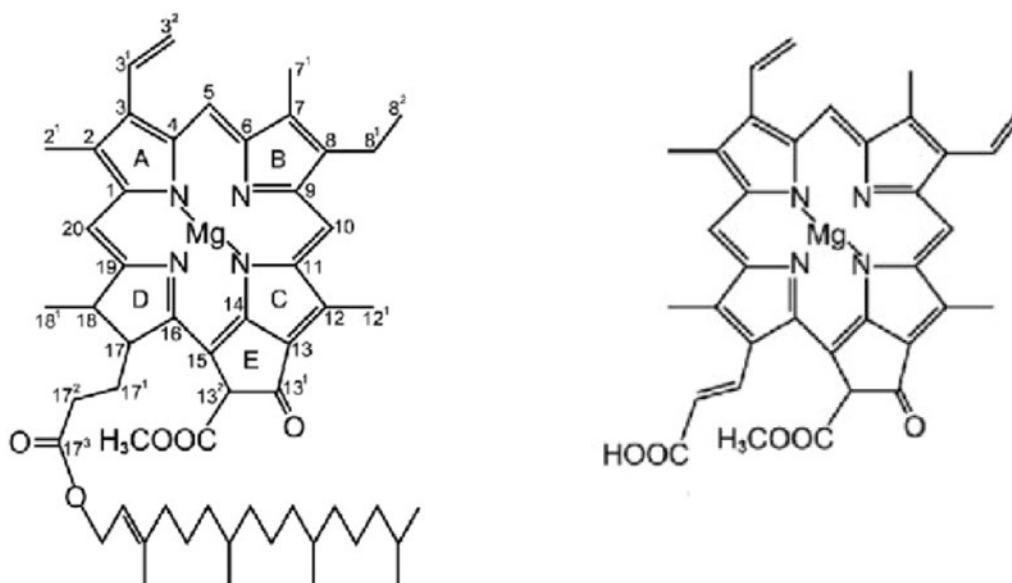
In FCP, two types of Chls can be found: Chl *a* and Chl *c₂*, depicted in figure 4.7. Chl *a* is characterized by the presence of a phytyl linked to the ring D, a vinyl group linked to the ring A and a methyl group linked to the ring B.[84] Chl *c₂*, instead, contains a vinyl group attached to the ring A and ring B and a *trans* acrylic acid at the ring D.[82]

Even if these are small structural differences, they have a strong impact on the spectroscopic features related to these molecules, as they lead to significant changes in their linear absorption spectra; more details will be presented later in section 5.2. These features are often explained using Gouterman's "four orbital model",[85,86] that employs group theory to predict the electronic transitions of chlorophylls. An ideal metalloporphyrin could be represented by the D_{4h} point group. In this model, Gouterman describes the possible transitions between four π-orbitals, i.e. the two Highest Occupied Molecular Orbitals (HOMO) and the two Lowest Unoccupied Molecular Orbitals (LUMO). This gives rise to four absorption bands divided into two groups: the B bands and the Q bands: the B bands, known as Soret bands, are stronger and at higher energies, while the Q bands are less intense and at lower energies. Generally the two B bands are not resolved in frequency, instead the Q bands can be distinguished and are labeled Q_y and Q_x.[87]

Chapter 5

Fucoxanthin Chlorophyll Protein – FCP

After a brief description of the spectroscopic properties of isolated chromophores, in this chapter we will look closely at the characteristics of the protein at the center of my project: the Fucoxanthin Chlorophyll Protein (FCP), in which fucoxanthin and chlorophylls can be found.

5.1 Light Harvesting Processes

In order to start the chemical reactions at the beginning of photosynthesis, the energy of the sunlight must be captured by *Light Harvesting Complexes* (LHCs) and transferred to the *Reaction Center* (RC). These two entities can be treated together as a photosynthetic unit.[5] LHCs are proteins that work like antennas: they are characterized by the presence of pigments inside their scaffold that absorb sunlight in the ultraviolet-visible region of the electromagnetic spectrum, and in some cases also in the near infrared.[12,88] Their arrangement in the protein has been tuned to maximize the efficiency of the energy transfer processes in which they are involved. The most common pigments found in LHCs are chlorophylls and carotenoids, which change in type and number depending on the specific LHC and organism. Moreover, another critical role of these antenna systems is the photoprotection of the photosystem from oxidation processes.[89–93]

These proteins have been widely studied to understand the fine details that govern the energy transfer processes among the pigments. More precisely, these processes are known as Excitation Energy Transfer (EET) and are particularly fascinating because they allow energy transport in a very efficient way. This is a quite challenging task for artificial devices such as photovoltaic cells, and biomimetic systems inspired by photosynthetic units represent a stimulating model for chemists and engineers trying to mimic the efficiency of the natural systems in artificial devices.

EET can be described by two different frameworks: a Förster incoherent hopping mechanism[94] or a coherent wavelike process that involves delocalized collective excitations.[95] Thanks to the advent of 2DES, and the access to very high temporal resolution (tens of femtoseconds), long-lived coherences have been captured, suggesting the possibility of a quantum coherent energy transport.[14–16,96] From that moment, 2DES has been qualified as one of the most interesting spectroscopic techniques to investigate this kind

of processes, thanks not only to its temporal resolution, but also to its capability of separating the signal along two frequency dimensions, excitation and emission frequency – a way to easily characterize interacting excited states.

5.2 Fucoxanthin Chlorophyll Protein

As already mentioned, several different LHCs are known: FCP is a particular kind of LHC found in diatoms and brown algae that live underwater and contribute to nearly a quarter of the global oxygen production.[17,18] It can be organized in monomers, dimers, trimers or tetramers. FCP is a membrane protein[97] and, differently from LHCs from higher plants, has a peculiar ratio of Chls and Cars. Indeed, usually, LHCs have a larger number of chlorophylls with respect to carotenoids, but for FCP and other related complexes the ratio is nearly 1:1.[98,99] As discussed in the previous chapter, the specific pigments that can be found in FCP are fucoxanthin, chlorophyll a and chlorophyll c_2 (from now on Chl c). The exact ratio between these chromophores depends on the specific organism from which FCP is obtained; the average is 4:4:1, respectively. In the FCP complex, also molecules of diadinoxanthin and diatoxanthin have been found, other carotenoids involved in regulation processes, whose spectroscopic relevance can be ignored. The large amount of Fxs and the presence of Chl c helps to increase the light absorption spectrum of FCP (fig. 5.1) in the blue-green region,[5,100] which is particularly helpful in the dim light conditions that rule underwater. Moreover, from an evolutionary point of view, the diatoms and brown algae that experience these challenging light conditions developed their LHCs to perform energy transfer with higher yields than higher plants. For this reason, these organisms have been largely studied throughout the years with different spectroscopic techniques. Nonetheless, several aspects of the structure, the function and the details of their energy transfer pathways are yet to be fully mapped.[19]

FCPs purified from different organisms present different features and relevant structural differences. The primary organisms from which FCP is more often extracted are: *Cyclotella meneghiniana* (a diatom), *Cladosiphon okamuranus* Tokida (brown algae), *Phaeodactylum tricornutum* (pennate diatom) and *Chaetoceros gracilis* (centric diatom). During my Ph.D. I worked on an FCP sample obtained from *Cyclotella meneghiniana*, which is known to possess two different types of complexes: FCPa and FCPb. These proteins differ in their quaternary structure: FCPa is structured as a trimer of three identical protein monomers, while FCPb is a nonamer (trimer of trimers). Nonetheless, their spectroscopic behavior does

not present any relevant discrepancies. The pigment distribution for *C. Meneghiniana* is 8 Fxs 8 Chl *a* and 2 Chl *c*.
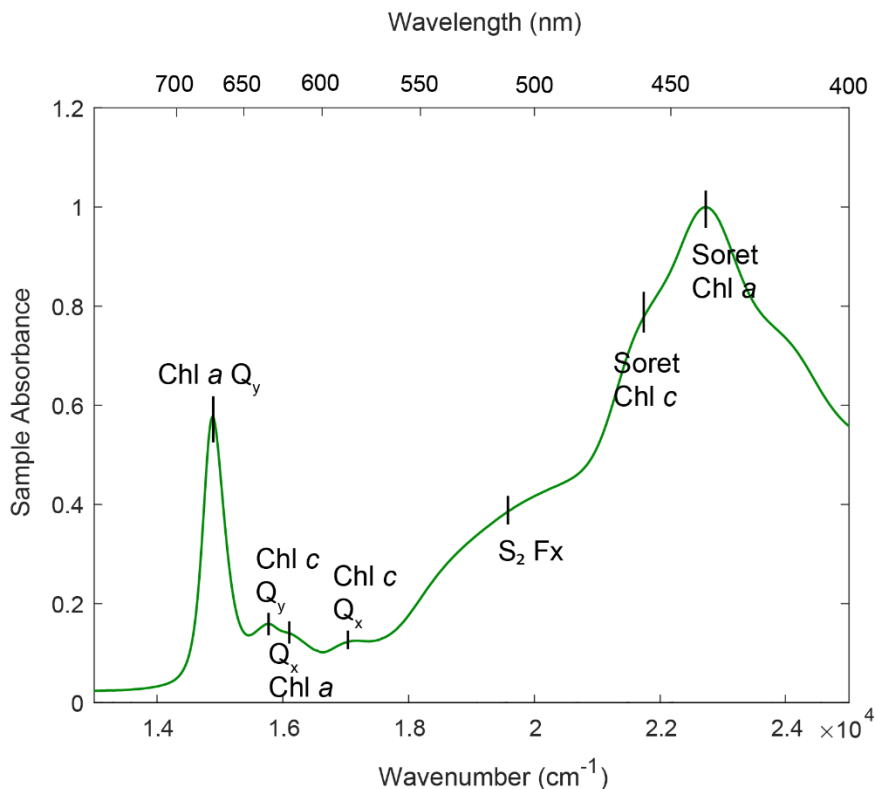

Figure 5.1 - Linear absorption spectrum of the FCP sample used in my 2DES measurements. The characteristic peaks from Fx, Chl a and Chl c can be distinguished.

5.3 Spectroscopic Characterization

The linear absorption spectrum of FCP is shown in figure 5.1. The different contributions from the three chromophores can be easily distinguished: the high-energy part of the spectrum is dominated by the Soret bands of Chl *a* and Chl *c*, partially overlapping with the Fx band that shows up at lower energies (around 500 nm). In the low-energy part of the spectrum the Q bands of the Chls can be identified. The most intense peak is attributed to the Q_y transition of Chl *a*; the other Q bands are less intense but still detectable and recognizable: the Q_y of Chl *c* and the Q_x of Chl *a* and Chl *c*.

Pump-probe spectroscopy has been useful in the characterization of the energy transfer dynamics among the FCP pigments. One of the main energy transfer channels of FCP is represented by the transfer from Fx to Chl *a* in the femtosecond and picosecond time scale.[98,101,102] The donor states of the carotenoid are the strongly allowed second excited state (S_2), the dark excited states S_1 and the intramolecular charge-transfer (ICT) state, which interacts with S_1.[71,103,104] The acceptor states of Chl *a* are the Q_y and the Q_x

bands. Additionally, also a very efficient energy transfer from Chl *c* to Chl *a* within a few hundred fs was found.[105]

5.3.1. 2DES on FCP

In the last ten years also 2DES has been exploited to investigate the ultrafast relaxation dynamics of FCP. The most relevant 2DES literature on FCP includes the works carried out by Gelzinis *et al.*[21], Songaila *et al.*[20] and Butkus *et al.*[106], all focusing on FCPs extracted from *Cyclotella meneghiniana*. The former study was performed with two-color 2DES, which allowed to successfully characterize the energy transfer between Fx and the Q_y band of Chl *a*. In this work, two different forms of Fx with two different relaxation dynamics have been identified: a "red" and a "blue" form, according to their excitation wavelength. The red form of Fx is characterized by a faster and more efficient EET than the blue form. The other two studies focused on the energy transfer among chlorophyll molecules. They verified the presence of a strong excitonic coupling driving an ultrafast energy transfer from Chl *c* to Chl *a* (60 fs). Moreover, two different types of Chl *c* were identified at cryogenic temperatures, characterized by different decaying timescales. As a result of the pump-probe and 2DES characterizations, the picture of the energetic cascade of the pigments of FCP is summarized in figure 5.2. In this figure we can observe the different energy transfer channels and the time constants that characterize them.
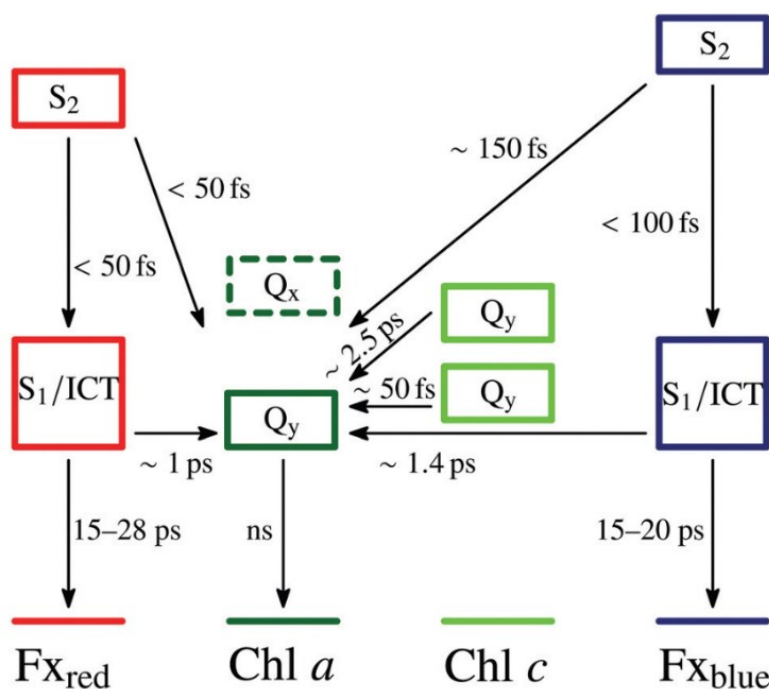

Figure 5.2 - Energy transfer scheme of the FCP complex from Cyclotella meneghiniana with timescales corresponding to room temperature, reproduced from Gelzinis et al.[107]

The red form of Fx transfers energy to the Q_y state of Chl a in less than 50 fs from S_2 and in about 1 ps from the S_1/ICT state. The blue form is generally slower, transferring the energy in circa 150 fs from S_2 and 1.4 ps from the S_1/ICT state. Also the different time constants of the EET from the Q_y states of the different Chls c to the Q_y state of Chl a can be appreciated: one Chl c transfers the energy in about 50 fs and the other one in about 2.5 ps.[107]

5.4 FCP Structure

All the previously reported data have been collected and interpreted without knowing the FCP's structure. In fact, the aim of several studies was also to understand the spatial arrangement of the pigments, in order to figure out their relaxation pathways in a better way. Finally, in 2019 three atomic structures of FCP complexes were published, hence filling this knowledge gap. In particular, the crystallographic structure of FCP from *Phaeodactylum tricornutum* has been resolved with a resolution of 1.8 Å.[108] The other two structures were obtained with cryo-electron microscopy with a resolution of 3.0 Å, investigating the centric diatom *Chaetoceros gracilis*.[109,110] These structures are related to the photosystem antenna supercomplex, which is comprehensive of the reaction center and a set of FCPs organized differently according to the organism. For example, in *C. gracilis* the supercomplex is arranged in two protomers, each with two tetrameric and three monomeric FCPs. The structures helped to define precisely the number of chromophores present in each FCP monomer and how they are arranged in the protein scaffold. This highlighted significant differences between the investigated organisms: in *P. tricornutum* the pigments are 7 Chls a, 7 Fxs and 2 Chls c, whereas the structure from *C. gracilis* revealed the presence of 7 Chls a, 7 Fxs and 3 Chls c. These numbers can also vary between tetramers and monomers. Note that these chromophores' stoichiometries are also different from the one expected for *C. meneghiniana*.

The pigment arrangement is also different, and this suggests possibly distinct interactions and EET pathways. All this information confirms that in the discussion of spectroscopic data, it is important to know the organism from which FCPs are obtained, as their structural variability can be significant. In fact, all the three works on the characterization of FCP through 2DES cited before used FCP samples from *C. meneghiniana*, whose structure is still unknown. For this reason, in 2021 Gelzinis *et al.*[107] tried to confront their spectroscopic data with the structures from the other two organisms, discussing the consistency of their experimental spectroscopic EET timescales with the crystallographic chromophores'

arrangement. The emerging result was that these two pieces of evidence were not easy to reconcile, revealing discrepancies and inconsistencies.
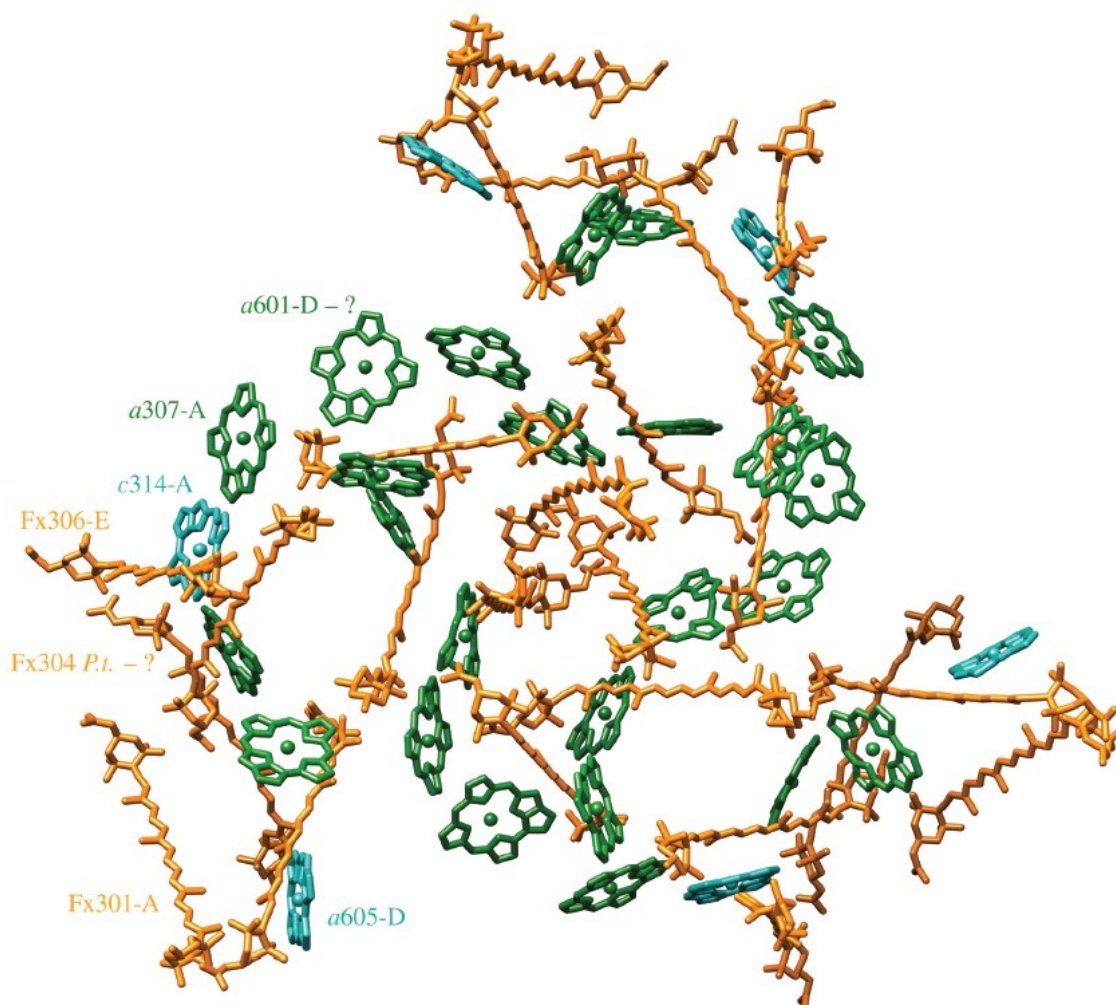

Figure 5.3 - Proposed FCP structure for Cyclotella meneghiniana. *Chl* a *are colored in green, Chl* c *in light blue, and Fx in orange. Figure created with UCSF Chimera, reproduced from Gelzinis et al.*[107]

Consequently, Gelzinis *et al.*[107] proceeded to propose a possible trimer–based FCP organization of the pigments in *Cyclotella meneghiniana*, that could account for the experimental findings of their 2DES measurements (figure 5.3). In order to build this structure, they considered a trimeric arrangement for FCP in *C. meneghiniana*, an expected stoichiometry of 8 Fxs, 8 Chl *a* and 2 Chl *c,* and the similarity to the available structures. The proposed arrangement successfully explains the presence of two Chls *c* molecules with different distances to Chls *a*, because of the different timescales found for Chl *c* to Chl *a* transfer. Moreover, (at least) one Fx molecule must be placed further away from the Chls *a*, to account for the two forms of Fxs (the blue and the red one) experimentally detected.

An interesting feature that can be found both in the actual structural data and in the reconstruction for the *C. meneghiniana*, is that Fx seems to be placed often near the Chls *c*, with a distance that would suggest the presence of an interaction between these two chromophores. Nonetheless, until now, no signatures of energy transfer from Fx to Chl *c* or any other interaction have been detected yet. It has thus been proposed that these interactions happen in an ultrafast timescale that could be too fast to be captured.[108]

Chapter 6

Experimental Results on Isolated Fucoxanthin

6.1 Sample Preparation

Fucoxanthin was purchased from Sigma–Aldrich® and dissolved in three different anhydrous solvents with different polarity: methanol (FxMe, ε_r = 33), acetone (FxAc, ε_r = 21) and toluene (FxTo, ε_r = 2.4). Solvents with different dielectric constants (ε_r) were chosen to characterize the solvent-dependent features of the ultrafast relaxation dynamics of the excited states of fucoxanthin described in chapter 4.

These solvents were selected also because they allow reaching a relatively high solubility of the carotenoid. In fact, before starting a 2DES experiment, the sample must be prepared so that its OD ranges from 0.2 to 0.3 at the exciting wavelength. In this way, the sample is concentrated enough to make its third-order signal detectable, but sufficiently diluted to avoid self-absorption phenomena. Carotenoids typically meet this condition easily thanks to their high molar extinction coefficient ($\varepsilon \sim 10^5\ M^{-1}cm^{-1}$). However, it should be noted that the steady-state spectrum of Fx does not match well with the laser emission profile used in 2DES, as only the red tail of the spectrum is excited by the pulse (figure 6.1). This is due to the technical properties of the TOPAS, whose output cannot be tuned further to the blue with respect to the spectrum shown in figure 6.1. Although this could appear as a limitation, this configuration focused the investigations only on the red tail of the absorption spectrum, allowing us to better characterize the formation of the ICT state in Fx, the ensuing relaxation dynamics, and its solvent-dependent properties, as discussed in chapter 4. Furthermore, this spectral window also allowed performing a spectral filtering action and neglecting all the relaxation dynamics involving higher energy vibrational levels within the S_2 manifold. This permitted a significant simplification in the interpretation of the complex dynamics of Fx.

In this particular case, because of the mismatch between the absorption spectrum of the system and the laser spectral profile, the wanted value of absorbance must be reached on the red side of the Abs spectrum (~ 520 nm). This led to the preparation of very concentrated samples that required solvents with high solubility. This is why toluene was chosen as the most apolar solvent, rather than the more common cyclohexane.

From an operational point of view, the absorbance of the prepared samples is checked by steady-state absorption spectroscopy. The linear absorption measurements on the sample solutions were carried out

using a Varian Cary® 5000 (Agilent Technologies). Linear absorption spectra were taken before and after each 2DES experiment to check the absorbance and verify that no photo-degradation occurred after the non-linear experiments.
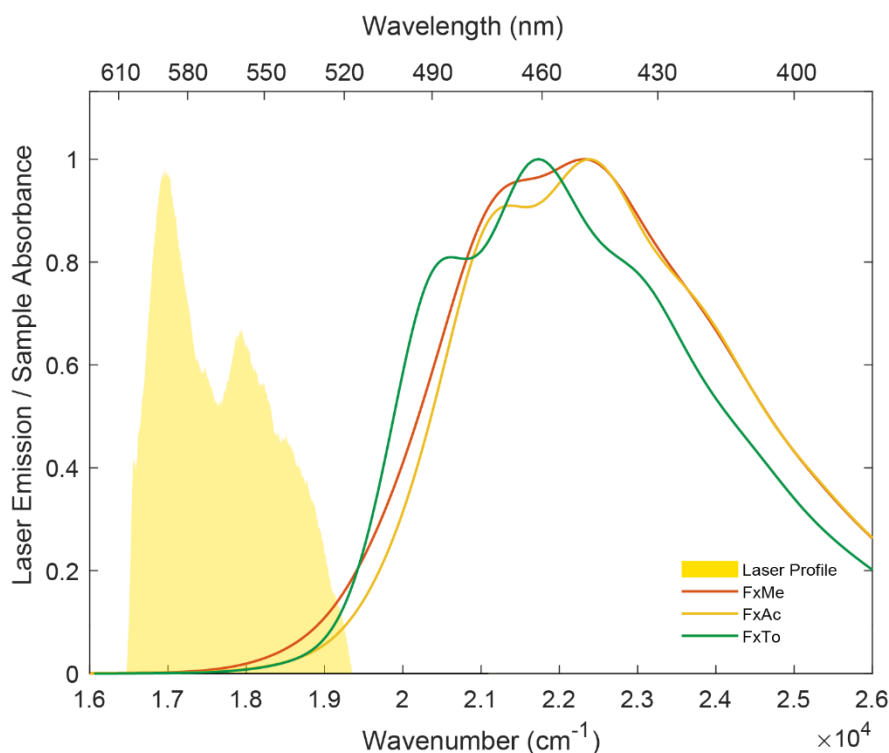

Figure 6.1 – Normalized linear absorption spectra of fucoxanthin in methanol (red line), acetone (yellow line), and toluene (green line), together with the laser emission profile (yellow area).

6.1.1 Concentration-Dependent Test

To rule out the presence of aggregates in these high concentration conditions, I conducted a concentration-dependent test, preparing different samples with increasing concentration of Fx and checking if their normalized steady-state spectra were identical. If not, those samples would likely contain aggregates and the related 2DES measure would not be reliable.

About 0.1 mg of fucoxanthin was weighed and dissolved in the three solvents used in the 2DES experiments: methanol, acetone, and toluene. Subsequent volumes of solvent were added in every sample, starting from 700 μL up to a total of 4200 μL, leading to a concentration range between 36 μM and 0.21 mM. After each addition, a linear absorption spectrum was collected. All the spectra were then normalized and compared. As example, in figure 6.2 the normalized spectra of Fx in methanol are reported. The other solvents show the same behavior. It was found that the normalized spectra present negligible differences until a concentration of 0.15 mM, while for higher concentrations non-negligible deviations start to be

recorded. This experiment sets the limit concentration for the Fx samples at 0.15 mM, which is the concentration of the 1000 μL sample. This test also allowed us to estimate the concentration of the sample used for the 2DES measurements, which is around 0.8 mM, using the Lambert–Beer law.
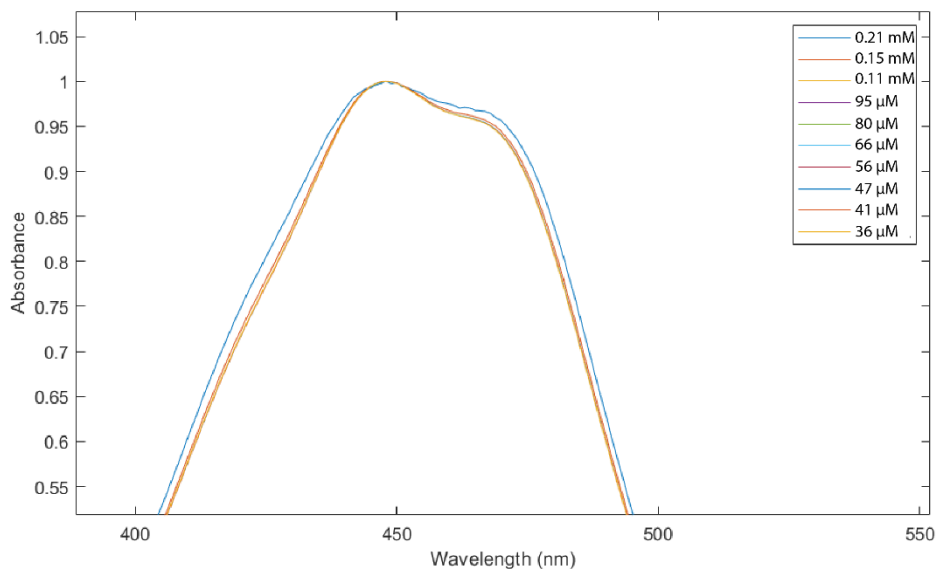

Figure 6.2 - Detail of the normalized absorption spectra of fucoxanthin in different concentrations of methanol.

6.2 2DES Maps

All the samples were investigated with the 2DES technique, probing their time evolution from 0 to 1000 fs. The measurements for each sample have been repeated between 2 and 6 times, depending on the quality of the signal, and then averaged to improve the signal–to–noise ratio. The time duration of the pulse has been characterized by a technique known as *frequency resolved optical grating* (FROG) and it has been estimated to be 8.7 fs.

 In this section, the 2DES maps of each sample will be discussed preliminarily, describing qualitatively their characteristic peaks and their energy values; the quantitative results of the fitting procedure and the overall discussion of the relaxation dynamics will be treated in the following sections. The results of the 2DES experiments, cast into a series of frequency-frequency maps at selected values of population time t_2, are summarized in figure 6.3 for the three fucoxanthin samples. The 2DES spectra of Fx are dominated by strong Excited State Absorption (ESA) signals, conventionally reported with a negative sign in 2D spectroscopy.[2,31] All the ESA signals are characterized by the same excitation frequency (*x*-coordinate), at around 18900 cm^{-1} (= 529 nm). The *x*-coordinate of the signal reflects what happens to the systems after

the first interaction with the laser pulse, i.e. the promotion of the strongly allowed $S_0 \rightarrow S_2$ transition. As previously discussed, this frequency value represents only the red tail of the absorption band, as the laser excitation profile does not cover frequencies higher than 19200 cm^{-1}.
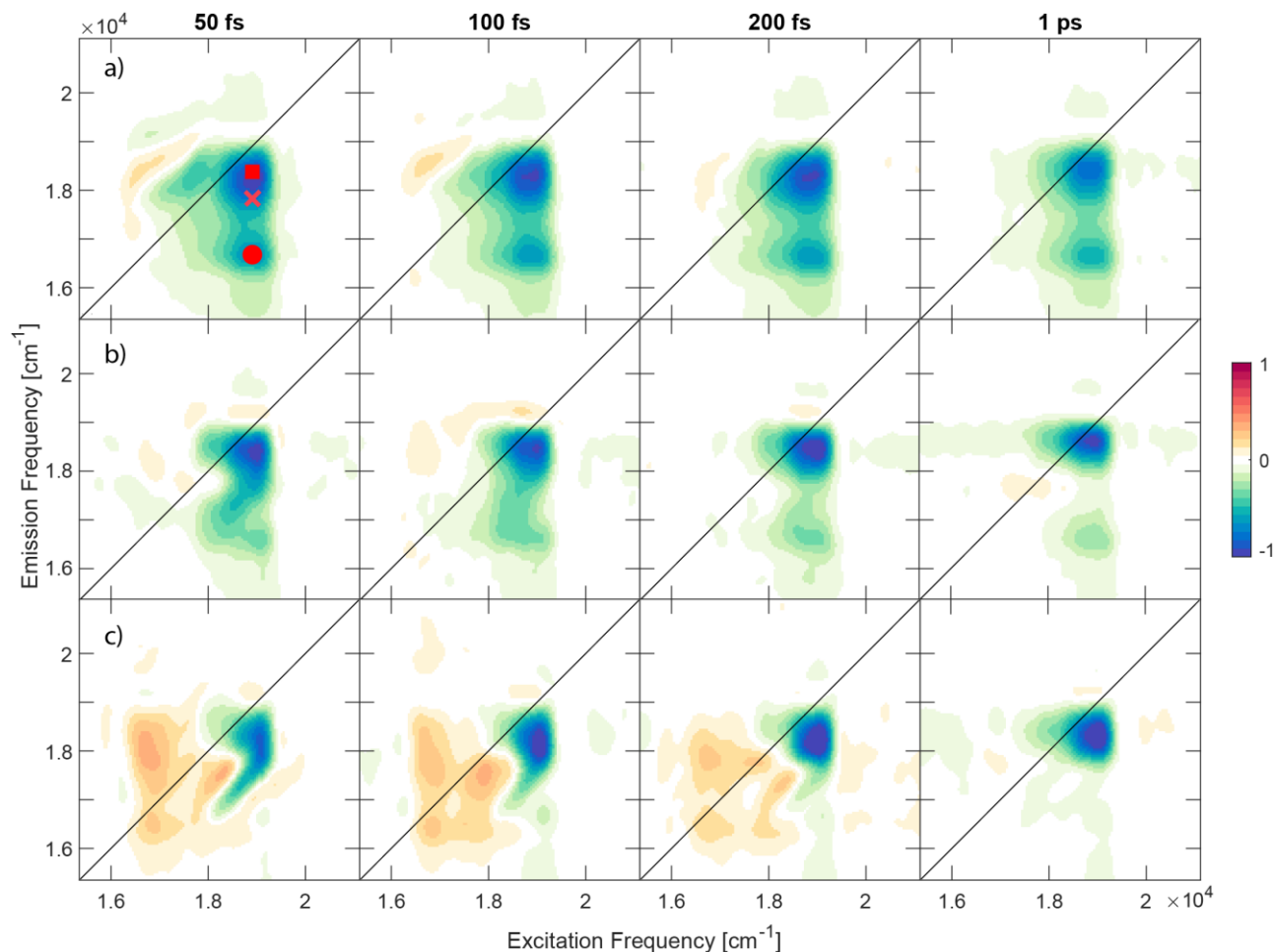

Figure 6.3 - 2DES total maps of fucoxanthin dissolved in (a) methanol, (b) acetone, and (c) toluene. The square and the circle identify the ESA signals from the S_1 state and from the ICT state, respectively. The cross indicates the coordinates of the 2D map where the hot vibrational states of S_1 contribute to the ESA signal.

Fucoxanthin in methanol (FxMe, figure 6.3a) displays two distinct ESA signals, one with an emission frequency (y-coordinate) of ~18300 cm^{-1} (square marker) and the other of ~16500 cm^{-1} (circle marker). The presence of two distinct ESA signals in the transient absorption spectra of Fx dissolved in polar solvents has already been captured by pump-probe spectroscopy, as seen in chapter 4.[23,62] The high-energy ESA signal is common to all carotenoids, and it has been attributed to the $S_1 \rightarrow S_n$ transition.[72] The cross marker in figure 6.3a indicates the coordinates where the hot vibrational states of S_1 are expected to contribute to the ESA signal through the $S_2 \rightarrow$ hot S_1 internal conversion and the hot S_1 relaxation processes. Commonly, the term hot vibrational states refers to the high energy vibrational states belonging to the same electronic state, in this case the S_1 state. The internal conversion process that transfers the

energy from the S_2 state to the S_1 state, also passes through the hot (high energy) vibrational states of S_1, and then the population in those states relaxes to the lower energy vibrational states of S_1, with a process known as hot vibrational relaxation.

The band at 16500 cm^{-1}, instead, can be found only in Fx and some other carbonyl carotenoids. This band is usually attributed to the presence of an ICT state in the excited states manifold indicating an ESA signal related to the ICT → S_n transition.[23,62,71,111]

The response of Fx in acetone (FxAc, figure 6.3b) is very similar to the one of FxMe. The main difference is that the lower energy ESA band is substantially less intense. This behavior can be explained through the destabilization of the ICT state in more apolar solvents.[23] In fact, this solvent-dependent trend is confirmed in the latest set of data collected on Fx in toluene (FxTo, figure 6.3c), where the low energy ESA band is not even detected, demonstrating how this latter is actually polarity-induced. The positive signals recorded at low excitation and emission frequency coordinates are due to non-resonant solvent contributions of toluene.

6.3 Global Fitting Analysis

After a first inspection of the main features of the 2DES maps, it is possible to analyze more in detail the data according to the procedures described in chapter 3, beginning with the global fitting analysis. The goal is to fit the evolution of the ESA signals along t_2 with a sum of exponential functions, with defined time constants. It is paramount to give a physical meaning to each time constant, otherwise the fitting procedure would not be useful for understanding the relaxation dynamics of Fx. The global fitting methodology was applied to the three sets of data after excluding the first 20 fs to avoid the artifacts originating during the time overlap of the exciting pulses. Two time constants has been used to fit the FxMe dataset, three for the FxAc and the FxTo datasets. The details of these constants (reported in Table 6.1 below) will be discussed together with the corresponding DAS maps.

6.3.1 DAS Maps

Figure 6.4 summarizes the results obtained for the FxAc sample. As seen in chapter 3, the outcome of the global fitting analysis includes time constants and their associated amplitude distribution along the 2D map, generating the so-called Decay Associated Spectra (DAS).

The DAS relative to the long-time constant (figure 6.4c) captures the main decaying component in both ESA bands, which represents the restoration of the ground state population in the picosecond time scale. The DAS relative to the shortest time constant (figure 6.4a) depicts a rising signal (positive red signal pinpointed by the square), which, considering the sign and the position, can be associated with the $S_2 \rightarrow S_1$ internal conversion.[75,111–113] The DAS in figure 6.4b, instead, is dominated by a decaying component on the lower part of the S_1–ESA band (blue signal highlighted by the cross). This signal appears at coordinates already associated with hot S_1 states' contributions and can been interpreted as the hot S_1 relaxation, in agreement with other studies.[113]
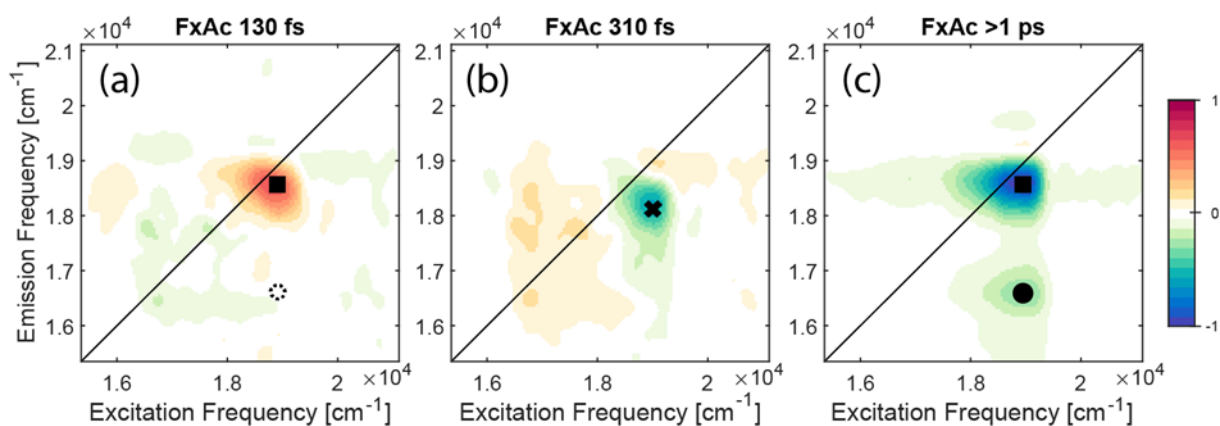

Figure 6.4 - DAS maps of fucoxanthin in acetone for the three time constants emerged from the fitting. The black square (circle) marks the ESA signal from the S_1 (ICT) state. The cross pinpoints the coordinates where hot S_1 states are mainly contributing. (a) DAS of the ultrafast time constant of 130 fs associated with the $S_2 \rightarrow S_1$ internal conversion. (b) DAS of the 310 fs component associated with the hot S_1 relaxation. (c) DAS of the longer time constant (>1 ps) associated with the S_1 relaxation.

The same analysis has also been applied to FxMe and FxTo samples. In FxMe, the overall dynamics appeared to be faster with respect to the less polar Ac solvent. In this case, it was not possible to identify signatures attributable to the hot S_1 relaxation, and an overall decay component with a time constant of 65 fs has been found, which we attribute to the $S_2 \rightarrow S_1$ internal conversion (figure 6.5a); the distortion and elongation of the positive peak on the first DAS is attributed to solvent contributions. The DAS related to the longer time decay >1 ps (figure 6.5b) has the same meaning as in the FxAc Sample.
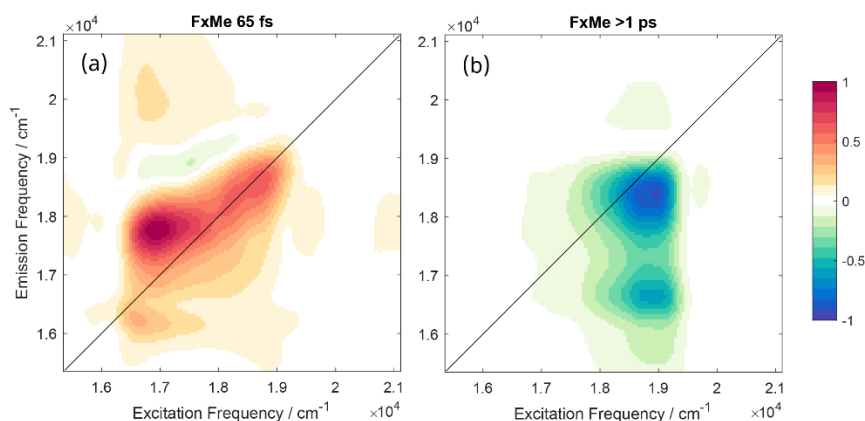
Figure 6.5 - DAS maps of fucoxanthin in methanol

In the FxTo sample, similar to FxAc, besides the >1 ps long time component, two time constants of 120 and 250 fs have been found. The sign and the amplitude distribution of these time components (figure 6.6) suggest a possible attribution to the $S_2 \rightarrow$ hot S_1 and $S_2 \rightarrow S_1$ processes, respectively. For FxAc (and FxMe), the $S_2 \rightarrow$ hot S_1 process is probably too fast to be clearly characterized.
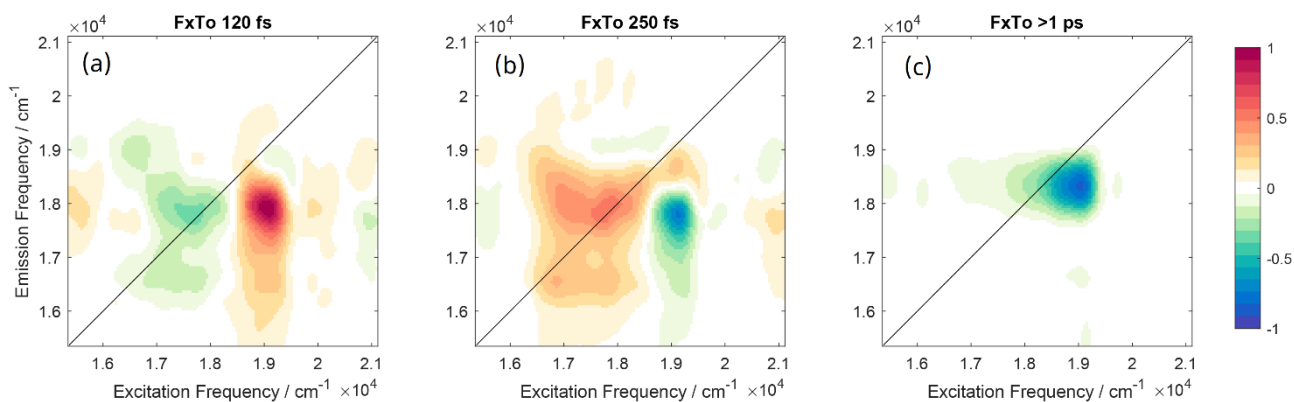
Figure 6.6 - DAS maps of fucoxanthin in toluene.

6.3.2 Hot Vibrational Relaxation

A closer analysis of the dynamic behavior of the signal at coordinates where hot S_1 states are expected to contribute (coordinates pinpointed by the cross marker in figure 6.4b) highlights the presence of an additional time component, which could not be reliably distinguished in the global fitting. A local fitting performed at these coordinates (figure 6.7a) and the comparison with the time decay of FxAc at the same position (figure 6.7b) lead to the identification of an additional kinetic component with a time constant

of 310 fs, which is likely attributed to the hot S_1 vibrational relaxation. The three colored bars on the bottom of figure 6.7a indicate the time ranges for the three processes that govern this evolution: the rising of the signal associated with the $S_2 \rightarrow$ hot S_1 internal conversion (orange), the fast decay related to the hot S_1 relaxation (yellow), and the slow decay as the population is restored to the ground state (green). The global fitting could not fully discriminate this component from the 250 fs one, given the slight difference between the associated time constants.
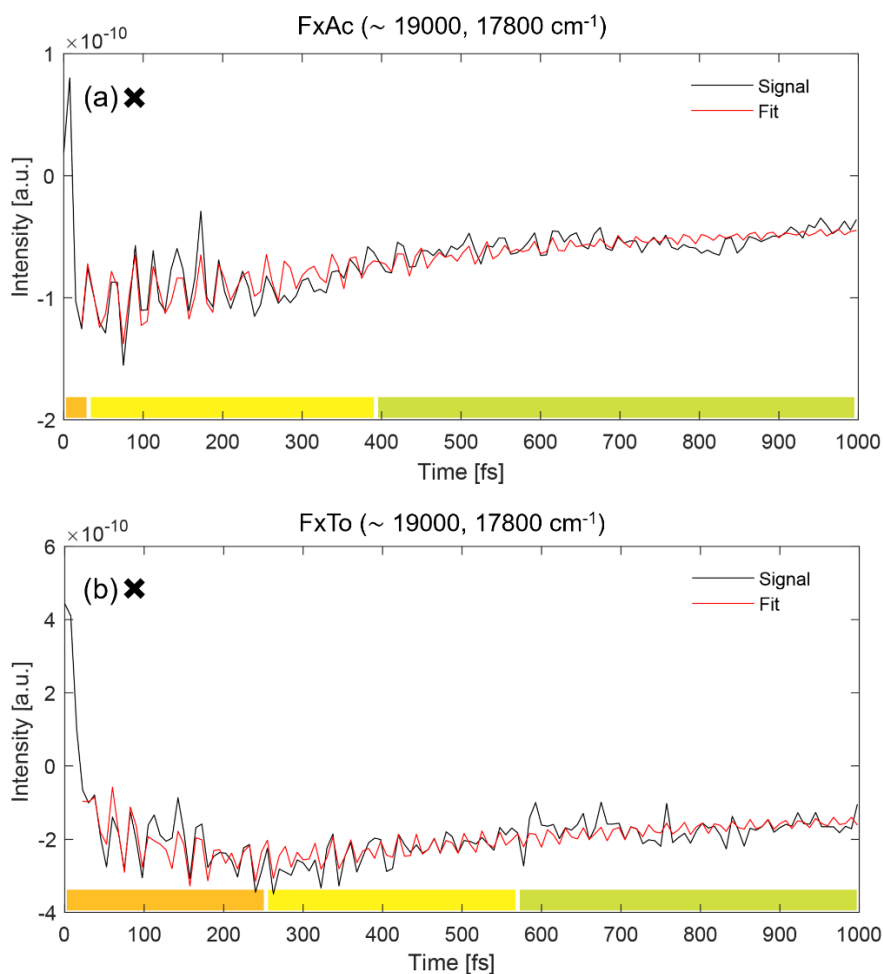

Figure 6.7 - Decay trace showing the t_2 evolution of the signal at the coordinates 19000, 17800 cm^{-1} for the (a) FxAc sample (time constants: < 10 fs, 310 fs and > 1 ps) (b) FxTo sample (time constants: 120 fs, 310 fs, >1 ps)

The time constants found for the FxTo sample are slightly different than those previously found by pump–probe experiments in other nonpolar solvents. For Fx in cyclohexane solutions, Kosumi et al. estimated a time constant of 60 and 620 fs for the S_2 decay and the S_1 vibrational relaxation, respectively.[62] This discrepancy can be explained by accounting for the different nature of the solvent used (toluene rather than cyclohexane) and the different time resolution (~10 fs vs. ~100 fs). Nonetheless, the important point is the confirmation of the progressive slowing down of the dynamics in less polar solvents.

Overall, although the relaxation dynamics of S_2 have been the object of an extensive investigation by pump–probe experiments, the improved time resolution of ~10 fs achieved with 2DES experiments and the possibility of inspecting the sign and the amplitude distribution of the components in the DAS plots allowed a better characterization and a robust interpretation of the early steps of relaxation, which also revealed a clear solvent-dependent trend. The obtained time constants for the three samples are summarized in Table 6.1.

Table 6.1 - **Time Constants Obtained from the Global Fitting Analysis of the Three Samples**
(The asterisk (*) indicates the time constants that could be discriminated only by a local fitting)

	$S_2 \rightarrow$ hot S_1	$S_2 \rightarrow S_1$	hot $S_1 \rightarrow S_1$	S_1 relaxation
FxMe		65 fs		>1 ps
FxAc		130 fs	310 fs	>1 ps
FxTo	120 fs	250 fs*	310 fs*	>1 ps

6.3.3 Population Traces

The time trace extracted at coordinates corresponding to the $S_1 \rightarrow S_n$ ESA (figure 6.8a) shows how the signal evolves in the first 1000 fs after the excitation. The rising and the decay of the ESA band can be observed. Instead, the time trace extracted where the ESA band associated with the ICT $\rightarrow S_{n'}$ transition contributes (figure 6.8b) does not present any rising component and starts to decay immediately after the laser excitation. This behavior is confirmed by the absence of any rising (red) signals in the corresponding portion of the DAS (figure 6.4a, dashed circle).
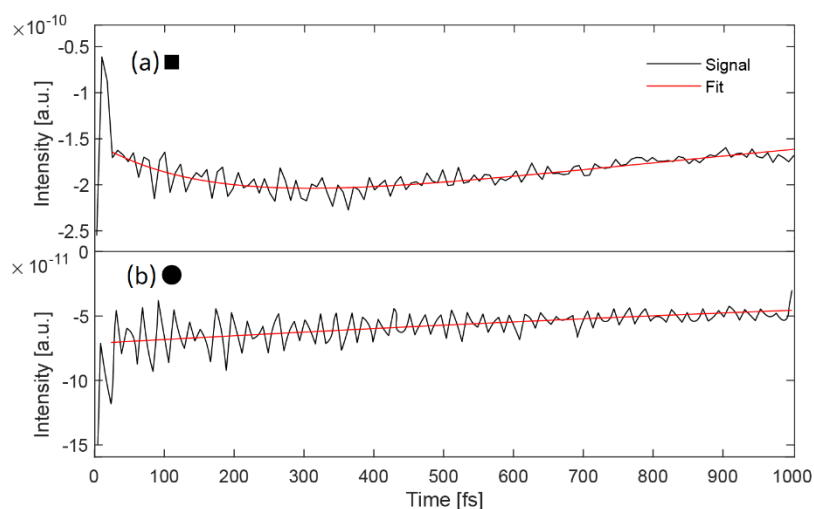

Figure 6.8 – (a) Decay trace showing the t_2 evolution of the signal at the coordinates of the ESA-S_1 signal (black square, fig. 6.4). (b) Decay trace at the coordinates of the ESA-ICT signal (black circle, fig. 6.4).

6.4 Beating Analysis

In addition, both traces reveal the presence of a lively beating behavior, due to the activation of vibrational modes of Fx. The main beating components in the 2DES signal were identified through Fourier spectra analysis, also known as Power Spectra analysis. The power spectra analysis is simple, but it is very useful to characterize the frequency of the oscillations, their relative intensity and to separate carotenoid and solvents contributions. As already described in chapter 3, a power spectrum is obtained from the residues of the global fitting analysis of the *rephasing* and *non-rephasing* datasets, that are Fourier-transformed, integrated along the excitation and emission frequencies, and finally arranged in a Raman–like fashion. The power spectra for R and N datasets of each sample are reported in figure 6.9.
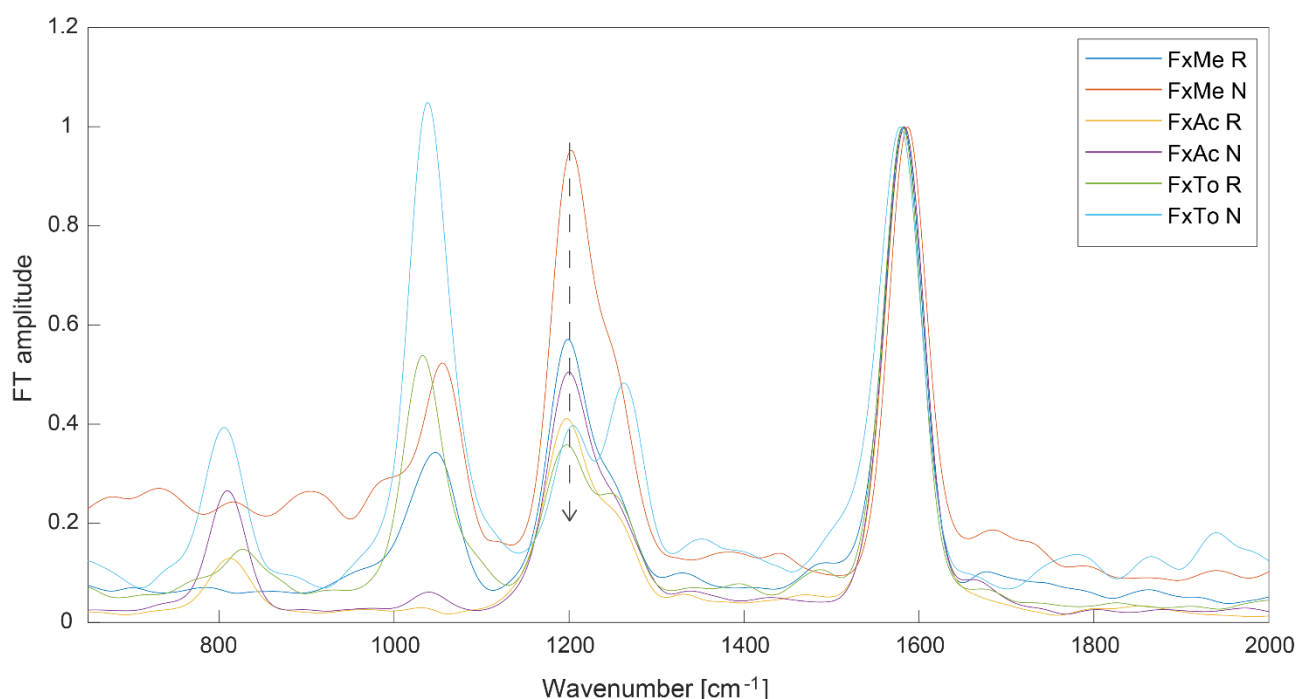

Figure 6.9 - Fourier spectrum analysis of the beatings in the t_2 evolution of the signal for the three samples (R = rephasing, N = non rephasing); the drop-down arrow indicates a solvent-dependent trend: the intensity of the C-C stretching mode decreases as the polarity of the solvent decreases.

The spectra are normalized with respect to the main peak at ~1580 cm^{-1}, present in all samples. Other two strong peaks can be distinguished: one at ~1200 cm^{-1}, and the other at ~1260 cm^{-1}, appearing as a shoulder of the former. In the literature, these peaks are assigned to the C=C stretching vibration (1580 cm^{-1}) and the C–C stretching (1200 cm^{-1}) that is mixed with the C–H in-plane bending. The C–CH$_3$ stretching, instead, should lie at 1010 cm^{-1}, but it is covered by non–resonant solvent contributions.[32,114] In fact, the main peak of methanol is centered at ~1050 cm^{-1} and the one of acetone at ~800 cm^{-1}. Toluene, instead, has two main components at ~800 cm^{-1} and ~1030 cm^{-1}.

Fucoxanthin exhibits a solvent dependence in the relative intensity of the two main peaks; the C-C stretching signal is the most intense in FxMe, while the least intense in FxTo. This could mean that the charge-transfer character of fucoxanthin plays a role in the vibrational modes of the carotenoid, even if they involve only the conjugated polyene chain. Nonetheless, the frequency of the beatings is not influenced by solvent polarity. High-level molecular orbital calculations on peridinin suggested that the charge-transfer character of the ICT state involves the motion of electron density within the polyene, and is accompanied by bond-order reversal in the central portion of the polyene chain.[71] Invoking a similar effect also in fucoxanthin could help explain this behavior.

6.5 Discussion of the Experimental Data

One of the most important pieces of evidence emerging from the analysis of the three samples is the increase of the rising ultrafast time constant as the polarity of the solvent decreases (Table 6.1). A similar solvent-dependent trend has already been detected by Kosumi et al.,[112] but the limited time resolution (~100 fs) did not allow for a detailed discussion of this behavior. An interesting explanation can be attempted following a model proposed by Wagner et al.[71] for peridinin. In this paper, the authors propose the use of an (S_1+S_2)/ICT state model, where the ICT state arises from a configurational mixing of the lowest two excited singlet states S_1 and S_2. The idea of a mixed state between S_1 and S_2 was already proposed in some early works on Peridinin-Chlorophyll Protein (PCP) to explain particular vibrational features.[74,115] This ICT state is characterized by an enhanced dipole moment and thus requires a polar solvent for stabilization. In this picture, the ICT and the S_1 states are separated by a polarity-dependent barrier of potential, expected to be very small in polar solvents. The application of a similar model also to Fx would explain the solvent-dependent $S_2 \rightarrow S_1$ conversion rates: in apolar solvents, the barrier is higher, leading to a longer internal conversion between S_2 and S_1.

This model is useful also to discuss the nature of the ICT state itself, focusing on another feature already glimpsed in the analysis of its trace along t_2 (figure 6.8b): the absence of a rising time constant related to the ICT-ESA band. In fact, at early delay times, the samples in methanol and acetone share the presence of the ICT-ESA immediately after the laser excitation. The S_1-ESA band instead is characterized by a rising component, derived from the internal conversion from the S_2 state. This new experimental evidence could only be captured with a high temporal resolution, and it goes together with recent studies that suggest that S_1 and ICT are indeed two distinct electronic states, since the temporal evolution of the

relative ESA signals is different.[116,117] The presence of an ESA from the ICT state already at $t_2 = 0$ suggests an instant population of that state (at least within our time resolution). This evidence has led to the hypothesis that the ICT state could be directly coupled to the S_2 state, an idea already presented in the (S_1+S_2)/ICT state model invoked previously. Indeed, according to Wagner et al.,[71] "in terms of most properties, the ICT state is S_2-like in character." This picture seems to be also supported by the work of Ghosh et al., who identified a <20 fs nonradiative decay of the S_2 of peridinin to an S_x state with a strong ICT character, assigned to a distorted configuration.[118,119]

This model refers to peridinin, whose ESA bands are indistinguishable, and it should also be tested for fucoxanthin; but the idea of a strong mixing between the various states of the system could explain this and other controversial features. Moreover, it is important to stress that, even though the S_1 and the ICT states are two distinct electronic states, an interplay between the two states is still possible, as recent pump–dump probe studies have proposed.[116,117] In this picture, more polar solvents, besides stabilizing the ICT and lowering its energy, would also promote a better mixing with S_2 and thus a lower barrier of potential. Another interesting insight of this model is the interpretation of the asymmetrical increase of the red tail of the linear absorption spectrum in polar solvents: if the ICT state, coupled with the S_2 state, can be populated instantly, there has to be a trace of this process also in the linear absorption, and this could be indeed related to the increased absorbance in the red tail. In fact, in apolar solvents, the ICT is not populated, and the red tail absorbance is less pronounced. It must finally be noted that all these results have been obtained with very specific excitation conditions, where only the most red portion of the absorption spectrum could be addressed (figure 6.1).

In conclusion, in this part of the project, the ultrafast relaxation dynamics of fucoxanthin was characterized with 2DES, a technique scarcely applied to carotenoid systems because of technical limitations. The obtained results permitted the unraveling of subtle details of the kinetics of the system, through the investigation of the time evolution of ESA signals promoted after the photoexcitation of the red tail of the S_2 absorption band and the ensuing relaxation to S_1 and ICT states.

Thanks to the 10 fs time resolution achieved in these experiments, the kinetic constants regulating the $S_2 \rightarrow S_1$ internal conversion of Fx in three solvents with different polarity have been determined with an unprecedented level of detail. Indeed, it is known that the relaxation dynamics of the S_2 state in carbonyl carotenoids takes place in the sub–100 fs time regime,[72] and therefore, conventional pump–probe experiments with a typical 100 fs time resolution so far could only provide rough estimates of the

associated kinetic constants. A clear solvent-dependent trend of the $S_2 \rightarrow S_1$ internal conversion rates has been found: the process becomes faster as the polarity of the solvent increases.

In addition, I found evidence for two distinct ESA signals developing from the S_1 and ICT states, whose relative intensities also depend on solvent polarity. The S_1-ESA signal rises in the first 100 fs, which clearly indicates that the S_1 state is progressively populated via relaxation from S_2. Instead, the ICT-ESA signal is instantaneously present immediately after photoexcitation, with no rise component, suggesting an instant population of the ICT state. These features have been interpreted on the basis of a model previously proposed in the literature for peridinin, which identified a strong coupling between the ICT and the strongly allowed S_2 state (figure 6.10).
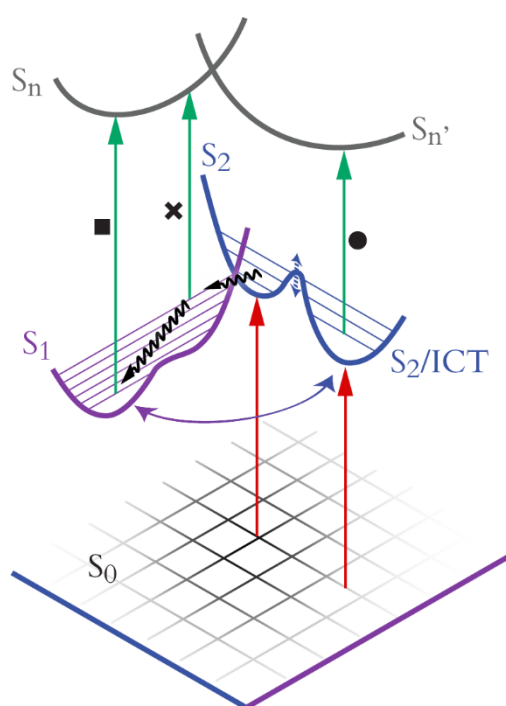

Figure 6.10 - Proposed scheme summarizing the main dynamic processes captured by the 2DES measurements on solutions of Fx. Red arrows: excitation; black wavy arrows: nonradiative processes; green arrows: ESA processes. The black markers (square, cross, and circle) pinpoint the processes identified in the 2D maps of figures 6.3 and 6.4. The barrier of potential between S_2 and ICT is solvent-dependent (dashed blue arrow). The purple/blue arrow represents the interplay between the S_1 and ICT states, leading to picosecond equilibration between the potential minima.

While the effective applicability of this model also to fucoxanthin needs to be supported by further studies, the instant presence of the ICT-ESA signal at early times and also its peculiar dependence on solvent polarity point toward a new interpretation of the nature of the ICT state.

These findings represent, in any case, an important piece of information about the nature and the dynamics of dark states in carotenoids. From a broader perspective, we believe that a better characterization of such dynamics is essential for a better comprehension of the ultrafast relaxation

dynamics taking place in more complex multi-chromophoric antenna systems. This preliminary characterization of Fx in vitro will also contribute to a deeper understanding of the excitation energy transfer processes that involve carotenoids *in protein*, as we will see in the next chapter on the characterization of FCP through 2DES.

Chapter 7

Experimental Results on Fucoxanthin Chlorophyll Protein

Taking into account the information summarized in chapter 5 about the spectroscopic features of FCP and their relation with the resolved crystallographic structure, now we can outline the aim of the 2DES characterization that I conducted during the Ph.D. Differently and complementarily to the other 2DES studies, the focus of this work is centered on the Fx behavior inside the protein environment and the aim is to characterize the possible interaction that may occur between Fx and Chl *c* inside FCP, considering the structure of the protein in the interpretation of the spectroscopic data. I considered both the published structures of *Phaeodactylum tricornutum* and *Chaetoceros gracilis* and also the proposed organization of the chromophores for *Cyclotella meneghiniana*. In fact, the arrangement of the chromophores proposed in the structural analysis of FCP highlights the presence of Fxs close to Chl *c* molecules. This perspective could lead to the discovery of new energy pathways and a better understanding of the role of Chl *c* in this proteic environment.

7.1 Sample Preparation

The sample for the 2DES measurements has been prepared from 45 μL of FCPa with a concentration of 575 μg/mL, diluted with a buffer composed of 25 mM of Tris (pH 7.5), 2 mM of KCl and 0.03% of β-dodecyl maltoside. The buffer composition is designed in order to maintain a constant pH in the protein solution, control the ionic force, and to stabilize the membrane protein with the presence of surfactants. The dilution has been carried out to obtain an OD of about 0.2 in the portion of the absorption spectrum that corresponds to the laser profile (figure 7.1a). The sample was successively put in a cuvette that was then sealed with a blowtorch. All these steps were performed keeping the sample in an ice bath. All these precautions were adopted as the sample is highly unstable, being a membrane protein. Nonetheless, we verified that the sample was usable for no more than 48 hours after its preparation because of severe oxidation processes and destabilization of the protein structure.
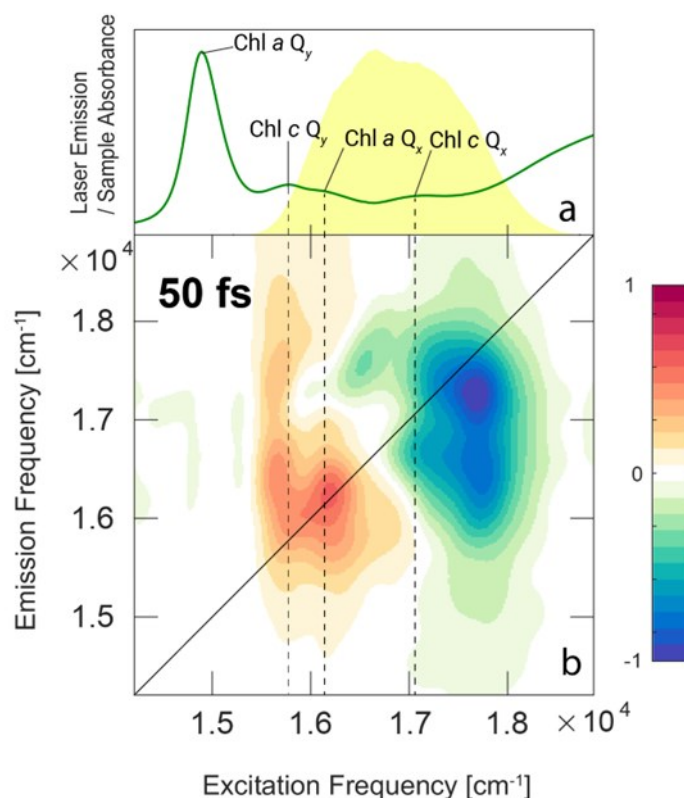
7.2 2DES Characterization

Figure 7.1 - a) Steady state absorption spectrum of FCP (green line), together with the laser emission profile used for 2DES experiments (yellow area). The main peaks of the spectrum are labelled with the associated attributions. b) 2DES total map at t_2 = 50 fs. The positive red signals are attributed to the GSB and SE of the chlorophylls and the negative blue signal is related to the ESA signal originated from the S_1 and ICT state of fucoxanthin.

In figure 7.1a, the steady state absorption spectrum of the FCP sample is shown, together with the laser emission profile used for the photoexcitation in the 2DES measurements (pulse duration: 11 fs, estimated by FROG measurements). Four main peaks can be noted, attributed to the Q_y and Q_x transitions of Chl a and Chl c.[20] The red tail of the S_2 transition of Fx dominates the high-energy part of the spectrum. The laser was tuned in order to focus on the interaction between Chl c and Fx: thus, its range of frequencies goes from ~15500 cm^{-1} to ~18000 cm^{-1}. In this way, it covers the red tail of the S_2 band of Fx and the Q_y and Q_x of Chl c, without the overwhelming presence of the Q_y signal of Chl a. As a result, with this setup, the 2DES maps have contributions both from Chl c (positive signal) and Fx (negative signal), as shown in figure 7.1b, which represents, as an example, the signal at 50 fs after the laser excitation.

Figure 7.2 shows instead 2D maps at different delay times. A first qualitative look at the maps immediately highlights a neat difference in the signal distribution for the early times sub-50 fs (panels a-d) and the >50 fs dynamics (panels e-h). At delay times longer than 50 fs, the 2DES map is composed of two main signals: a negative band with an excitation frequency (x-coordinate) of ~17700 cm^{-1}, corresponding to the ESA

of the S_1 and ICT states of Fx (upper and lower lobe of the band),[72] and a positive peak with an excitation frequency of ~16200 cm^{-1}, related to the SE and the GSB of the Chls bands.[87]
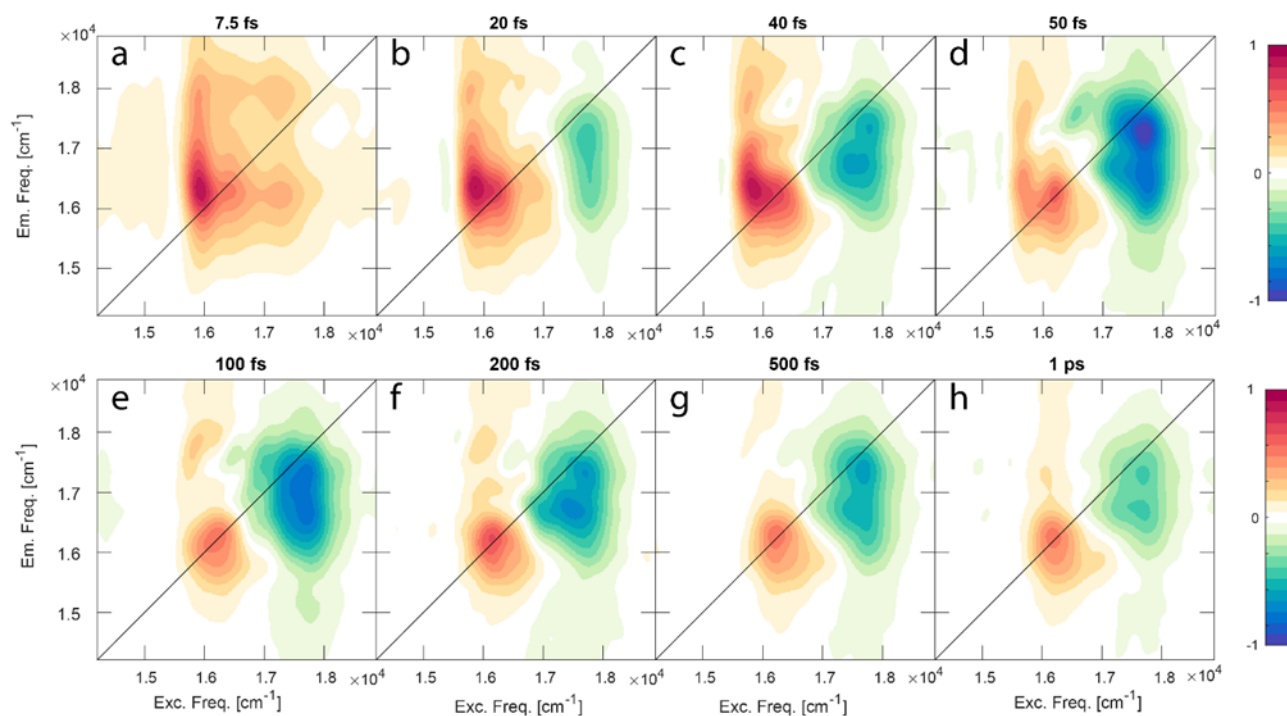

Figure 7.2 - 2DES total maps of FCP; the first four maps (a–d) are normalized on their maximum absolute value, in order to highlight the shape variations of the signals at early times. Panels (e–h) are normalized on the absolute maximum of the map at 50 fs so that the decay of the signals at increasing time can be better appreciated.

The evolution of the signal in the first 50 fs is displayed in figure 7.2a-d. In this timeframe, the early time dynamics shown in the maps are dominated by a strong positive signal that appears concomitantly with the photoexcitation. In figure 7.2a the total signal includes three distinct positive bands at different excitation frequencies. The lowest one (x-coordinate at 16000 cm^{-1}) is the most intense and it is clearly detectable until 50 fs. The other two signals (x-coordinate at ~16500 cm^{-1} and ~17200 cm^{-1}, respectively) are less intense, and they are damped in a timescale comparable with the laser pulse duration (11 fs). The excitation frequency of these three ultrafast signals agrees with the position of the Q_x and Q_y bands of Chls in the absorption spectrum of FCP, suggesting that these excited states of the chlorophylls are stimulated synchronously by the exciting pulse. The decay of these ultrafast signals allows for the main positive and negative signals already discussed for the longer time maps to emerge, which then slowly diminish at longer time scales, indicating that the system is relaxing to the ground states.

7.3 Global Fitting and DAS Analysis

As for the analysis of the isolated fucoxanthin datasets, to characterize quantitatively the rates regulating the dynamics, a global complex multiexponential fitting procedure was used. In this way, all the coordinates of the 2D maps are fitted simultaneously.[38] The result of the global fitting is described by three time constants (8 and 18 fs and >1 ps) together with the amplitude distribution of these components as a function of the excitation and emission frequencies. This amplitude distribution can be visualized in the form of DAS associated with each time constant resulting from the fitting.[38] The DAS maps are reported in figure 7.3(a–c).
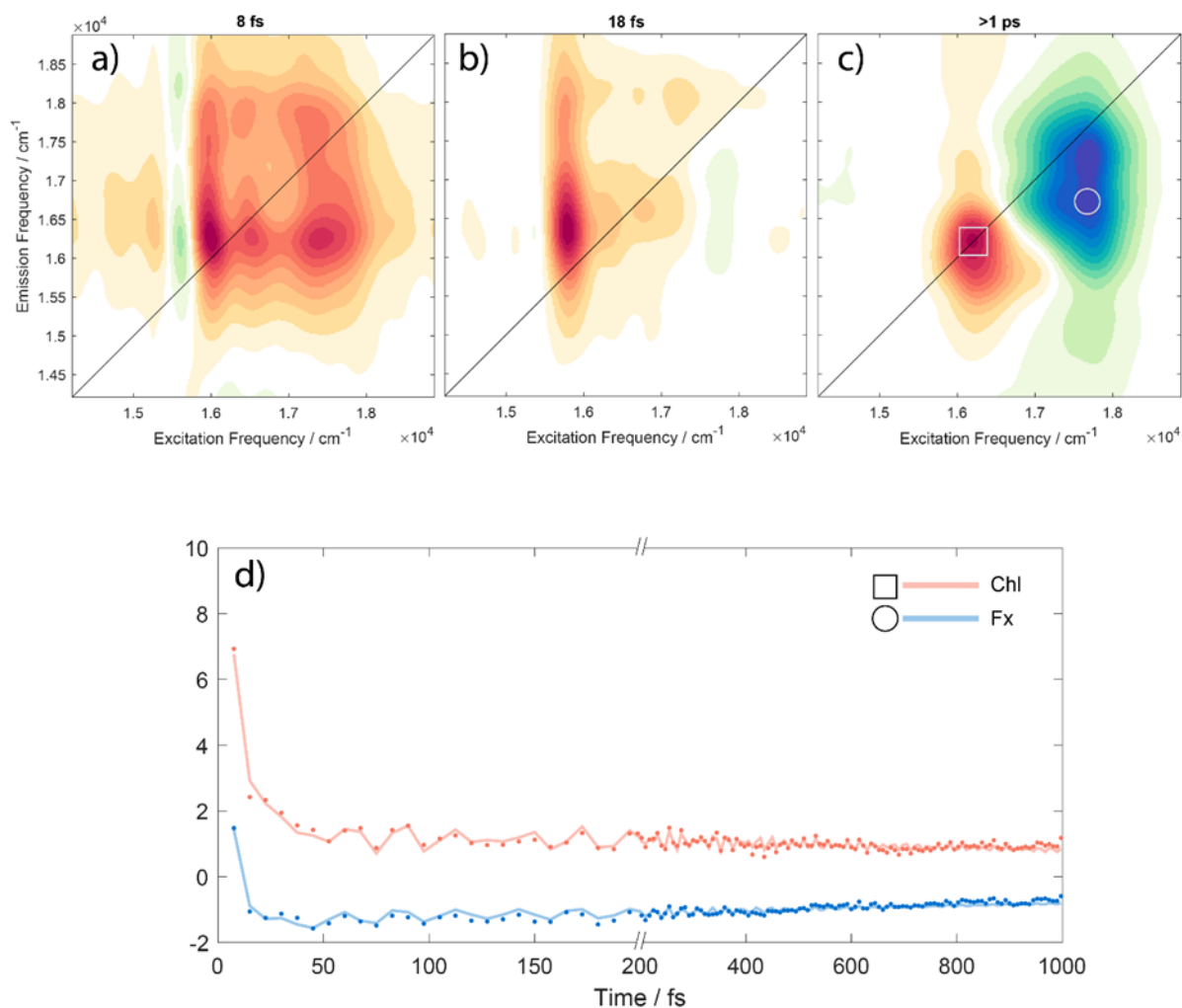
Figure 7.3 - DAS for the three time constants emerged from the fitting and relative traces. a) DAS of the ultrafast time constant of 8 fs related to the damping of the strong positive signal prepared with the excitation of the laser. b) DAS of the 18 fs time component associated with the ultrafast energy transfer from the Q_y of Chl c to the Q_y Chl a. c) DAS of the longer time constant (>1ps) associated with the restoration of the ground state population. d) Time decay traces (circles: experimental data; solid lines: fitting curves) of the ESA band of Fx (circle marker, blue, coordinates: 17700, 16700 cm^{-1}) and the GSB/SE band of Chl (square marker, red, coordinates: 16200, 16200 cm^{-1}).

Following the conventions presented in the previous chapters about the meaning of the color spectrum for DAS maps, in this particular case, each of the three DAS has positive peaks for signals with positive amplitude (Chls) and negative peaks for signals with negative amplitude (Fx). Thus, this means that all the components that regulate the fitting are related to a decay of the population of the states involved. These trends can be easily verified inspecting the time traces at the coordinates of the main peaks (square and circle marks), as shown in figure 7.3d. Though it may seem that the ESA signal is rising in the first 20 fs, this behavior is caused by the decay of the strong positive signal.

The three dynamic components consist of: (i) an ultrafast sub-10 fs time constant, comparable with the pulse duration, describing the quick damping of signals initially prepared by the pulse excitation (figure 7.3a); (ii) another ultrafast decay component (~20 fs) mainly contributing at lower values of excitation frequency (figure 7.3b) and (iii) a longer time constant that can be associated with the relaxation dynamics of the main peaks (figure 7.3c). This latter DAS captures the main decaying component in both chlorophyll and fucoxanthin bands, representing the restoration of the ground state population in a timescale >1ps, longer than the investigated time window. The attribution of the first two DAS in the sub-50 fs timescale is less trivial.

7.3.1 DAS Interpretation

The positive signal generated by the laser pulse at early delay times (figure 7.2a) is characterized by a particularly strong intensity that dominates the maps in the first tens of femtoseconds. It features three different peaks separated on the x-axis and elongated on the y-axis. The first DAS map (figure 7.3a) indicates that this signal decays (positive red peaks) in around ten femtoseconds, which is the duration of the laser pulse. This signal includes three main diagonal components at excitation energies corresponding to the excited states of Chls and Fx and all the corresponding cross-peaks symmetrically above and below the diagonal. The peculiar positions of the peaks suggests that these signals are capturing something different than the mere pulse overlap effect. My hypothesis is that all the FCP chromophores are excited concurrently by the ultrafast pulse, which prepares a coherent superposition of the excited states causing the delocalization of excitation among the Chls and the Fx. This superposition dephases within the duration of the pulse itself; therefore, I cannot attribute any functional meaning to these overdamped coherences. It is indeed important to stress that the DAS of figure 7.3a does not imply an ultrafast energy transfer between the chromophores but rather suggests the presence of an actual coupling between their

excited states. A similar situation was recently found in another pigment-protein complex where the amplitude distribution of the signal in an ultrashort DAS maps was exploited to pinpoint the energies of the excitonic states in the early stages of the relaxation dynamics with greater precision.[120] The presence of a similar signal at early time delays was previously detected also by Gelzinis *et al.*, but it was not analyzed, because it "should be related to the fifth-order response, non-resonant and/or the pulse overlap effects."[21] While we cannot fully exclude the possible contribution of these spurious effects, the peculiar signal distribution in this DAS seems to point towards a more specific attribution.

The second DAS map (figure 7.3b) depicts the presence of a second femtosecond dynamics, longer and independent from the one previously discussed, which contributes mainly to the early decay of the lowest energy peak, attributed to Chl *c*. As also confirmed by the maps in figure 7.2, this peak decays with a time constant of ~20 fs, making it detectable until 50 fs. My interpretation is that the ultrafast decay of this signal could be evidence for the ultrafast energy transfer between Chl *c* and the Q_y state of Chl *a*, not fully detectable in our spectral range. This attribution is in agreement with the most recent models that invoke an ultrafast energy transfer between these states shorter than 50 fs.[107] These data allowed providing a better estimate of this time constant.

7.4 S_1–ESA vs ICT–ESA

Additional details can be obtained by exploring the time traces at specific coordinates in the 2D map. In particular, I analyzed the signal looking at possible differences between the traces extracted at the coordinates of the two lobes that belong to the ESA band of the Fx, attributed to the ESA from the S_1 state (upper lobe) and the ICT state (lower lobe). As seen in chapter 6, I demonstrated that the relative amplitude of these two lobes and their dynamics strongly depends on solvent polarity. Therefore, the analysis of the time traces extracted at these peculiar coordinates might provide crucial indications about the polarity of the medium in which Fx molecules are embedded. In the case of FCP, no relevant difference has been found between these traces (figure 7.4), in the current experimental conditions. By comparison with the previous evidence on isolated Fx in solution, one should thus deduce that in FCP the protein environment surrounding Fxs can be considered, on average, strongly polar. Moreover, the simple presence of a strong ESA from the ICT state is evidence of this assumption. However, FCP is a membrane protein and inside the membrane the environment should be apolar.
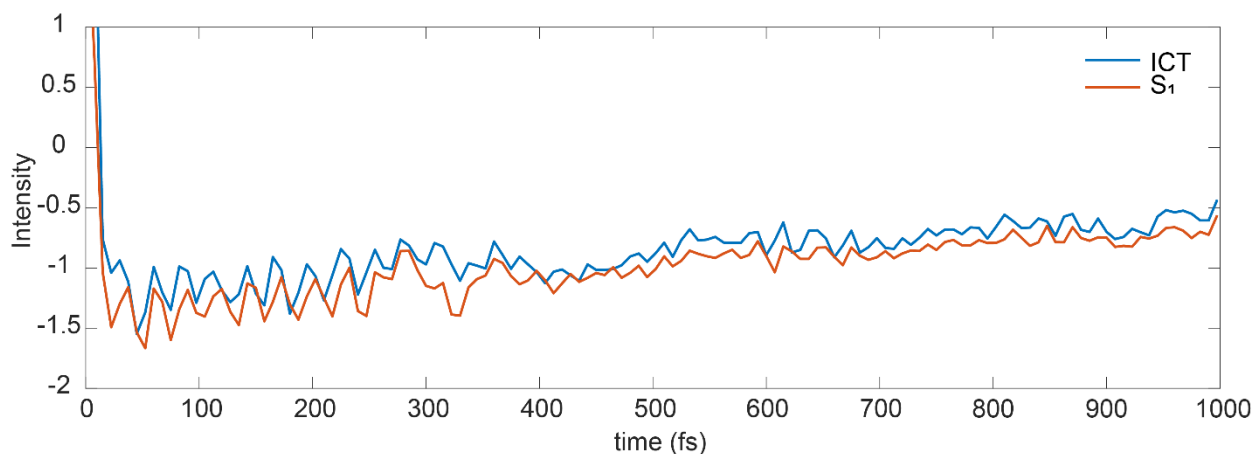
Figure 7.4 – Time decay traces of the ESA band of fucoxanthin. Blue line: trace related to the ESA signal generated from the ICT state (coordinates: 17600, 16450 cm^{-1}); orange line: trace related to the ESA signal generated from the S$_1$ state (coordinates: 17700, 17100 cm^{-1}).

Thus, a meaningful comparison between the response of Fx in solution or in protein should take into account that the various Fx molecules in FCP experience different surroundings inside the protein, due to the presence of different amino acids that could provide local polarized environments. The crystallographic structure and the chromophores' arrangement deduced from X-ray experiments[108] suggest in particular that some Fxs are conditioned by polar binding environments, thanks also to the closeness to Chl *c* molecules. These are the molecules labelled as Fx306 and Fx307,[108] known to contribute to the red side of the absorption band and thus the ones more likely addressed in our experimental conditions. For these molecules, the polyene chains of the carotenoids are running parallel to the tetrapyrrole rings of Chl *c*, and their C-rings are hydrogen-bonded to the two propenoic acids of Chls *c*, contributing to the hydrophilic polar environment that the Fxs experience.[108] Therefore, these experimental findings seem to be in agreement with structural investigations.

However, it is important to remember that the available structures of FCP were obtained for *Phaeodactylum tricornutum* and *Chaetoceros gracilis*; there is no available structure of *Cyclotella meneghiniana* yet. So, the assumptions made on those structures have to be pondered carefully. Previous investigations[107] explicitly comparing spectroscopic data of *Cyclotella meneghiniana* with the chromophores arrangement of *Phaeodactylum tricornutum* and *Chaetoceros gracilis* highlighted some discrepancies, suggesting that FCP's spectroscopic features depend strongly on the type of organism from which they are extracted.

7.5 Beating Analysis

Moreover, we carried out an analysis of the lively beating behavior contributing to the time traces of the signal, related to the activation of the vibrational modes of the Fx. The main beating components in the 2DES signal have been determined through Fourier spectrum analysis (figure 7.5). The frequencies identified agree with the well-known vibrational modes of carotenoids (~1200, ~1580 cm^{-1}).[32,114] The third previously identified mode at 1280 cm^{-1} appears here as a shoulder of the strong 1200 cm^{-1} band.
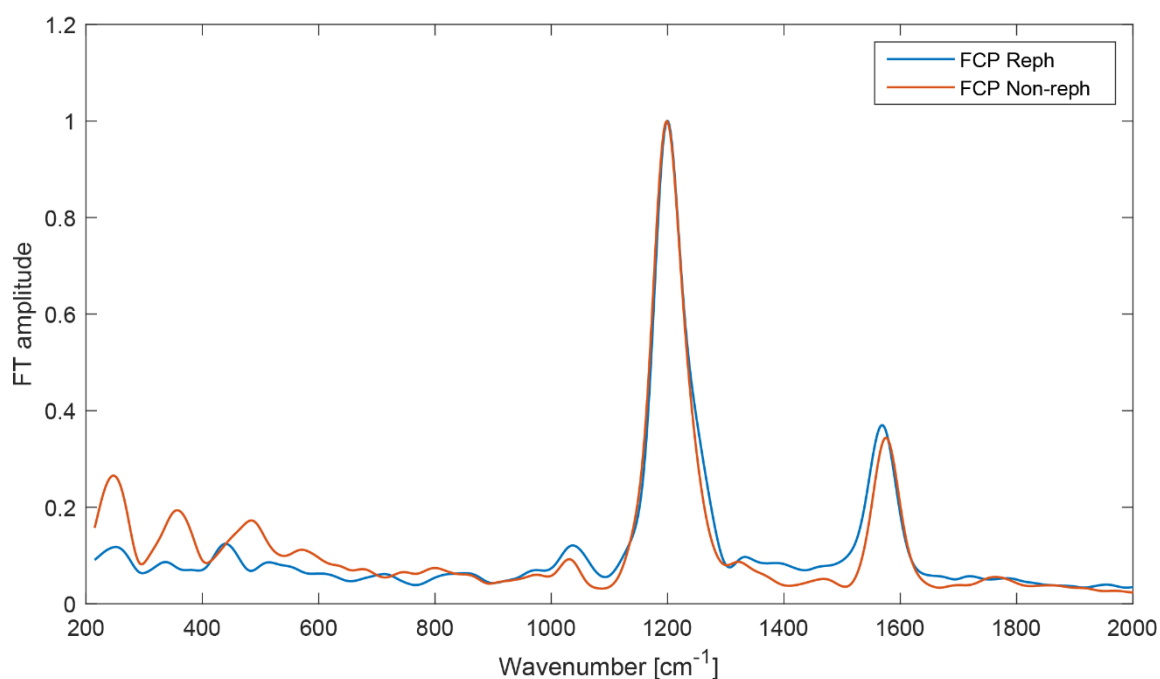

Figure 7.5 - Fourier spectrum analysis of the beatings in the t$_2$ evolution of the FCP dataset
(Reph = rephasing, Non-reph = non rephasing)

Another vibrational analysis makes use of Coherent decay Associated Spectra (CAS), where the amplitude of the beating components is reported in the whole 2D map, similarly to the DAS maps used for the fitting of the populations. Interestingly, the Fx vibrational frequencies do not affect only the ESA band explicitly attributed to dynamics within the Fx, but they strongly contribute in the whole map, including positions where the Chls' signals are typically identified (figure 7.6). These contributions are well defined and specific, nonetheless, a clear attribution has not been proposed yet. However, the finding that the vibrational oscillation of Fx is delocalized throughout the 2D map could imply that the nuclear degrees of freedom of Fx play a functional role in the redistribution of the energy between chromophores. This interpretation, although very suggestive, remains a hypothesis and further targeted experiments are needed to confirm it.
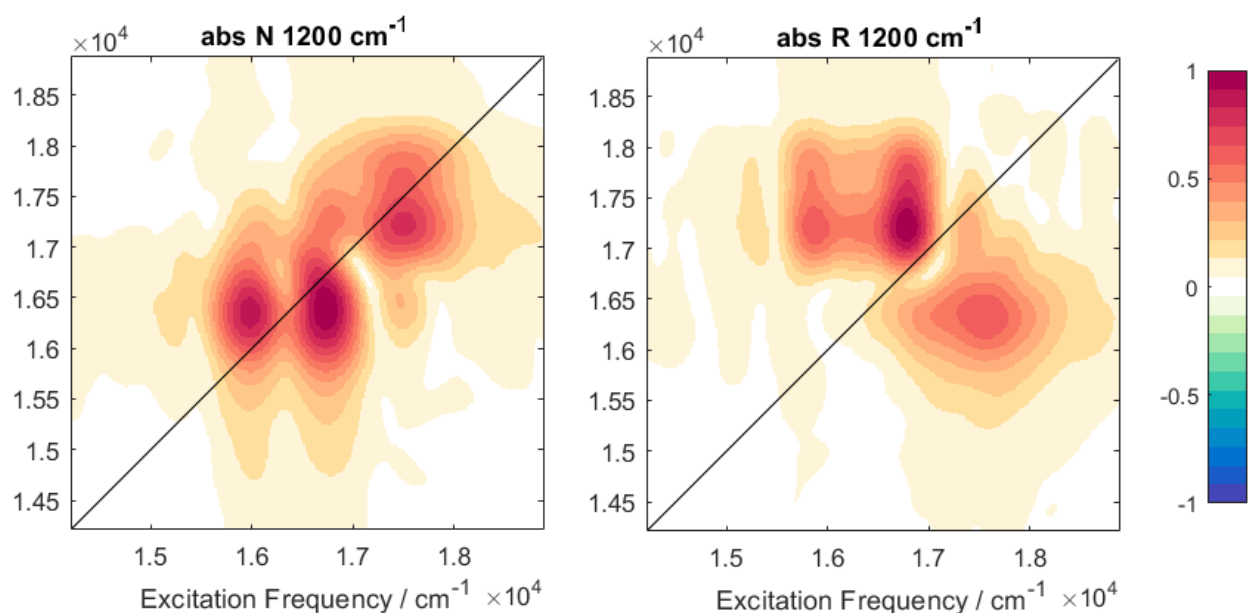
Figure 7.6 – CAS maps relative to the absolute of the vibrational mode with frequency of 1200 cm^{-1}.
Left: Non-rephasing dataset; right: Rephasing dataset.

7.6 Final Remarks

Thanks to these measurements, the ultrafast relaxation dynamics of Fx and Chl in the FCP extracted by *Cyclotella meneghiniana* has been characterized with the 2DES, one of the most solid and suitable techniques for the investigation of Light Harvesting Complexes. By following an approach different and complementary with respect to the 2DES studies on FCP already published by other groups,[20,21,106] I focused on a particular spectral window that permitted to specifically investigate the interaction between Chl *c* and Fx without the overwhelming contribution of the signal from the Q$_y$ band of Chl *a*.

Thanks to the 11 fs time resolution achieved with the 2DES experiment, I have been able to investigate the first hundreds of femtoseconds with improved time resolution. In particular, I shed light on a strong positive signal that I associated with the delocalization of excitation among the Chls and the Fx, and on another ultrafast feature related to the energy transfer between Chl *c* and Chl *a*. This latter feature was described in the models proposed in the literature as an energy transfer with a rate constant <50 fs. With a global fitting analysis, I can state that the rate constant of this dynamics is ~20 fs.

These findings help me to draw a better picture of the complex interactions that happen inside the protein complex. Energy-transfer features between Chl *c* and Fx have not been found, in agreement with the previous studies. However, I captured signs of delocalization among chromophores, suggesting the presence of interactions lasting only for the first femtoseconds and supporting the predictions based on

structural information. Another structural information that has been confirmed is the closeness between Fx and Chl *c*, because of the polar environment experienced by Fxs inside the FCP scaffold.

From a broader perspective, I believe that these new pieces of information and the consolidation of the already known spectroscopic features of FCP contribute to a better understanding of the complex ultrafast dynamics of these systems, still posing many open questions. While the recently published structural studies helped us clarify certain hypotheses, at the same time they raised new questions and opened perspectives, making even more appealing the study of these fascinating complexes.

Chapter 8

Conclusions

The aim of this Ph.D. project was to characterize the ultrafast relaxation dynamics of the Fucoxanthin Chlorophyll Protein with Two-Dimensional Electronic Spectroscopy, keeping a particular focus on the investigation of the spectroscopic features of the main carotenoid embedded in its protein scaffold: fucoxanthin. Although the measurements of FCP have been the culmination of my project, the common thread that accompanied me over these three years and gave structure to my project was the interest in the photophysics of fucoxanthin, indeed. The "carotenoid part" of light harvesting has always been particularly challenging to face because of the presence of dark states, their specific interactions with other electronic states, and the peculiar behavior of ketocarotenoids as regards charge transfer character and solvent polarity.

For these reasons, what started as a preliminary investigation on isolated fucoxanthin before the characterization of FCP, became a substantial and independent research topic. The characterization performed with the 2DES technique led to high-quality data with a time resolution that permitted the unraveling of subtle details in the ultrafast time regime. Many dynamical aspects were already characterized before, with other techniques and different resolutions; the 2DES characterization confirmed the kinetic constants regulating the $S_2 \rightarrow S_1$ internal conversion of Fx, with a higher and more robust level of detail. These rate constants also helped to find solvent-dependent trends. Moreover, and more interestingly, a new piece of evidence was found in the analysis of the traces of the ESA signals originating from the S_1 and the ICT state. In the first hundreds of femtoseconds, the dynamics of the two traces are different: the ESA from the S_1 state rises over time (with rate constants dependent on the polarity of the solvent); the ESA from the ICT state, instead, does not present any rising component, suggesting that the signal most likely come from an instant population of that state. This evidence is particularly relevant for the ongoing dispute about the nature of the ICT state itself, and it is pointing towards a distinction between the S_1 state and the ICT state, which can interact and interplay reciprocally, but in this framework, they are not strongly coupled. Consequently, I proposed for Fx a model similar to one previously proposed for peridinin. This model takes into account the various spectroscopic features collected and describes the ICT state as coupled to the S_2 state, separated by a solvent-dependent barrier of potential.

These findings helped to gain awareness of the ultrafast relaxation dynamics of Fx as an isolated pigment and provided a reference in the following characterization of FCP. The measurements on FCP were conducted following a different approach compared to other previous 2DES studies on the same protein. Thanks to the recent publication of the resolved structure of FCP, it was possible to specifically design the 2DES experiment to answer the new questions that arose with the knowledge of the structure and the relative arrangement of the pigments. Maintaining the focus on the Fx molecule, one of the questions that needed to be answered concerned the interaction that may exist between Fx and Chl c: the two molecules are spatially close, but no sign of interaction between the two was detected before. Aiming to contribute to this quest, the laser profile of the 2DES measurements was adjusted to capture the red tail of the Fx band and the Q_y and Q_x bands of Chl c.

Even though an energy transfer process between the two chromophores was not detected, the 2DES experiment was able to capture a strong positive signal at early delay times, associated with the delocalization of excitation among the chromophores. This signal suggests that the chromophores of FCP interact together, and this piece of information answers the original question motivating this experiment. Moreover, similarly to the analysis of the fucoxanthin samples, I confirmed already known features such as the Chl $c \rightarrow$ Chl a energy transfer, characterizing the associated dynamics with better resolution. From the structural point of view, I was able also to confirm spectroscopically the spatial closeness between a Fx molecule and Chl c through the analysis of the traces of the ESA signal originating from the ICT state. I found that the ESA–ICT is present also in FCP and its dynamics are similar to the ones of the isolate Fx in the polar solvent, suggesting that the environment experienced by fucoxanthin in FCP must be polar, and this is provided by the closeness to Chl c. This last significant deduction would not be possible without the preliminary work done on Fx.

Lastly, from a broader perspective, this Ph.D. project tried to answer difficult questions related to complex systems, whose photophysical properties are still a matter of debate. It was challenging but also exciting, with the thrill of being able to exploit one of the most up-to-date spectroscopic techniques. As the advent of the FCP structure teaches us, new answers lead to new questions. In no way has what I did during these three years put a full stop to the general characterization of fucoxanthin or even FCP; what I achieved deals more with the metaphor of finding new pieces for a puzzle that still needs to be completed. I hope that my work will help to get closer and closer to a full picture of these mysterious systems, which are so crucial for life on this planet and the management of solar energy.

Bibliography

(1)   Hybl, J. D.; Albrecht, A. W.; Gallagher Faeder, S. M.; Jonas, D. M. Two-Dimensional Electronic Spectroscopy. *Chem. Phys. Lett.* **1998**, *297* (3–4), 307–313. https://doi.org/10.1016/S0009-2614(98)01140-3.

(2)   Bránczyk, A. M.; Turner, D. B.; Scholes, G. D. Crossing Disciplines - A View on Two-Dimensional Optical Spectroscopy. *Ann. Phys.* **2014**, *526* (1–2), 31–49. https://doi.org/10.1002/andp.201300153.

(3)   Cho, M. *Coherent Multidimensional Spectroscopy*; Springer Singapore, 2019.

(4)   Collini, E. Spectroscopic Signatures of Quantum-Coherent Energy Transfer. *Chem. Soc. Rev.* **2013**, *42* (12), 4932–4947. https://doi.org/10.1039/c3cs35444j.

(5)   Croce, R.; van Amerongen, H. Natural Strategies for Photosynthetic Light Harvesting. *Nat. Chem. Biol.* **2014**, *10* (7), 492–501. https://doi.org/10.1038/nchembio.1555.

(6)   Meneghin, E.; Volpato, A.; Cupellini, L.; Bolzonello, L.; Jurinovich, S.; Mascoli, V.; Carbonera, D.; Mennucci, B.; Collini, E. Coherence in Carotenoid-to-Chlorophyll Energy Transfer. *Nat. Commun.* **2018**, *9* (1), 1–9. https://doi.org/10.1038/s41467-018-05596-5.

(7)   Ostroumov, E. E.; Mulvaney, R. M.; Cogdell, R. J.; Scholes, G. D. Broadband 2D Electronic Spectroscopy Reveals a Carotenoid Dark State in Purple Bacteria. *Science* **2013**, *340* (6128), 48–52. https://doi.org/10.1126/science.1229495.

(8)   Maiuri, M.; Réhault, J.; Carey, A. M.; Hacking, K.; Garavelli, M.; Lüer, L.; Polli, D.; Cogdell, R. J.; Cerullo, G. Ultra-Broadband 2D Electronic Spectroscopy of Carotenoid-Bacteriochlorophyll Interactions in the LH1 Complex of a Purple Bacterium. *J. Chem. Phys.* **2015**, *142* (212433), 1–10. https://doi.org/10.1063/1.4919056.

(9)   Toa, Z. S. D.; Degolian, M. H.; Jumper, C. C.; Hiller, R. G.; Scholes, G. D. Consistent Model of Ultrafast Energy Transfer in Peridinin Chlorophyll- A Protein Using Two-Dimensional Electronic Spectroscopy and Förster Theory. *J. Phys. Chem. B* **2019**, *1231*, 6410–6420. https://doi.org/10.1021/acs.jpcb.9b04324.

(10)   Schlau-Cohen, G. S.; Ishizaki, A.; Fleming, G. R. Two-Dimensional Electronic Spectroscopy and Photosynthesis: Fundamentals and Applications to Photosynthetic Light-Harvesting. *Chem. Phys.* **2011**, *386* (1–3), 1–22. https://doi.org/10.1016/j.chemphys.2011.04.025.

(11)   McDermott, G.; Prince, S. M.; Freer, A. A.; Hawthornthwaite-Lawless, A. M.; Papiz, M. Z.; Cogdell, R. J.; Isaacs, N. W. Crystal Structure of an Integral Membrane Light-Harvesting Complex from Photosynthetic Bacteria. *Nature* **1995**, *374* (6522), 517–521. https://doi.org/10.1038/374517a0.

(12)   Van Amerongen, H.; Van Grondelle, R. *Photosynthetic Excitons*; World Scientific, 2000.

(13)   Plenio, M. B.; Almeida, J.; Huelga, S. F. Origin of Long-Lived Oscillations in 2D-Spectra of a Quantum Vibronic Model: Electronic versus Vibrational Coherence. *J. Chem. Phys.* **2013**, *139* (235102), 1–10. https://doi.org/10.1063/1.4846275.

(14)   Engel, G. S.; Calhoun, T. R.; Read, E. L.; Ahn, T. K.; Mančal, T.; Cheng, Y. C.; Blankenship, R. E.; Fleming, G. R. Evidence for Wavelike Energy Transfer through Quantum Coherence in Photosynthetic Systems. *Nature* **2007**, *446* (7137), 782–786. https://doi.org/10.1038/nature05678.

(15)   Scholes, G. D. Quantum-Coherent Electronic Energy Transfer: Did Nature Think of It First? *J. Phys. Chem. Lett.* **2010**, *1* (1), 2–8. https://doi.org/10.1021/jz900062f.

(16)   Collini, E.; Wong, C. Y.; Wilk, K. E.; Curmi, P. M. G.; Brumer, P.; Scholes, G. D. Coherently Wired Light-Harvesting in Photosynthetic Marine Algae at Ambient Temperature. *Nature* **2010**, *463* (7281), 644–647. https://doi.org/10.1038/nature08811.

(17)   Field, C. B.; Behrenfeld, M. J.; Randerson, J. T.; Falkowski, P. Primary Production of the Biosphere: Integrating Terrestrial and Oceanic Components. *Science* **1998**, *281* (5374), 237–240. https://doi.org/10.1126/science.281.5374.237.

(18)   Falkowski, P. G.; Barber, R. T.; Smetacek, V. Biogeochemical Controls and Feedbacks on Ocean Primary Production. *Science* **1998**, *281* (5374), 200–206. https://doi.org/10.1126/science.281.5374.200.

(19)   Mirkovic, T.; Ostroumov, E. E.; Anna, J. M.; Van Grondelle, R.; Govindjee; Scholes, G. D. Light Absorption and Energy Transfer in the Antenna Complexes of Photosynthetic Organisms. *Chem. Rev.* **2017**, *117* (2), 249–293. https://doi.org/10.1021/acs.chemrev.6b00002.

(20)   Songaila, E.; Augulis, R.; Gelzinis, A.; Butkus, V.; Gall, A.; Büchel, C.; Robert, B.; Zigmantas, D.; Abramavicius, D.; Valkunas, L. Ultrafast Energy Transfer from Chlorophyll c_2 to Chlorophyll a in Fucoxanthin-Chlorophyll Protein Complex. *J. Phys. Chem. Lett.* **2013**, *4* (21), 3590–3595. https://doi.org/10.1021/jz401919k.

(21)   Gelzinis, A.; Butkus, V.; Songaila, E.; Augulis, R.; Gall, A.; Büchel, C.; Robert, B.; Abramavicius, D.; Zigmantas, D.; Valkunas, L. Mapping Energy Transfer Channels in Fucoxanthin-Chlorophyll Protein Complex. *Biochim. Biophys. Acta - Bioenerg.* **2015**, *1847* (2), 241–247. https://doi.org/10.1016/j.bbabio.2014.11.004.

(22)   Meneghin, E.; Leonardo, C.; Volpato, A.; Bolzonello, L.; Collini, E. Mechanistic Insight into Internal Conversion Process within Q-Bands of Chlorophyll A. *Sci. Rep.* **2017**, 7 (1), 1–7. https://doi.org/10.1038/s41598-017-11621-2.

(23)   Polívka, T.; Sundström, V. Ultrafast Dynamics of Carotenoid Excited States-from Solution to Natural and Artificial Systems. *Chem. Rev.* **2004**, *104* (4), 2021–2071. https://doi.org/10.1021/cr020674n.

(24)   Polívka, T.; Sundström, V. Dark Excited States of Carotenoids: Consensus and Controversy. *Chem. Phys. Lett.* **2009**, *477* (1–3), 1–11. https://doi.org/10.1016/j.cplett.2009.06.011.

(25)   Mukamel, S. Principles of Nonlinear Optical Spectroscopy. Oxford 1996, p 549.

(26)   Tokmakoff, A. *Time-Dependent Quantum Mechanics and Spectroscopy*; 2014.

(27)   Yee, T. K.; Gustafson, T. K. Diagrammatic Analysis of the Density Operator for Nonlinear Optical Calculations: Pulsed and Cw Responses. *Phys. Rev. A* **1978**, *18* (4), 1597–1617.

(28)   Aihara, M. Transient Polarization Characteristics Associated with Resonant Light Scattering by a Degenerate Two-Level System. *Phys. Rev. A* **1978**, *18* (2), 606–616. https://doi.org/10.1103/PhysRevA.18.606.

(29)   Collini, E. Spectroscopic Signatures of Quantum-Coherent Energy Transfer. *Chem. Soc. Rev.* **2013**, *42* (12), 4932–4947. https://doi.org/10.1039/c3cs35444j.

(30)   Scholes, G. D. Long-Range Resonance Energy Transfer in Molecular Systems. *Annu. Rev. Phys. Chem.* **2003**, *54* (18), 57–87. https://doi.org/10.1146/annurev.physchem.54.011002.103746.

(31)   Gelzinis, A.; Augulis, R.; Butkus, V.; Robert, B.; Valkunas, L. Two-Dimensional Spectroscopy

for Non-Specialists. *Biochim. Biophys. Acta - Bioenerg.* **2019**, *1860* (4), 271–285. https://doi.org/10.1016/j.bbabio.2018.12.006.

(32)   Rimai, L.; Heyde, M. E.; Gill, D. Vibrational Spectra of Some Carotenoids and Related Linear Polyenes. A Raman Spectroscopic Study. *J. Am. Chem. Soc.* **1973**, *95* (14), 4493–4501.

(33)   Prokhorenko, V. I.; Halpin, A.; Miller, R. J. D. Coherently-Controlled Two-Dimensional Photon Echo Electronic Spectroscopy. *Opt. Express* **2009**, *17* (12), 9764. https://doi.org/10.1364/oe.17.009764.

(34)   Bolzonello, L.; Volpato, A.; Meneghin, E.; Collini, E. Versatile Setup for High-Quality Rephasing, Non-Rephasing, and Double Quantum 2D Electronic Spectroscopy. *J. Opt. Soc. Am. B* **2017**, *34* (6), 1223–1233. https://doi.org/10.1364/josab.34.001223.

(35)   Nemeth, A.; Milota, F.; Mančal, T.; Pullerits, T.; Sperling, J.; Hauer, J.; Kauffmann, H. F.; Christensson, N. Double-Quantum Two-Dimensional Electronic Spectroscopy of a Three-Level System: Experiments and Simulations. *J. Chem. Phys.* **2010**, *133* (94505), 1–15. https://doi.org/10.1063/1.3474995.

(36)   De Camargo, F. V. A.; Grimmelsmann, L.; Anderson, H. L.; Meech, S. R.; Heisler, I. A. Resolving Vibrational from Electronic Coherences in Two-Dimensional Electronic Spectroscopy: The Role of the Laser Spectrum. *Phys. Rev. Lett.* **2017**, *118* (3), 1–6. https://doi.org/10.1103/PhysRevLett.118.033001.

(37)   Collini, E. 2D Electronic Spectroscopic Techniques for Quantum Technology Applications. *J. Phys. Chem. C* **2021**, *125* (24), 13096–13108. https://doi.org/10.1021/acs.jpcc.1c02693.

(38)   Volpato, A.; Bolzonello, L.; Meneghin, E.; Collini, E. Global Analysis of Coherence and Population Dynamics in 2D Electronic Spectroscopy. *Opt. Express* **2016**, *24* (21), 24773–24785. https://doi.org/10.1364/oe.24.024773.

(39)   Volpato, A. Innovative Strategies in Coherent Multidimensional Electronic Spectroscopy, Ph.D. Thesis, Department of Chemical Sciences, University of Padua, **2017**.

(40)   Meneghin, E.; Pedron, D.; Collini, E. Raman and 2D Electronic Spectroscopies: A Fruitful Alliance for the Investigation of Ground and Excited State Vibrations in Chlorophyll A. *Chem. Phys.* **2018**, *514*, 132–140. https://doi.org/10.1016/j.chemphys.2018.03.003.

(41) Turner, D. B.; Dinshaw, R.; Lee, K. K.; Belsley, M. S.; Wilk, K. E.; Curmi, P. M. G.; Scholes, G. D. Quantitative Investigations of Quantum Coherence for a Light-Harvesting Protein at Conditions Simulating Photosynthesis. *Phys. Chem. Chem. Phys.* **2012**, *14* (14), 4857–4874. https://doi.org/10.1039/c2cp23670b.

(42) Calhoun, T. R.; Ginsberg, N. S.; Schlau-Cohen, G. S.; Cheng, Y. C.; Ballottari, M.; Bassi, R.; Fleming, G. R. Quantum Coherence Enabled Determination of the Energy Landscape in Light-Harvesting Complex II. *J. Phys. Chem. B* **2009**, *113* (51), 16291–16295. https://doi.org/10.1021/jp908300c.

(43) Christensson, N.; Žídek, K.; Magdaong, N. C. M.; Lafountain, A. M.; Frank, H. A.; Zigmantas, D. Origin of the Bathochromic Shift of Astaxanthin in Lobster Protein: 2D Electronic Spectroscopy Investigation of β-Crustacyanin. *J. Phys. Chem. B* **2013**, *117* (38), 11209–11219. https://doi.org/10.1021/jp401873k.

(44) Volpato, A.; Collini, E. Optimization and Selection of Time-Frequency Transforms for Wave-Packet Analysis in Ultrafast Spectroscopy. *Opt. Express* **2019**, *27* (3), 2975. https://doi.org/10.1364/oe.27.002975.

(45) Cohen, L. *Time-Frequency Analysis*; Prentice-Hall: New Jersey, 1995.

(46) Britton, G.; Liaaen-Jensen, S.; Pfander, H. *Carotenoids*; Birkhäuser Verlag: Basel, 1995.

(47) Polli, D.; Cerullo, G.; Lanzani, G.; De Silvestri, S.; Yanagi, K.; Hashimoto, H.; Cogdell, R. J. Conjugation Length Dependence of Internal Conversion in Carotenoids: Role of the Intermediate State. *Phys. Rev. Lett.* **2004**, *93* (16), 1–4. https://doi.org/10.1103/PhysRevLett.93.163002.

(48) Schulten, K.; Karplus, M. On the Origin of a Low-Lying Forbidden Transition in Polyenes and Related Molecules. *Chem. Phys. Lett.* **1972**, *14* (3), 305–309. https://doi.org/10.1016/0009-2614(72)80120-9.

(49) Hudson, B. S.; Kohler, B. E. A Low-Lying Weak Transition in the Polyene α,ω-Diphenyloctatetraene. *Chem. Phys. Lett.* **1972**, *14* (3), 299–304. https://doi.org/10.1016/0009-2614(72)80119-2.

(50) Polívka, T.; Herek, J. L.; Zigmantas, D.; Åkerlund, H.-E.; Sundström, V. *Direct Observation of the*

(Forbidden) S 1 State in Carotenoids; 1999; Vol. 96.

(51)   Walla, P. J.; Linden, P. A.; Hsu, C. P.; Scholes, G. D.; Fleming, G. R. Femtosecond Dynamics of the Forbidden Carotenoid S1 State in Light-Harvesting Complexes of Purple Bacteria Observed after Two-Photon Excitation. *Proc. Natl. Acad. Sci. U. S. A.* **2000**, *97* (20), 10808–10813. https://doi.org/10.1073/pnas.190230097.

(52)   Kosumi, D.; Abe, K.; Karasawa, H.; Fujiwara, M.; Cogdell, R. J.; Hashimoto, H.; Yoshizawa, M. Ultrafast Relaxation Kinetics of the Dark S1 State in All-Trans-β-Carotene Explored by One- and Two-Photon Pump-Probe Spectroscopy. *Chem. Phys.* **2010**, *373* (1–2), 33–37. https://doi.org/10.1016/j.chemphys.2009.12.013.

(53)   Greco, J. A.; LaFountain, A. M.; Kinashi, N.; Shinada, T.; Sakaguchi, K.; Katsumura, S.; Magdaong, N. C. M.; Niedzwiedzki, D. M.; Birge, R. R.; Frank, H. A. Spectroscopic Investigation of the Carotenoid Deoxyperidinin: Direct Observation of the Forbidden $S_0 \rightarrow S_1$ Transition. *J. Phys. Chem. B* **2016**, *120* (10), 2731–2744. https://doi.org/10.1021/acs.jpcb.6b00439.

(54)   Fiedor, L.; Heriyanto; Fiedor, J.; Pilch, M. Effects of Molecular Symmetry on the Electronic Transitions in Carotenoids. *J. Phys. Chem. Lett.* **2016**, 7 (10), 1821–1829. https://doi.org/10.1021/acs.jpclett.6b00637.

(55)   Craft, N. E.; Soares, J. H. Relative Solubility, Stability, and Absorptivity of Lutein and β-Carotene in Organic Solvents. *J. Agric. Food Chem.* **1992**, *40* (3), 431-434.

(56)   Frank, H. a; Desamero, R. Z. B.; Chynwat, V.; Gebhard, R.; Hoef, I. Van Der; Jansen, F. J.; Lugtenburg, J.; Gosztola, D.; Wasielewski, M. R. Spectroscopic Properties of Spheroidene Analogs Having Different Extents of π-Electron Conjugation. *J. Phys. Chem. A* **1997**, *101* (2), 149–157.

(57)   Zigmantas, D.; Hiller, R. G.; Yartsev, A.; Sundström, V.; Polívka, T. Dynamics of Excited States of the Carotenoid Peridinin in Polar Solvents: Dependence on Excitation Wavelength, Viscosity, and Temperature. *J. Phys. Chem. B* **2003**, *107* (22), 5339–5348. https://doi.org/10.1021/jp0272318.

(58)   Christensen, R. L.; Goyette, M.; Gallagher, L.; Duncan, J.; DeCoster, B. S_1 and S_2 States of Apo- and Diapocarotenes. *J. Phys. Chem. A* **1999**, *103* (14), 2399–2407.

https://doi.org/10.1021/jp983946s.

(59)   Ricci, M.; Bradforth, S. E.; Jimenez, R.; Fleming, G. R. Internal Conversion and Energy Transfer Dynamics of Spheroidene in Solution and in the LH-1 and LH-2 Light-Harvesting Complexes. *Chem. Phys. Lett.* **1996**, *259* (3–4), 381–390. https://doi.org/10.1016/0009-2614(96)00832-9.

(60)   Macpherson, A. N.; Gillbro, T. Solvent Dependence of the Ultrafast S_2-S_1 Internal Conversion Rate of β-Carotene. *J. Phys. Chem. A* **1998**, *102* (26), 5049–5058. https://doi.org/https://doi.org/10.1021/jp980979z.

(61)   Akimoto, S.; Yamazaki, I.; Sakawa, T.; Mimuro, M. Temperature Effects on Excitation Relaxation Dynamics of the Carotenoid β-Carotene and Its Analogue β-Apo-8′-Carotenal, Probed by Femtosecond Fluorescence Spectroscopy. *J. Phys. Chem. A* **2002**, *106* (10), 2237–2243. https://doi.org/10.1021/jp0125653.

(62)   Kosumi, D.; Kusumoto, T.; Fujii, R.; Sugisaki, M.; Iinuma, Y.; Oka, N.; Takaesu, Y.; Taira, T.; Iha, M.; Frank, H. A.; Hashimoto, H. One- and Two-Photon Pump-Probe Optical Spectroscopic Measurements Reveal the S1 and Intramolecular Charge Transfer States Are Distinct in Fucoxanthin. *Chem. Phys. Lett.* **2009**, *483* (1–3), 95–100. https://doi.org/10.1016/j.cplett.2009.10.077.

(63)   Zhang, J.-P.; Skibsted, L. H.; Fujii, R.; Koyama, Y. Transient Absorption from the 1Bu+ State of All-Trans-β-Carotene Newly Identified in the Near-Infrared Region. *Photochem. Photobiol.* **2001**, *73* (3), 219. https://doi.org/10.1562/0031-8655(2001)073<0219:taftus>2.0.co;2.

(64)   Andersson, P. O.; Bachilo, S. M.; Chen, R. L.; Gillbro, T. Solvent and Temperature Effects on Dual Fluorescence in a Series of Carotenes. Energy Gap Dependence of the Internal Conversion Rate. *J. Phys. Chem.* **1995**, *99* (44), 16199–16209. https://doi.org/10.1021/j100044a002.

(65)   Polívka, T.; Zigmantas, D.; Frank, H. A.; Bautista, J. A.; Herek, J. L.; Koyama, Y.; Fujii, R.; Sundström, V. Near-Infrared Time-Resolved Study of the S_1 State Dynamics of the Carotenoid Spheroidene. *J. Phys. Chem. B* **2001**, *105* (5), 1072–1080. https://doi.org/10.1021/jp002206s.

(66)   Frank, H. A.; Bautista, J. A.; Josue, J.; Pendon, Z.; Hiller, R. G.; Sharples, F. P.; Gosztola, D.; Wasielewski, M. R. Effect of the Solvent Environment on the Spectroscopic Properties and Dynamics of the Lowest Excited States of Carotenoids. *J. Phys. Chem. B* **2000**, *104* (18), 4569–4577. https://doi.org/10.1021/jp000079u.

(67)   Bautista, J. A.; Connors, R. E.; Raju, B. B.; Hiller, R. G.; Sharples, F. P.; Gosztola, D.; Wasielewski, M. R.; Frank, H. A. Excited State Properties of Peridinin: Observation of a Solvent Dependence of the Lowest Excited Singlet State Lifetime and Spectral Behavior Unique among Carotenoids. *J. Phys. Chem. B* **1999**, *103* (41), 8751–8758. https://doi.org/10.1021/jp9916135.

(68)   Premvardhan, L.; Papagiannakis, E.; Hiller, R. G.; Van Grondelle, R. The Charge-Transfer Character of the $S_0 \rightarrow S_2$ Transition in the Carotenoid Peridinin Is Revealed by Stark Spectroscopy. *J. Phys. Chem. B* **2005**, *109* (32), 15589–15597. https://doi.org/10.1021/jp052027g.

(69)   Bovi, D.; Mezzetti, A.; Vuilleumier, R.; Gaigeot, M. P.; Chazallon, B.; Spezia, R.; Guidoni, L. Environmental Effects on Vibrational Properties of Carotenoids: Experiments and Calculations on Peridinin. *Phys. Chem. Chem. Phys.* **2011**, *13* (47), 20954–20964. https://doi.org/10.1039/c1cp21985e.

(70)   Kusumoto, T.; Horibe, T.; Kajikawa, T.; Hasegawa, S.; Iwashita, T.; Cogdell, R. J.; Birge, R. R.; Frank, H. A.; Katsumura, S.; Hashimoto, H. Stark Absorption Spectroscopy of Peridinin and Allene-Modified Analogues. *Chem. Phys.* **2010**, *373* (1–2), 71–79. https://doi.org/10.1016/j.chemphys.2010.01.018.

(71)   Wagner, N. L.; Greco, J. A.; Enriquez, M. M.; Frank, H. A.; Birge, R. R. The Nature of the Intramolecular Charge Transfer State in Peridinin. *Biophys. J.* **2013**, *104* (6), 1314–1325. https://doi.org/10.1016/j.bpj.2013.01.045.

(72)   Zigmantas, D.; Hiller, R. G.; Sharples, F. P.; Frank, H. A.; Sundström, V.; Polívka, T. Effect of a Conjugated Carbonyl Group on the Photophysical Properties of Carotenoids. *Phys. Chem. Chem. Phys.* **2004**, *6* (11), 3009–3016. https://doi.org/10.1039/b315786e.

(73)   Premvardhan, L.; Sandberg, D. J.; Fey, H.; Birge, R. R.; Büchel, C.; Van Grondelle, R. The Charge-Transfer Properties of the S_2 State of Fucoxanthin in Solution and in Fucoxanthin Chlorophyll-a/c_2 Protein (FCP) Based on Stark Spectroscopy and Molecular-Orbital Theory. *J. Phys. Chem. B* **2008**, *112* (37), 11838–11853. https://doi.org/10.1021/jp802689p.

(74)   Shima, S.; Ilagan, R. P.; Gillespie, N.; Sommer, B. J.; Hiller, R. G.; Sharples, F. P.; Frank, H. A.; Birge, R. R. Two-Photon and Fluorescence Spectroscopy and the Effect of Environment on the Photochemical Properties of Peridinin in Solution and in the Peridinin-Chlorophyll-Protein from Amphidinium Carterae. *J. Phys. Chem. A* **2003**, *107* (40), 8052–8066.

https://doi.org/10.1021/jp022648z.

(75)   Kosumi, D.; Kusumoto, T.; Fujii, R.; Sugisaki, M.; Iinuma, Y.; Oka, N.; Takaesu, Y.; Taira, T.; Iha, M.; Frank, H. A.; Hashimoto, H. Ultrafast Excited State Dynamics of Fucoxanthin: Excitation Energy Dependent Intramolecular Charge Transfer Dynamics. *Phys. Chem. Chem. Phys.* **2011**, *13* (22), 10762–10770. https://doi.org/10.1039/c0cp02568b.

(76)   Rechthaler, K.; Köhler, G. Excited State Properties and Deactivation Pathways of 7-Aminocoumarins. *Chem. Phys.* **1994**, *189* (1), 99–116. https://doi.org/10.1016/0301-0104(94)80010-3.

(77)   Okada, T.; Malaga, N.; Baumann, W.; Siemiarczuk, A. Picosecond Laser Spectroscopy of 4-(9-Anthryl)-*N,N*-Dlmethylaniline and Related Compounds. *J. Phys. Chem* **1987**, *91* (17), 4490-4495.

(78)   Christensson, N.; Milota, F.; Nemeth, A.; Pugliesi, I.; Riedle, E.; Sperling, J.; Pullerits, T.; Kauffmann, H. F.; Hauer, J. Electronic Double-Quantum Coherences and Their Impact on Ultrafast Spectroscopy: The Example of β-Carotene. *J. Phys. Chem. Lett.* **2010**, *1* (23), 3366–3370. https://doi.org/10.1021/jz101409r.

(79)   Christensson, N.; Milota, F.; Nemeth, A.; Sperling, J.; Kauffmann, H. F.; Pullerits, T.; Hauer, J. Two-Dimensional Electronic Spectroscopy of β-Carotene. *J. Phys. Chem. B* **2009**, *113* (51), 16409–16419. https://doi.org/10.1021/jp906604j.

(80)   Christensson, N.; Polívka, T.; Yartsev, A.; Pullerits, T. Photon Echo Spectroscopy Reveals Structure-Dynamics Relationships in Carotenoids. *Phys. Rev. B - Condens. Matter Mater. Phys.* **2009**, *79* (245118), 1–14. https://doi.org/10.1103/PhysRevB.79.245118.

(81)   Tanaka, R.; Tanaka, A. Chlorophyll Cycle Regulates the Construction and Destruction of the Light-Harvesting Complexes. *Biochim. Biophys. Acta - Bioenerg.* **2011**, *1807* (8), 968–976. https://doi.org/10.1016/j.bbabio.2011.01.002.

(82)   Zapata, M.; Garrido, J. L.; Jeffrey, S. W. Chlorophyll *c* Pigments: Current Status. In *Chlorophylls and Bacteriochlorophylls*; 2007; pp 39–53. https://doi.org/10.1007/1-4020-4516-6_3.

(83)   Qiu, N. W.; Jiang, D. C.; Wang, X. S.; Wang, B. S.; Zhou, F. Advances in the Members and Biosynthesis of Chlorophyll Family. *Photosynthetica* **2019**, *57* (4), 974–984.

https://doi.org/10.32615/ps.2019.116.

(84)   Scheer, H. *Structure and Occurence of Chlorophylls*; 1991.

(85)   Gouterman, M.; Wagnière, G. H.; Snyder, L. C. Spectra of Porphyrins. Part II. Four Orbital Model. *J. Mol. Spectrosc.* **1963**, *11* (1–6), 108–127. https://doi.org/10.1016/0022-2852(63)90011-0.

(86)   Ceulemans, A.; Oldenhof, W.; Görller-Walrand, C.; Vanquickenborne, L. G. Gouterman,'s "Four-Orbital" Model and the MCD Spectra of High-Symmetry Metalloporphyrins. *J. Am. Chem. Soc.* **1986**, *108* (6), 1155–1163. https://doi.org/10.1021/ja00266a007.

(87)   Reimers, J. R.; Cai, Z. L.; Kobayashi, R.; Rätsep, M.; Freiberg, A.; Krausz, E. Assignment of the Q-Bands of the Chlorophylls: Coherence Loss via Q_x-Q_y Mixing. *Sci. Rep.* **2013**, *3* (2761), 1–8. https://doi.org/10.1038/srep02761.

(88)   Collini, E.; Curutchet, C.; Mirkovic, T.; Scholes, G. D. *Electronic Energy Transfer in Photosynthetic Antenna Systems*; 2009; Vol. 93. https://doi.org/10.1007/978-3-642-02306-4.

(89)   Pascal, A. A.; Liu, Z.; Broess, K.; Van Oort, B.; Van Amerongen, H.; Wang, C.; Horton, P.; Robert, B.; Chang, W.; Ruban, A. Molecular Basis of Photoprotection and Control of Photosynthetic Light-Harvesting. *Nature* **2005**, *436* (7047), 134–137. https://doi.org/10.1038/nature03795.

(90)   Ruban, A. V.; Berera, R.; Ilioaia, C.; Van Stokkum, I. H. M.; Kennis, J. T. M.; Pascal, A. A.; Van Amerongen, H.; Robert, B.; Horton, P.; Van Grondelle, R. Identification of a Mechanism of Photoprotective Energy Dissipation in Higher Plants. *Nature* **2007**, *450* (7169), 575–578. https://doi.org/10.1038/nature06262.

(91)   Cazzaniga, S.; Bressan, M.; Carbonera, D.; Agostini, A.; Dall'osto, L. Differential Roles of Carotenes and Xanthophylls in Photosystem I Photoprotection. *Biochemistry* **2016**, *55* (26), 3636–3649. https://doi.org/10.1021/acs.biochem.6b00425.

(92)   Jahns, P.; Holzwarth, A. R. The Role of the Xanthophyll Cycle and of Lutein in Photoprotection of Photosystem II. *Biochim. Biophys. Acta* **2012**, *1817* (1), 182–193. https://doi.org/10.1016/j.bbabio.2011.04.012.

(93)   Santabarbara, S.; Horton, P.; Ruban, A. V. Comparison of the Thermodynamic Landscapes of Unfolding and Formation of the Energy Dissipative State in the Isolated Light Harvesting

Complex II. *Biophys. J.* **2009**, *97* (4), 1188–1197. https://doi.org/10.1016/j.bpj.2009.06.005.

(94)   Förster, T. Energiewanderung Und Fluoreszenz. *Naturwissenschaften* **1946**, *33*, 166–175.

(95)   Davydov, A. S. The Theory of Molecular Excitons. *Uspekhi Fiz. Nauk* **1964**, *82* (3), 393–448.
https://doi.org/10.3367/ufnr.0082.196403a.0393.

(96)   Scholes, G. D.; Fleming, G. R.; Olaya-Castro, A.; Van Grondelle, R. Lessons from Nature about
Solar Light Harvesting. *Nat. Chem.* **2011**, *3* (10), 763–774. https://doi.org/10.1038/nchem.1145.

(97)   Lavaud, J. Fast Regulation of Photosynthesis in Diatoms : Mechanisms , Evolution and
Ecophysiology. *Functional Plant Science and Biotechnology*, **2007**, *1*, 267-287.

(98)   Papagiannakis, E.; Van Stokkum, I. H. M.; Fey, H.; Büchel, C.; Van Grondelle, R. Spectroscopic
Characterization of the Excitation Energy Transfer in the Fucoxanthin-Chlorophyll Protein of
Diatoms. *Photosynth. Res.* **2005**, *86*, 241–250. https://doi.org/https://doi.org/10.1007/s11120-005-
1003-8.

(99)   Premvardhan, L.; Robert, B.; Beer, A.; Büchel, C. Pigment Organization in Fucoxanthin
Chlorophyll a/c$_2$ Proteins (FCP) Based on Resonance Raman Spectroscopy and Sequence
Analysis. *Biochim. Biophys. Acta - Bioenerg.* **2010**, *1797* (9), 1647–1656.
https://doi.org/10.1016/j.bbabio.2010.05.002.

(100)   Kuczynska, P.; Jemiola-Rzeminska, M.; Strzalka, K. Photosynthetic Pigments in Diatoms. *Mar.
Drugs* **2015**, *13* (9), 5847–5881. https://doi.org/10.3390/md13095847.

(101)   Ramanan, C.; Berera, R.; Gundermann, K.; Van Stokkum, I.; Büchel, C.; Van Grondelle, R.
Exploring the Mechanism(s) of Energy Dissipation in the Light Harvesting Complex of the
Photosynthetic Algae Cyclotella Meneghiniana. *Biochim. Biophys. Acta - Bioenerg.* **2014**, *1837* (9),
1507–1513. https://doi.org/10.1016/j.bbabio.2014.02.016.

(102)   Gildenhoff, N.; Amarie, S.; Gundermann, K.; Beer, A.; Büchel, C.; Wachtveitl, J.
Oligomerization and Pigmentation Dependent Excitation Energy Transfer in Fucoxanthin-
Chlorophyll Proteins. *Biochim. Biophys. Acta - Bioenerg.* **2010**, *1797* (5), 543–549.
https://doi.org/10.1016/j.bbabio.2010.01.024.

(103)   West, R. G.; Bína, D.; Fuciman, M.; Kuznetsova, V.; Litvín, R.; Polívka, T. Ultrafast Multi-Pulse
Transient Absorption Spectroscopy of Fucoxanthin Chlorophyll a Protein from Phaeodactylum

Tricornutum. *Biochim. Biophys. Acta - Bioenerg.* **2018**, *1859* (5), 357–365. https://doi.org/10.1016/j.bbabio.2018.02.011.

(104) Marcolin, G.; Collini, E. Solvent-Dependent Characterization of Fucoxanthin through 2D Electronic Spectroscopy Reveals New Details on the Intramolecular Charge-Transfer State Dynamics. *J. Phys. Chem. Lett.* **2021**, *12* (20), 4833–4840. https://doi.org/10.1021/acs.jpclett.1c00851.

(105) Akimoto, S.; Teshigahara, A.; Yokono, M.; Mimuro, M.; Nagao, R.; Tomo, T. Excitation Relaxation Dynamics and Energy Transfer in Fucoxanthin- Chlorophyll a/c-Protein Complexes, Probed by Time-Resolved Fluorescence. *Biochim. Biophys. Acta - Bioenerg.* **2014**, *1837* (9), 1514–1521. https://doi.org/10.1016/j.bbabio.2014.02.002.

(106) Butkus, V.; Gelzinis, A.; Augulis, R.; Gall, A.; Büchel, C.; Robert, B.; Zigmantas, D.; Valkunas, L.; Abramavicius, D. Coherence and Population Dynamics of Chlorophyll Excitations in FCP Complex: Two-Dimensional Spectroscopy Study. *J. Chem. Phys.* **2015**, *142* (212414), 1–9. https://doi.org/10.1063/1.4914098.

(107) Gelzinis, A.; Augulis, R.; Büchel, C.; Robert, B.; Valkunas, L. Confronting FCP Structure with Ultrafast Spectroscopy Data: Evidence for Structural Variations. *Phys. Chem. Chem. Phys.* **2021**, *23* (2), 806–821. https://doi.org/10.1039/d0cp05578f.

(108) Wang, W.; Yu, L. J.; Xu, C.; Tomizaki, T.; Zhao, S.; Umena, Y.; Chen, X.; Qin, X.; Xin, Y.; Suga, M.; Han, G.; Kuang, T.; Shen, J. R. Structural Basis for Blue-Green Light Harvesting and Energy Dissipation in Diatoms. *Science* **2019**, *363* (6427), 1–8. https://doi.org/10.1126/science.aav0365.

(109) Pi, X.; Zhao, S.; Wang, W.; Liu, D.; Xu, C.; Han, G.; Kuang, T.; Sui, S. F.; Shen, J. R. The Pigment-Protein Network of a Diatom Photosystem II–Light-Harvesting Antenna Supercomplex. *Science* **2019**, *365* (6452), 1–10. https://doi.org/10.1126/science.aax4406.

(110) Nagao, R.; Kato, K.; Suzuki, T.; Ifuku, K.; Uchiyama, I.; Kashino, Y.; Dohmae, N.; Akimoto, S.; Shen, J. R.; Miyazaki, N.; Akita, F. Structural Basis for Energy Harvesting and Dissipation in a Diatom PSII–FCPII Supercomplex. *Nat. Plants* **2019**, *5* (8), 890–901. https://doi.org/10.1038/s41477-019-0477-x.

(111) Kosumi, D.; Kusumoto, T.; Fujii, R.; Sugisaki, M.; Iinuma, Y.; Oka, N.; Takaesu, Y.; Taira, T.;

Iha, M.; Frank, H. A.; Hashimoto, H. Ultrafast S1 and ICT State Dynamics of a Marine Carotenoid Probed by Femtosecond One- and Two-Photon Pump–Probe Spectroscopy. *J. Lumin.* **2011**, *131* (3), 515–518. https://doi.org/10.1016/j.jlumin.2010.09.018.

(112)   Kosumi, D.; Fujii, R.; Sugisaki, M.; Oka, N.; Iha, M.; Hashimoto, H. Characterization of the Intramolecular Transfer State of Marine Carotenoid Fucoxanthin by Femtosecond Pump–Probe Spectroscopy. *Photosynth. Res.* **2014**, *121* (1), 61–68. https://doi.org/10.1007/s11120-014-9995-6.

(113)   Kosumi, D.; Kajikawa, T.; Yano, K.; Okumura, S.; Sugisaki, M.; Sakaguchi, K.; Katsumura, S.; Hashimoto, H. Roles of Allene-Group in an Intramolecular Charge Transfer Character of a Short Fucoxanthin Homolog as Revealed by Femtosecond Pump–Probe Spectroscopy. *Chem. Phys. Lett.* **2014**, *602* (2014), 75–79. https://doi.org/10.1016/j.cplett.2014.04.022.

(114)   Merlin, J. C. Resonance Raman Spectroscopy of Carotenoids and Carotenoid-Containing Systems. *Pure Appl. Chem* **1985**, *57* (5), 785–792.

(115)   Zimmermann, J.; Linden, P. A.; Vaswani, H. M.; Hiller, R. G.; Fleming, G. R. Two-Photon Excitation Study of Peridinin in Benzene and in the Peridinin Chlorophyll a-Protein (PCP). *J. Phys. Chem. B* **2002**, *106* (36), 9418–9423. https://doi.org/10.1021/jp020565c.

(116)   Redeckas, K.; Voiciuk, V.; Vengris, M. Investigation of the S1/ICT Equilibrium in Fucoxanthin by Ultrafast Pump-Dump-Probe and Femtosecond Stimulated Raman Scattering Spectroscopy. *Photosynth. Res.* **2016**, *128* (2), 169–181. https://doi.org/10.1007/s11120-015-0215-9.

(117)   West, R. G.; Fuciman, M.; Staleva-Musto, H.; Šebelík, V.; Bína, D.; Durchan, M.; Kuznetsova, V.; Polívka, T. Equilibration Dependence of Fucoxanthin S_1 and ICT Signatures on Polarity, Proticity, and Temperature by Multipulse Femtosecond Absorption Spectroscopy. *J. Phys. Chem. B* **2018**, *122* (29), 7264–7276. https://doi.org/10.1021/acs.jpcb.8b04217.

(118)   Ghosh, S.; Bishop, M. M.; Roscioli, J. D.; Lafountain, A. M.; Frank, H. A.; Beck, W. F. Femtosecond Heterodyne Transient Grating Studies of Nonradiative Deactivation of the S_2 (1^1Bu^+) State of Peridinin: Detection and Spectroscopic Assignment of an Intermediate in the Decay Pathway. *J. Phys. Chem. B* **2016**, *120* (15), 3601–3614. https://doi.org/10.1021/acs.jpcb.5b12753.

(119)   Ghosh, S.; Roscioli, J. D.; Bishop, M. M.; Gurchiek, J. K.; Lafountain, A. M.; Frank, H. A.; Beck, W. F. Torsional Dynamics and Intramolecular Charge Transfer in the S_2 (1^1Bu^+) Excited State of

Peridinin: A Mechanism for Enhanced Mid-Visible Light Harvesting. *J. Phys. Chem. Lett.* **2016**, 7 (18), 3621–3626. https://doi.org/10.1021/acs.jpclett.6b01642.

(120) Fresch, E.; Meneghin, E.; Agostini, A.; Paulsen, H.; Carbonera, D.; Collini, E. How the Protein Environment Can Tune the Energy, the Coupling, and the Ultrafast Dynamics of Interacting Chlorophylls: The Example of the Water-Soluble Chlorophyll Protein. *J. Phys. Chem. Lett.* **2020**, *11* (3), 1059–1067. https://doi.org/10.1021/acs.jpclett.9b03628.